Programmable Deployable Structures

Exploring the Potential of Mechanical Meta-Materials and Large-Scale 3D Printing for Fast Production and Assembly of Deployable Structures.

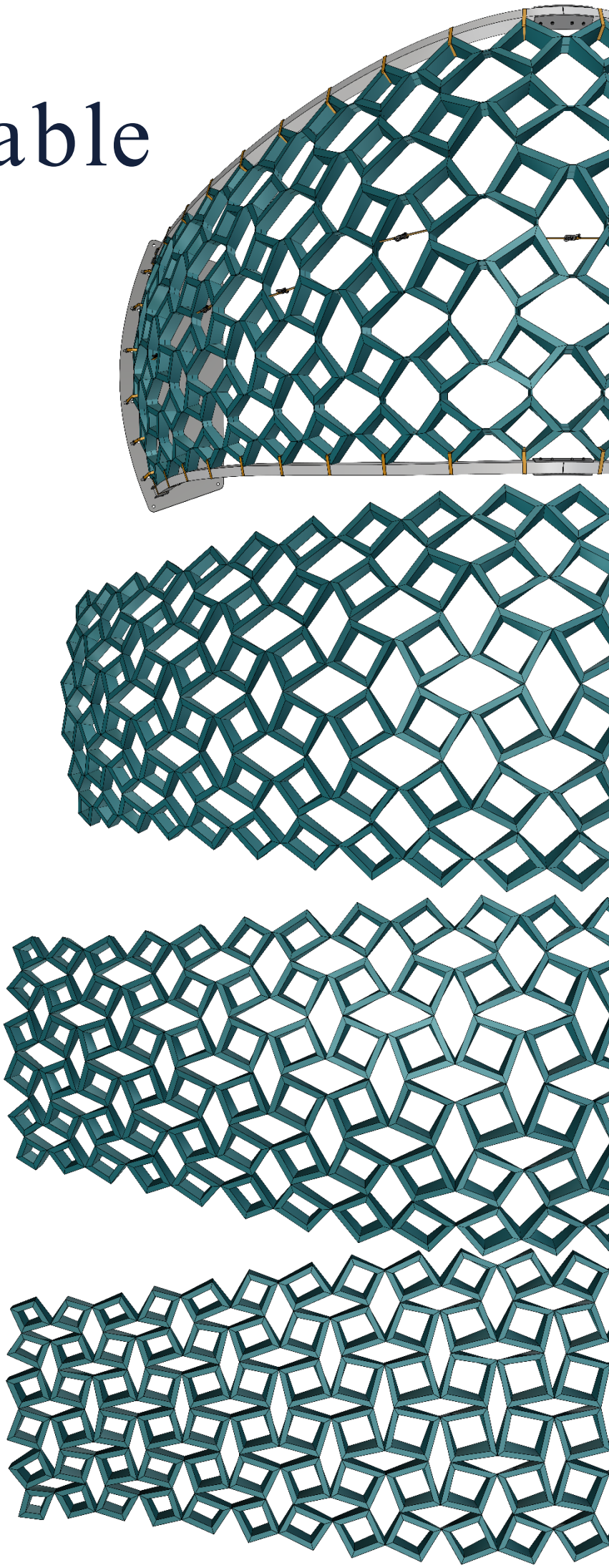

Pepijn Feijen

First mentor: Mauro Overend

Second mentor: Gabriele Mirra

Table of Contents

1 ABSTRACT

This study presents a computational and experimental framework for translating arbitrary doubly curved surfaces into 3D-printed, deployable structures based on programmable mechanical metamaterials. A rotating-polygon auxetic lattice is employed for its ability to expand or contract while preserving in-plane geometry. A dynamic-relaxation workflow implemented in Grasshopper/Kangaroo links flattened and target configurations through a global equal-length constraint, automatically resolving element dimensions and hinge rotations. This approach is validated on test shapes with three types of curvature: mono-, syn-, and anticlastic. Physical models of these test shapes were printed to demonstrate the feasibility of the method.

In addition, the potential for scaling the system to full-scale structures was explored through large-format additive manufacturing. Deployment techniques were investigated, and discussions with industry experts informed decisions on manufacturability and material selection. Full-scale printing trials were conducted to balance the flexibility required for compliant hinges with the rigidity needed in structural elements.

Finally, the developed method was applied to a case study: a temporary shelter for festivals and events. A deployable design was created, and optimisation strategies were explored for both the surface geometry and the applied lattice grid. Finite element analyses were performed to evaluate deformations during deployment as well as structural performance under operational loads. A 1:10 scale prototype was constructed to illustrate how the structure can be divided into printable segments and assembled to form the complete system.

2 INTRODUCTION

2.1 Background

Deployable structures are engineered systems designed to transition from a compact state to a larger, functional configuration through a process known as deployment. These structures address the need for efficient storage and transportation (S. Pellegrino, 2001). Although simple deployable structures, like umbrellas, have existed for centuries, advanced engineered deployable systems started to emerge in the mid-20th century. Today, these systems are widely used in diverse applications such as spacecraft antennas, retractable roofs, and medical devices (S. Pellegrino, 2001; Fenci & Currie, 2017).

Origami, derived from the Japanese words "ori" (folding) and "kami" (paper), involves folding flat sheets, usually paper, along straight creases to create three-dimensional shapes (Park et al., 2019; Jiang et al., 2020). Origami has evolved into a field influencing mathematics, computer science, and material science research (Jiang et al., 2020).

Kirigami, derived from "kiri" (to cut) and "kami" (paper), extends origami by adding cutting into the folding process (Park et al., 2019; Jiang et al., 2020). Kirigami enables the creation of more intricate structures that folding alone cannot achieve (Jiang et al., 2020).

Origami and kirigami together offer various kinematic systems useful for developing deployable structures. These methods have been studied extensively and demonstrate effective techniques for material transformation. Recent advancements in material science and engineering have further expanded these methods, offering new possibilities for innovation.

Metamaterials are engineered materials whose unique properties come from their designed microstructures rather than their composition (Zadpoor, 2016; Shaw et al., 2019). These materials can exhibit unusual behaviors, such as negative Poisson's ratios (auxetic materials), where materials expand laterally when stretched. Auxetic materials have properties beneficial for designing flexible, deployable structures, such as their ability to undergo significant shape changes while maintaining structural integrity (Ou et al., 2018; Zadpoor, 2016). Applications of metamaterials range from acoustic cloaking to soft robotics and materials capable of transforming into predetermined shapes under compression (Ou et al., 2018).

Despite these advantages, metamaterials are often difficult and expensive to produce. 4D printing technology makes manufacturing metamaterials feasible, as it extends traditional 3D printing by enabling printed objects to change shape, properties, or functionality over time (Campbell et al., 2014). Smart materials, like shape-memory polymers, allow 4D-printed structures to respond to external stimuli such as temperature, light, or water (Aldawood, 2023). MIT's Self-Assembly Lab has demonstrated 4D-printed objects that transform into predefined shapes when exposed to water, showing great potential for aerospace and architectural applications (Campbell et al., 2014).

These principles are relevant to architecture and structural engineering as they allow structures to adapt to environmental conditions, simplify construction, and enhance sustainability by reducing resource use. While adaptive deployable structures using origami, kirigami, and 4D printing have primarily been explored at smaller scales, significant opportunities remain for their development and application at larger architectural scales.

2.2 Problem Statement

Origami and Kirigami structures, deployable systems, self-assembly methods, programmable metamaterials, and 4D printing technologies each offer innovative approaches to controlling material behaviour, geometry, and functionality. These methods and principles lie at the intersection of design, material science, and engineering, and enable the creation of adaptive systems capable of dynamically responding, transforming, or adjusting to external stimuli. Such adaptive systems utilize advanced geometric principles, novel manufacturing techniques, and programmable materials to achieve flexibility and versatility.

A significant challenge shared by all adaptive structures is accurately predicting their transformations. Specifically, the core difficulty lies in translating an initial flat configuration into a reliably functioning structure that precisely assumes the desired deployed shape. Achieving this requires an in-depth understanding of both geometric transformations and the dynamic responses of materials subjected to external stimuli.

This prediction challenge relates closely to the broader "inverse design problem." According to Panetta et al. (2021), inverse design involves determining the optimal initial configuration of a structure that, once deployed, closely matches a target shape. This contrasts with forward design methods, where a known initial configuration is simulated to predict the resulting deployed shape. Forward design is generally simpler but often demands iterative experimentation to handle complex adaptive structures effectively. In contrast, inverse design (though technically more complex) directly aims at achieving specific desired outcomes, thereby potentially reducing extensive trial-and-error processes.

Current research predominantly investigates specific patterns or techniques for self-assembling or deployable structures. For example:

- **Chen et al. (2021)** propose deployable structures using bistable auxetic cells that transform from flat elastic sheets into stable, double-curved shapes, requiring no additional supports upon deployment.
- **Konaković et al. (2016)** introduce methods for creating auxetic surfaces through cutting patterns that form triangular linkages, employing conformal mapping to reliably translate a 2D layout into an accurate 3D geometry.
- **Panetta et al. (2021)** address inverse design in inflatable structures by optimizing networks of air channels, ensuring the inflated structure reliably achieves predetermined shapes.

Despite their innovation, these studies are primarily limited to planar materials and conventional manufacturing techniques such as CNC machining or laser cutting.

One approach to predicting structural transformations, as demonstrated by Dudte et al. (2023) and Ou et al. (2018), involves linear algebraic modelling. However, this method demands a strong mathematical and algorithmic background, skills typically less common among designers. Moreover, such abstract mathematical models provide limited visual feedback, creating a disconnect from the intuitive, visual processes designers prefer.

Demoly et al. (2021) underscore the broader lack of accessible predictive modelling tools for simulating material behaviour in adaptive structures, particularly those involving 4D printing. Without such predictive capabilities, designers frequently revert to trial-and-error experimentation, significantly slowing development and limiting the practical deployment of programmable and adaptive structures.

Ultimately, addressing the inverse design challenge through intuitive and accurate modelling frameworks is critical for broader adoption of adaptive methodologies in architectural and structural contexts.

2.2.1 Relevance

This research aims to address a significant gap in the design and fabrication of deployable structures by developing a computational method that minimizes the complexity of components, streamlines assembly processes, and leverages automation to simplify design and manufacturing workflows. By developing accessible, predictive design tools, this project seeks to facilitate broader integration of adaptive deployable structures into architectural applications, with the potential to fundamentally alter the way these structures are conceived and implemented.

The project specifically addresses current shortcomings by:

- Creating a computational tool capable of predicting the deployment and behaviour of adaptive structures without relying on extensive trial-and-error approaches.
- Developing a robust methodology that is accessible to designers, blending algorithmic precision with intuitive visual feedback to facilitate creative design exploration.
- Demonstrating the feasibility of manufacturing complex, adaptive structural systems using automated methods such as large-format additive manufacturing (LFAM).

The research holds relevance for various architectural and structural applications where adaptability, efficient transportation, rapid assembly, and reusability are key requirements. Potential use cases include:

- **Temporary shelters and event structures**: Rapidly deployable structures for exhibitions, outdoor events, or emergency response scenarios, benefiting from efficient transportation, minimal assembly, and reusability.
- **Adaptive building facades:** Dynamically responsive facades that adjust to environmental conditions such as sunlight, temperature, or airflow, contributing to sustainable building practices.
- **Interactive installations and exhibitions:** Visually engaging architectural elements capable of dynamic transformations that enhance user interaction, engagement, and spatial experience.

By addressing these critical issues, the research not only fills a gap in current computational modelling methods but also opens new possibilities for deploying innovative adaptive systems at a practical architectural scale.

2.3 Objective

The objective of this research is to investigate to what extent principles from emerging research fields—particularly self-assembling structures, mechanical metamaterials, and 4D printing—can improve the design and performance of deployable architectural structures. Specifically, this project aims to determine how these principles can enhance key characteristics such as ease of transport, rapid deployment, cost-effectiveness, and structural performance.

The challenges described in the problem statement highlight the absence of intuitive and accessible predictive modelling tools capable of reliably simulating the deployment and transformation behaviours of adaptive structures. Existing modelling methods, such as linear algebraic modelling, typically require advanced mathematical knowledge and do not provide designers with intuitive visual feedback, resulting in a disconnect from practical architectural applications. This gap underscores the need for a specialized computational tool tailored explicitly to designers. The proposed computational design tool will generate and optimize a kinematic mechanism capable of transitioning between multiple stable deployment states, ensuring that the final structure closely matches a predefined target shape.

The focus of this project is primarily on the mechanical performance of deployable structures, deliberately emphasizing mechanical and structural functionality over the use of responsive or smart materials. This prioritization is motivated by current limitations in large-scale manufacturing and predictability associated with responsive materials. Concentrating on mechanical solutions provides greater control and reliability, particularly for structural-scale applications that demand stability, safety, and predictable behaviour.

To evaluate the scalability, effectiveness, and practical applicability of the developed design methodology, a case study will be conducted, focusing specifically on deployable shelters. Deployable shelters represent an ideal test scenario for this research, as they are typically characterized by the need for rapid assembly, efficient transportability, reusability, and structural reliability. Additionally, shelters intended for exhibitions and events offer opportunities to demonstrate aesthetically compelling and innovative designs, enhancing public visibility and acceptance of deployable architectural solutions.

2.4 Research Question

2.4.1 Main research question

- How can the principles of mechanical-meta material be scaled up to design deployable shelters?

2.4.2 Background questions

- Can advancements in self-assembling structures, meta-materials, and 4D printing be of potential use for the creation of adaptive deployable structures?
- What principles, techniques, and materials enable adaptive deployable structures for diverse geometries?
- How can deployment methods, be evaluated for their effectiveness in creating adaptive deployable structures for diverse geometries?
- What computational techniques are used to address the inverse design problem in deployable structures or shape-changing materials?

2.4.3 Sub-questions

- How can a computational tool be developed to support the design of adaptive deployable structures?
- To what extent can programmable mechanical metamaterials be scaled to enable the creation of large, safe, and stable structures?
- In what ways can the developed computational tool be applied to design a functional, deployable shelter for events?

2.5 Approach and methodology

This study draws from a wide range of academic resources, including peer-reviewed papers from the ACM Digital Library, ScienceDirect, and online lectures. They were selected to ensure a comprehensive review of the current state of research and practice. Additionally, Notebook LM was utilized to compare and extract information from these papers, while ChatGPT was employed to assist with writing, refining, and checking the text.

This study will consist of 3 parts:

- Literature study on topic
- Development of a computation tool
- Application to a case study

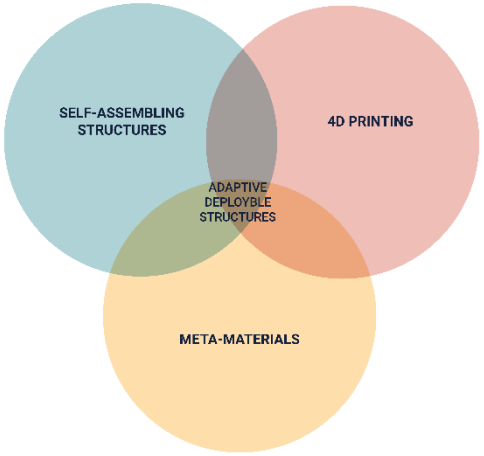

Figure 1: *Relation Self-assembling structures, 4D printing and Meta materials*

2.5.1 Literature review on topic

Emerging research in self-assembling structures, meta-material and 4d printing

This part of the research involves conducting a detailed literature review on self-assembling structures, meta-materials, and 4D printing. Each subject will be individually explored to define key concepts, categorize these technologies, examine current examples, and identify challenges that limit their development. The study will also analyse how these technologies interrelate (see figure 1) and if they can potentially be used for adaptive deployable structures.

Principles, techniques, and materials used for deployable structures

This part of the research focuses on identifying the principles, techniques, and materials that enable adaptive deployable structures with diverse geometries. Multiple case studies are examined to explore their deployment methods, applied materials, and manufacturing techniques, particularly their adaptability to various input shapes. By comparing these approaches, the study aims to identify effective techniques with the potential for scalability and broader application.

Computational methods

The computational methods aspect of this research will examine the approaches used in the case studies to address the inverse design problem. This includes analyzing the various techniques and algorithms employed to achieve adaptive deployable structures, focusing on how these methods were utilized to optimize geometry, materials, and functionality.

2.5.2 Development of a computation tool

Building on insights from the literature review, this phase explores kinematic mechanisms through a series of small-scale TPU prototypes produced by 3D printing. A computational design tool built on the principles of mechanical metamaterials and dynamic relaxation, then converts selected geometries into deployable structures. To verify versatility, the workflow is applied to three test surfaces exhibiting mono-, syn- and anticlastic curvature.

The process begins by generating a reference grid on the target surface in its fully deployed state and subsequently flattening this grid for fabrication. A kinematic system defines allowable variations in cell geometry, and constraint sets preserve desired behaviour while permitting the deformations required for deployment. Form-finding is performed with the Kangaroo physics engine, which iteratively minimises the difference between the flat and deployed configurations, thereby achieving minimal strain and faithful shape approximation.

The tool is validated through dynamic simulations and physical models, and the results inform further optimisation aimed at increasing scale, reducing material use, and integrating large-format additive manufacturing.

2.5.3 Application to a case study

This phase of the research involves adapting and applying the developed computational tool and insights gained from earlier modelling to a practical, large-scale case study. The aim is to evaluate the method's scalability and practicality within architectural applications, specifically through designing a deployable shelter for exhibitions and events.

Key considerations for scaling the methodology include:

- Selecting appropriate materials that balance flexibility for compliant hinges with the stiffness needed for structural stability.
- Addressing constraints and limitations inherent to large-format additive manufacturing, such as bead dimensions, continuous printing paths, and thermal management.
- Optimizing joint designs to maintain functionality and durability during repeated deployments.

Collaboration with industry partners BouwLab and CEAD Group provides essential feedback on manufacturability. Discussions cover the feasibility of proposed structures, constraints posed by large-format additive manufacturing, and potential improvements in material selection and hinge detailing.

Structural optimization is conducted to refine shelter geometry and grid configurations, considering surface curvature and element density. These parameters are fine-tuned to minimize weight and material use while meeting structural performance criteria defined by Eurocode standards for wind loads and service deflections.

Structural analysis conducted using Karamba3D, couples large-deformation deployment simulations with linear static load cases to verify that the structure achieves the target shape and withstands operational loads. Simulation results guide further adjustments to ensure both structural integrity and functional reliability.

Finally, validation of the scaling approach involves constructing full-scale prototype segments. These prototypes are tested for print quality, ease of assembly, and repeatability of deployment, confirming that the method remains robust, economical, and practical at architectural scales. This comprehensive approach ensures the developed methodology can effectively transition from conceptual design to tangible, deployable structures.

3 LITERATURE REVIEW

This section examines recent advances in self-assembling structures, mechanical metamaterials, and 4D printing to identify strategies relevant to the design of adaptive and deployable architectural systems.

3.1 The state of the art of Self-Assembling Structures, Meta materials and 4D Printing

3.1.1 Self Assembling Structures

Papadopoulou et al. (2017) define self-assembly as "the process by which disordered parts build an ordered structure without humans or machines." This phenomenon is observable in natural processes such as cellular replication, crystal formation, animal or insect swarming, and weather patterns.

The Self-Assembly Lab at MIT identifies three essential components for self-assembly:

1. **Components**: The physical characteristics of the components—such as geometry, texture, size, mass, weight, and polarity—encode the necessary information for the self-assembly process.
2. **Environment**: The surrounding medium, like fluids or air, provides a context for the components to interact. Activation energy, such as turbulence or agitation, initiates movement within the system.
3. **Interactions**: Interactions between the components and their environment drive the formation of ordered structures. These interactions involve two key mechanisms:
    - **Equilibration**: Alternating between aggregated and non-aggregated states.
    - **Error-Correction**: Adjusting positions and eliminating errors in the assembly process.

Papadopoulou et al. (2017) further distinguish between two types of self-assembly:

- **Static self-assembly**: Produces a fixed and stable structure.
- **Dynamic self-assembly**: Results in a continuously evolving structure that dissipates energy over time.

Examples

The Self-Assembly Lab at MIT is at the forefront of innovations in programmable materials and self-assembling systems. Their work investigates how objects and materials can autonomously organize or adapt by leveraging natural forces such as gravity, magnetism, and fluid dynamics.

Despite the name "Self-Assembly Lab," their research spans a broad range of topics, including: 4D printing, liquid printing, smart Active Textiles and programmable materials

The lab's projects often involve creating shape-shifting materials, self-folding structures, and responsive designs for applications in architecture, robotics, and manufacturing. By integrating design, engineering, and science, they aim to revolutionize production processes, focusing on adaptability, efficiency, and sustainability.

Most of the lab's projects start as manufactured structures that later change shape. Examples include:

1. **Biased Chains**:
   This project features a one-dimensional chain of elements, each containing a binary switch to control its orientation and fold angle. The user assembles the chain in a pre-determined sequence and activates it by shaking. The motion supplies energy, enabling the parts to reorient and fold into a desired 3D structure. (Tibbits, 2012)

Figure 2 *Biased Chains (Tibbits, 2012)*

2. **Programmable Table**:
   Developed in collaboration with Wood-Skin S.r.l., this furniture piece transforms from a flat-packed shipping form into a fully functional table. Using pre-stressed textiles and Wood-Skin® technology, the table eliminates complex assembly and efficiently transitions between forms for shipping, storage, and use, representing a new generation of reconfigurable, self-transforming household products. (*Programmable Table — Self-Assembly Lab*, n.d.)

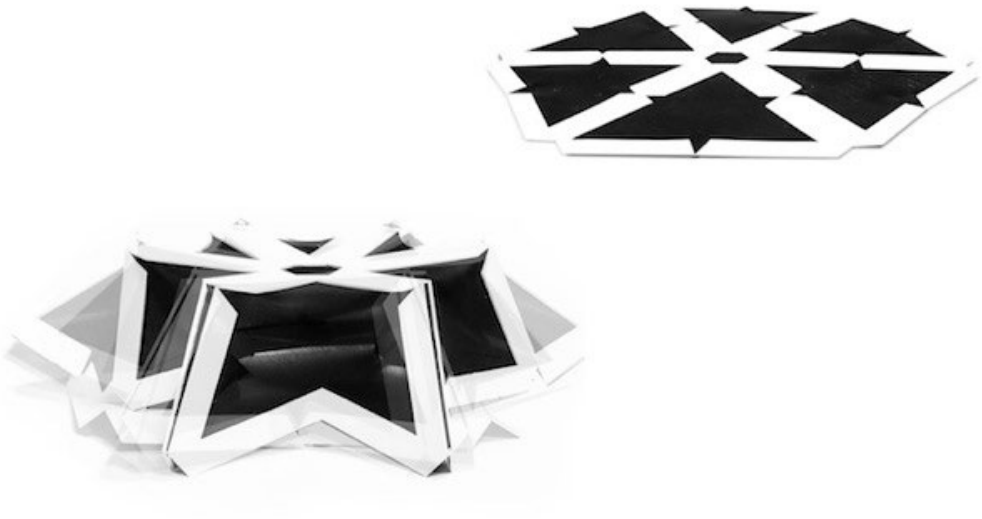

Figure 3: *Programmable Table (Programmable Table — Self-Assembly Lab, n.d.)*

However, only a few of the lab's projects meet the strict definition of self-assembly as outlined by Papadopoulou et al. (2017), which defines it as:
"The process by which disordered parts build an ordered structure without humans or machines."

Projects aligning with this definition include:

1. **Fluid Lattices**:
   In this project, identical truncated cube units embedded with magnets are released into a water tank. Pumps create turbulence, causing the units to move and connect, forming a 3D lattice structure. The lattice configuration emerges naturally, influenced by water flow, resulting in diverse and unpredictable structures. (Papadopoulou et al., 2017)

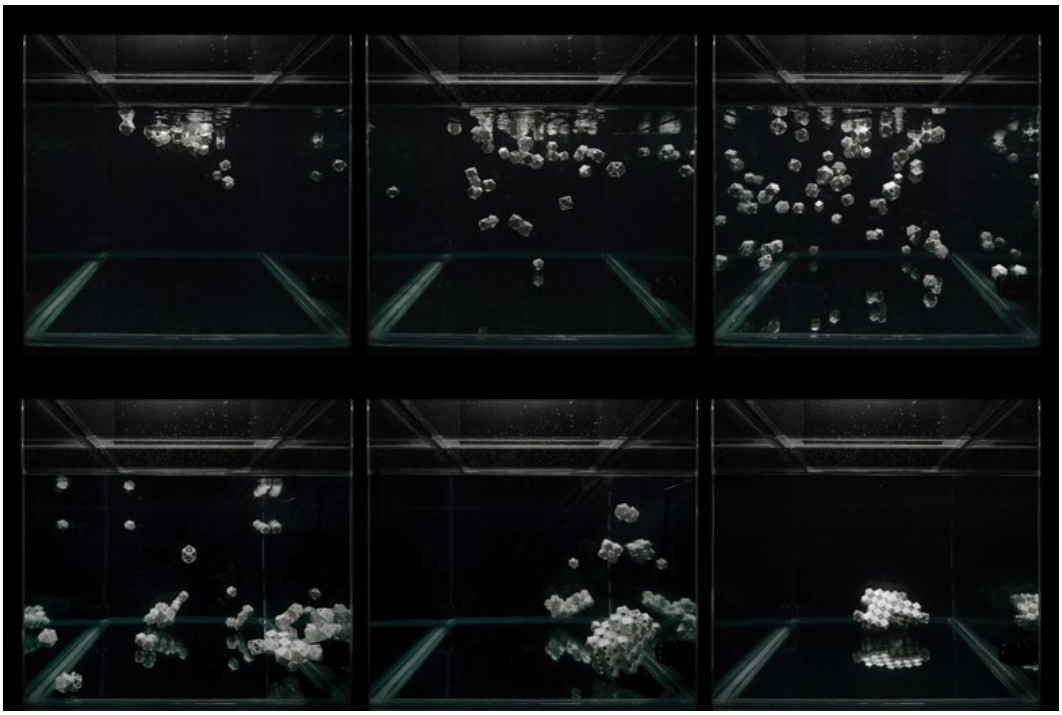

Figure 4: *Fluid Lattices (Papadopoulou et al., 2017)*

2. **Self-Assembly Chair**:
   This project demonstrates the assembly of a pre-designed chair from six unique components. Made of folded plastic sheets and 3D-printed connectors with embedded magnets, the components have distinct male/female node geometries. Placed randomly in a water tank, they assemble autonomously through magnetic attraction and geometric guidance. (Papadopoulou et al., 2017)

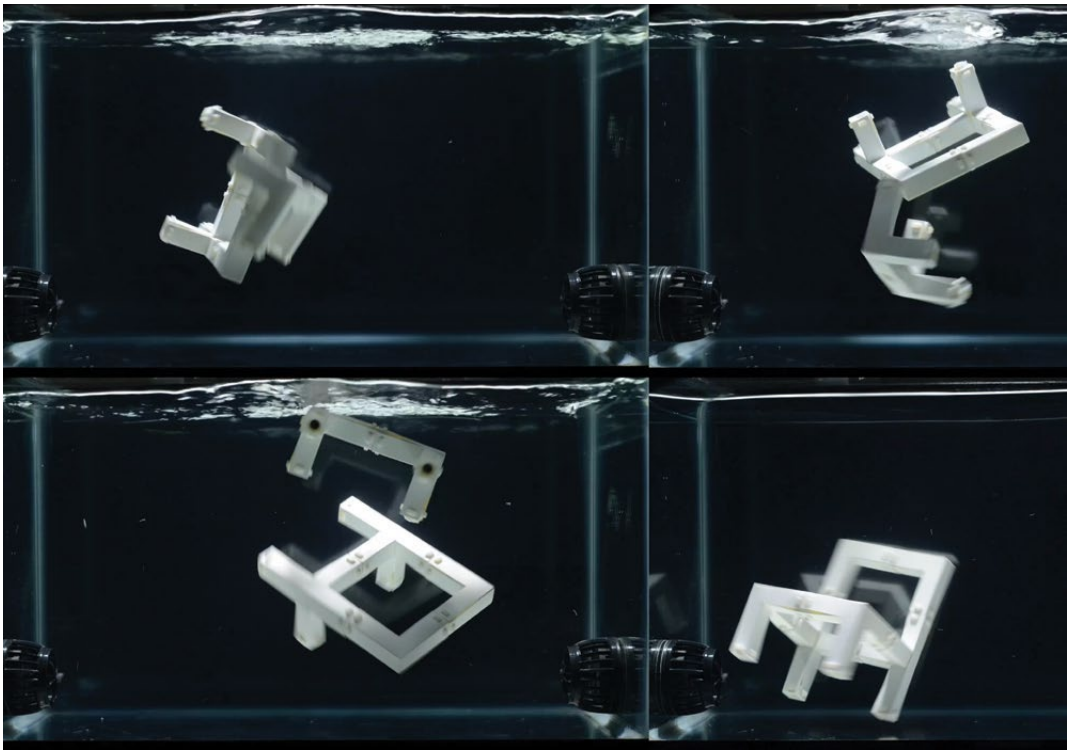

Figure 5: *The Self-Assembly Chair (Papadopoulou et al., 2017)*

3. **Aerial Balloon Assembly**:
   Large-scale self-assembly is explored using thirty-six identical truncated octahedron units made from fiberglass rods with Velcro-equipped nodes for connection and error correction. Each unit contains a helium-filled balloon for buoyancy. Released into a courtyard, they interact with turbulent air from fans, forming various structures such as lattices, cubes, and beams. (Papadopoulou et al., 2017)

Figure 6*: Aerial Balloon Assembly (Papadopoulou et al., 2017)*

4. **Self-Replicating Spheres**:
   Inspired by cellular replication, this project uses spherical units with hollow shells containing metal spheres and magnets. Placed on an oscillating table, the spheres move and connect, forming rings. As the rings grow, they destabilize and split into smaller rings, mimicking cellular mitosis. (Papadopoulou et al., 2017)

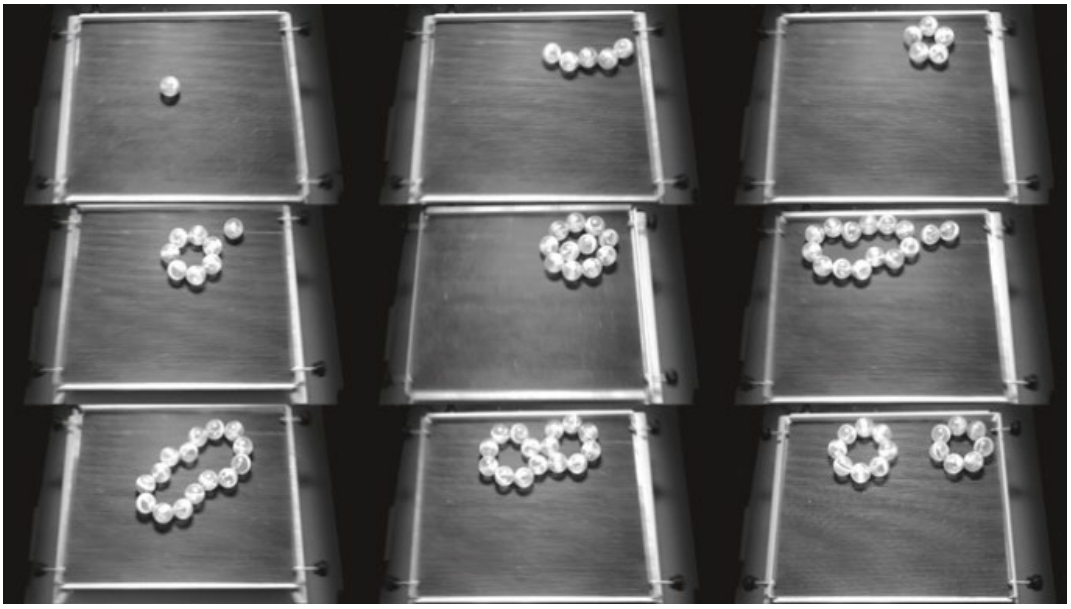

Figure 7: *Self-Replicating Spheres (Papadopoulou et al., 2017)*

5. **Aerial Fan Assembly**:
   This project explores evolutionary assembly based on environmental fitness criteria. Lightweight plastic truncated octahedron units with embedded magnets are released into a chamber with upward airflow created by a fan. The units collide and assemble, with the most successful configurations demonstrating the ability to both fly and grow in complexity. (Papadopoulou et al., 2017)

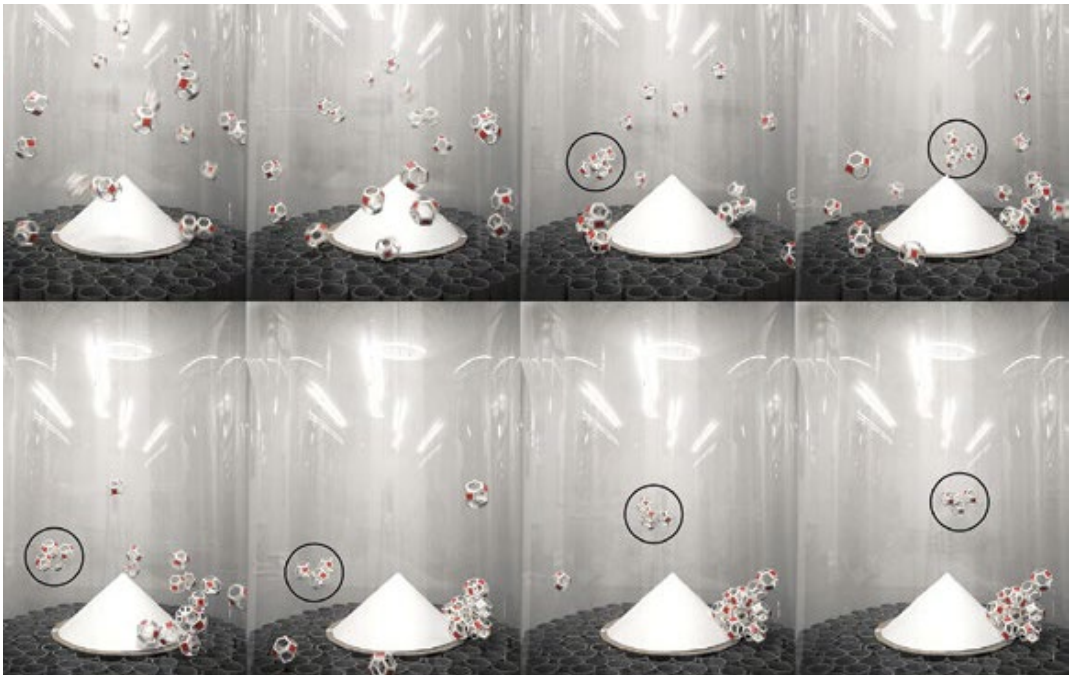

Figure 8: *Aerial Fan Assembly (Papadopoulou et al., 2017)*

Summary

The projects aligning with the definition of “self-assembling” including: Fluid Lattices, Self-Assembly Chair, Aerial Balloon Assembly, Self-Replicating Spheres, and Aerial Fan Assembly (Papadopoulou et al., 2017), are undoubtedly impressive and innovative. However, their operation still relies on carefully controlled environmental conditions, such as turbulent water tanks or enclosed spaces with forced airflows (ibid.). Although these demonstrations mark significant progress in the field of self-assembly, they remain several developmental stages away from practical deployment and widespread integration within the built environment. Further research is required to demonstrate their potential in solving real-world problems.

3.1.2 Meta materials

The concept of meta-materials initially emerged in the context of optics and electromagnetism, where they were primarily developed and studied. This focus has led to the term "meta-material" often being understood as specific to optical and electromagnetic applications. However, a relatively new and less explored category, mechanical meta-materials, has been introduced in recent years. Although certain classes of mechanical meta-materials, such as auxetic materials, have been recognized for decades, the broader exploration of this field remains in its early stages (Zadpoor, 2016).

Shaw et al. (2019) also describe mechanical meta-materials as "architected materials." In their research, they introduced an approach called Freedom and Constraint Topologies (FACT), which enables engineers to "reverse engineer" a desired mechanical behaviour. This method involves first defining the freedom space and then using its complementary constraint space as a blueprint to design the material's geometry.

Mechanical meta-materials stand apart in the spectrum ranging from natural materials with inherent mechanical properties to large-scale structures engineered with highly specific design characteristics. At the micro- and nanoscale, mechanical meta-materials behave more like structures due to their intricate designs. Yet, when viewed on a macro scale, their homogenized behavior aligns more closely with that of conventional materials, bridging the gap between structure and material (Zadpoor, 2016).

categories

Amir A. Zadpoor. (2016) discusses several categories of mechanical metamaterials:

- Extremal Materials: These materials are extremely stiff in certain modes of deformation while being extremely compliant in others. Examples include:
    - Penta-mode meta-materials: These materials have five very small eigenvalues, meaning they are very compliant in five out of six principal directions. This results in a very large bulk modulus compared to their shear modulus, making them almost incompressible. (Ibid)
    - Dilational meta-materials: These materials have an extremely small bulk modulus compared to their shear modulus. Their shape remains the same regardless of deformation; only their size changes. (Ibid)
    - Auxetic meta-materials: These materials have a negative Poisson's ratio, meaning they expand in the direction perpendicular to the tensile loading direction. Dilational materials are a specific case of auxetic materials. (Ibid)
- Negative Meta-materials: These materials exhibit negative moduli, such as a negative bulk modulus or negative elastic modulus.6 Examples include:
    - Materials with negative compressibility: These materials expand in response to hydrostatic pressure. They can have negative line, area, or volume compressibility. (Ibid)
    - Materials with negative stiffness: These materials deform in a direction opposite to the applied force. They can be combined with positive stiffness materials to create composites with high damping coefficients and stiffness values. (Ibid)

- Ultra-property meta-materials: These materials are designed to possess multiple desirable properties simultaneously, such as high stiffness, high strength, high toughness, and low mass density. (Ibid)
- Emerging areas of meta-materials: The source also discusses emerging areas in the field of mechanical meta-materials, including:(Ibid)
    - Origami-based meta-materials: These materials are inspired by the Japanese art of paper folding and utilize folding patterns to achieve desired properties and functionalities. (Ibid)
    - Active, adaptive, and programmable meta-materials: These materials can change their mechanical behaviour in response to external stimuli. They often make use of soft materials, large deformations, and instability. (Ibid)

Examples

To gain a better understanding of the possibilities offered by mechanical meta-materials, the following examples will be examined.

Ou et al. (2018) developed a system for designing deformable material mechanism, focusing on creating structures capable of diverse shape-changing possibilities. The system utilizes a set of cellular-based material structure units composed of rigid plates connected by elastic or rotary hinges. By adjusting the location and angle of these hinges, each unit can be programmed to perform unique transformations, such as uniform scaling, shearing, folding, and twisting. This allows for a wide range of design possibilities. For example, the position of the hinges can be parametrically tuned to create a gradual change in transformation. Additionally, the deformation of a single hinge can propagate throughout the entire system, enabling global transformations with local actuation.

Figure 9: *Spatial transformation includes bending and twisting. Combining these can achieve desired transformation (Ou et al., 2018)*

Ion et al. (2019) aims to develop a computational design tool that enables users to create customized mechanisms. The project is based on mechanisms composed of two types of cells arranged on a regular grid: rigid cells and cells capable of shearing. Users can input their desired motion paths, define the size of the mechanism, and draw the desired input and output paths. The tool then employs a heuristic optimization algorithm to find a cell configuration that fulfills these boundary conditions, essentially allowing users to "program" the desired mechanical behaviour of the metamaterial. This approach aims to make the design and fabrication of complex mechanisms more accessible.

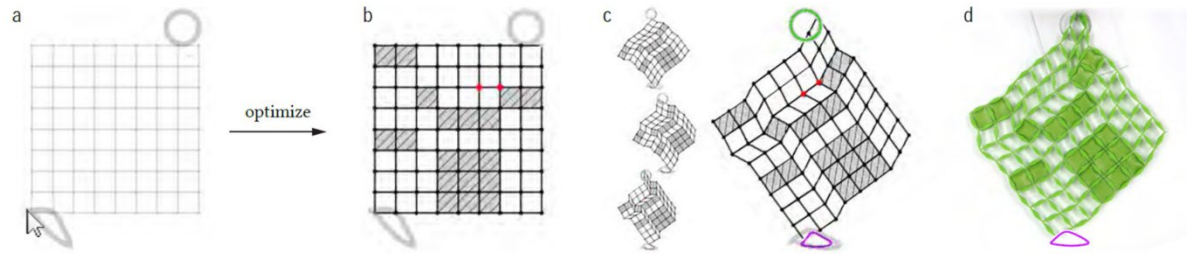

Figure 10: *Computational design tool for mechanical metamaterials (Ion et al., 2019)*

Both the research of Ou et al. (2018) and Ion et al. (2019) can be considered programmable mechanical metamaterials because they enable the creation of materials with customized mechanical properties and behaviours through the arrangement of specific structural units or cells. The specific arrangement of rigid plates and hinges in the research from Ou et al. (2018), or shearing and rigid cells in the research from Ion et al. (2019), controls the overall deformation and motion transformation of the material. This arrangement acts as a "program" that determines how the material will respond to external stimuli, like compression or force, enabling the design of materials with predictable and tuneable mechanical responses. This programmability distinguishes them from traditional materials, whose properties are determined solely by their chemical composition.

Both the research of Ou et al. (2018) and Ion et al. (2019) show promise for scalability and potential use in deployable structures. Ou et al. (2018) highlight its modularity, enabling the creation of larger-scale structures by tessellating individual units. This scalability is demonstrated through examples like the 15x15 panel showcasing the auxetic effect and the 8x8 panel with a gradient of hinge positions. This inherent scalability, combined with the ability to achieve controlled deformations, makes their research a strong candidate for deployable structures like foldable shelters, medical devices, or even large-scale architectural elements.

The research from Ion et al. (2019), while primarily focused on 2D structures, also exhibit scalability. The paper notes that their constraint graph representation can handle larger grids and more complex cell arrangements, suggesting potential for larger deployable structures. Extending this concept to 3D structures, as hinted at in the paper, could unlock new possibilities for designing intricate and efficient deployable systems across various scales.

Conclusion

In summary, mechanical meta-materials are a subset of meta-materials defined by their unique mechanical properties. Although called "materials," they often function more like structures due to their design and engineered functionalities. This characteristic allows them to bridge the gap between natural materials and engineered structures.

Most of these materials are designed and fabricated on the micro- and nanoscale, and no large-scale examples have been reported.

Programmable meta-materials are particularly notable for their ability to achieve controlled deformation through structured arrangements of units. This programmability has potential applications in deployable structures such as foldable shelters and scalable architectural systems. Their modularity and scalability make them a promising area for further research and practical use in dynamic, shape-changing designs.

3.1.3 4D Printing

4D printing is an advanced form of additive manufacturing where a 3D-printed object can deform and change its shape over time in response to external stimuli. Unlike traditional 3D printing, 4D printing incorporates time as the fourth dimension, allowing objects to transition from a static to a dynamic state (Aldawood, 2023).

The concept was introduced in 2013 by Skylar Tibbits, founder of the Self-Assembly Lab at MIT, and has since grown into a rapidly advancing field. By combining 3D printing with smart materials, 4D printing enables objects to respond dynamically to environmental factors (Aldawood, 2023).

Aldawood (2023) identifies three primary approaches for fabricating 4D objects:

1. **Stimulus-Responsive Smart Materials**: These materials alter their behavior in response to stimuli such as temperature, light, or moisture. Examples include shape-memory polymers that react to heat and hydrogels that swell when exposed to water.
2. **Implanted 3D-Printed Devices**: Polymer-based components are embedded in 3D-printed devices to accommodate tissue growth, particularly in biomedicine and tissue engineering. Applications include personalized implants and scaffolds for tissue regeneration.
3. **Self-Organization through Patterning**: This approach leverages self-assembly principles by precisely placing components in patterns to enable automatic assembly, inspired by natural phenomena like protein folding.

Programmable materials are central to 4D printing, allowing objects to transform their shape and properties post-production. This is achieved by designing materials that react predictably to specific stimuli (Campbell et al., 2014).

Challenges

Despite its promise, 4D printing faces significant challenges (Demoly et al., 2021):

1. **Material Limitations**: Smart materials often have low mechanical strength, actuation force, and efficiency. Repeated cycles of transformation can degrade these materials, reducing the lifespan of 4D-printed objects.
2. **Process Limitations**: Limited compatibility between smart materials and existing 3D printing techniques complicates multi-material printing. Additionally, precise and continuous stimuli application is required for transformations, posing a technical challenge.
3. **Design Limitations**: Current design processes rely heavily on trial and error due to the lack of robust predictive models for simulating material behavior. Developing predictive tools and methodologies is essential for advancing the field.

Aldawood (2023) emphasizes that the absence of predictive design models is directly tied to the "inverse design problem," where designers work backward from a desired outcome to determine the necessary materials, shapes, and stimuli. This lack of tools significantly hinders progress in 4D printing.

Examples

Researchers at MIT, Stratasys, and Autodesk have demonstrated various applications of 4D printing using Stratasys' Connex multi-material printer and polymers capable of expanding up to 150% when submerged in water (Campbell et al., 2014). Examples include:

- A snake-like object forming the letters "MIT" when exposed to water.
- A flat surface folding into a closed cube.
- A single strand folding into a wireframe cube.
- A strand transforming from the letters "MIT" into "SAL" (Self-Assembly Lab).
- A flat surface folding into a truncated octahedron.
- A flat disc folding into a curved origami saddle structure.

Figure 11: *4D Printing (4D Printing — Self-Assembly Lab, n.d.)*

Applications and Challenges in Architecture

While 4D printing's architectural applications remain in early exploration stages, researchers are investigating its potential in construction (Aldawood, 2023). Possible benefits include:

- **Adaptive Building Components**: Structures could adapt to environmental stimuli, enabling dynamic building designs and simplifying construction processes.
- **Responsive Facades**: Materials could create facades that adjust to weather changes, optimizing energy efficiency and aesthetics.
- **Customized Architectural Elements**: The ability to tailor complex geometries and material properties could allow for highly personalized designs.

However, several challenges must be addressed for large-scale architectural applications:

1. **Scalability**: Current technologies focus on small-scale objects. Advancements are required to scale up for large building components.
2. **Structural Integrity**: Ensuring the safety and stability of large structures necessitates rigorous testing and the development of new design principles.
3. **Cost**: High costs of materials and processes remain a barrier to adoption in construction.

Further research and innovation are essential to overcome these obstacles and unlock 4D printing's full potential in architecture.

Conclusion

4D printing, an innovative extension of additive manufacturing, enables 3D-printed objects to transform their shape over time in response to environmental stimuli, with programmable materials playing a central role in achieving these dynamic changes. By embedding responsiveness into the material design, 4D printing unlocks possibilities for adaptive structures across various fields. However, as a relatively new technology, it faces several challenges that hinder its widespread adoption. Among these, the lack of robust predictive models is particularly significant, as it forces designers to rely on trial-and-error processes, limiting efficiency and scalability. Overcoming these challenges is critical to realizing the full potential of 4D printing in industries such as architecture, biomedicine, and beyond.

3.2 Principles, techniques, and materials used for deployable structures

This part of the research investigates what principles, techniques, and materials enable adaptive deployable structures for diverse geometries. The selected projects explore varied deployment methods, applied materials, and manufacturing techniques, including adaptability to multiple input shapes. By comparing these approaches, the study aims to highlight their unique contributions and uncover key connections for advancing deployable structures.

3.2.1 Different studies

Elastic Geodesic Grids

Pillwein and Musialski (2021) focused on creating spatial grids made of bent lamellas that can be deployed from a planar configuration. These structures approximate freeform surfaces and are easy to fabricate and deploy. The deployment process is governed by the rules of physics, with the lamellas acting as thin elastic beams that can bend, rotate, and slide at their intersections.

The structures are deployed from a planar configuration using a simple kinematic mechanism. The deployment process is governed by the physics of the elastic lamellas.

Bistable Auxetic Surface Structures

Chen et al. (2021) utilizes optimized bistable auxetic cells to create deployable structures. The structures can be flat-fabricated from elastic sheet material and then deployed into a desired double-curved target shape by activating the bistable mechanism of its component cells. The deployed model is stable and does not require external supports or boundary constraints.

The structures are deployed by activating the bistable mechanism of the auxetic cells, causing the planar sheet to transform into the desired double-curved shape. The deployment can be triggered manually or through environmental stimuli.

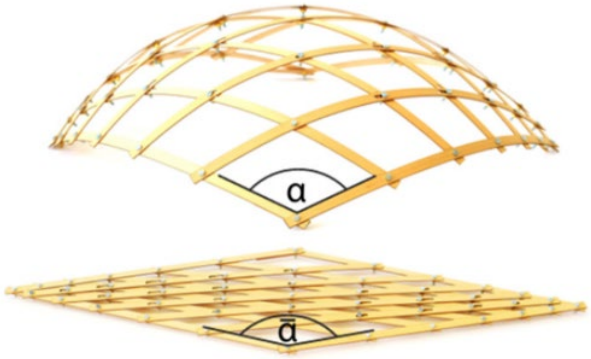

Figure 12: *Elastic Geodesic Grids (Pillwein et al., 2020)*

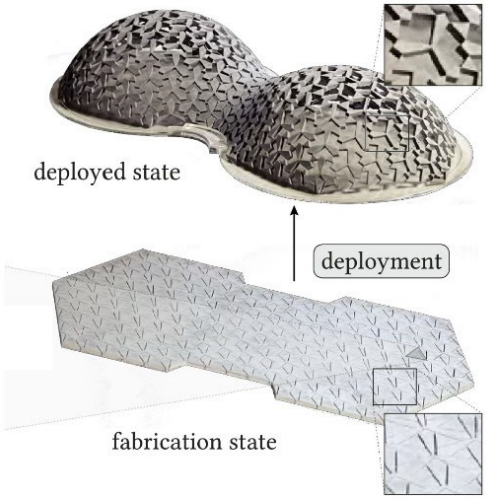

Figure 13: *Bistable Auxetic Surface Structures (Chen et al., 2021)*

Computational Design with Auxetic Materials

Konaković et al. (2016) focuses on designing and fabricating surfaces with auxetic materials, which exhibit a negative Poisson's ratio. By introducing a cutting pattern that creates a triangular linkage, the method allows for spatially varying stretching of initially inextensible flat sheets.

Deployment is achieved through the controlled expansion of the auxetic material, guided by the specific cutting pattern and linkage design. The method utilizes conformal mapping to relate the 2D layout to the 3D deployed shape.

Surface-Based Inflatables

Panetta et al. (2021) tackles the inverse design problem for inflatable structures, aiming to find the optimal network of air channels that deploy to approximate a given target surface. The structures are fabricated by fusing together sheets of airtight inextensible fabrics along computed air channel curves.

The structures are deployed by inflating the network of air channels. The pressure forces expand the channels, causing the initially flat sheets to transform into the desired shape. The deployed state is determined by a static equilibrium condition, which is achieved when the internal pressure balances the elastic forces of the material.

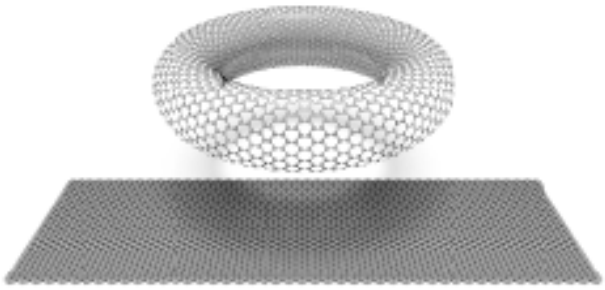

Figure 14: *Design with Auxetic Materials (Konaković et al., 2016)*

Figure 15: *Surface-Based Inflatables (Panetta et al., 2021)*

Differentiable Stripe Patterns

Maestre et al. (2023) investigates the use of stripe patterns for the design and fabrication of various deployable surfaces. The approach involves generating unique and differentiable stripe patterns and incorporating equilibrium state derivatives to enable an end-to-end differentiable pipeline for optimizing the design.

The deployment method depends on the specific material system employed, but the core concept relies on the geometric arrangement and deformation of stripe patterns to achieve the desired shape transformation. Examples include inflatable membranes, surfaces made from elastic curves, and auxetic structures.

Freeform Quad-Based Kirigami

Jiang et al. (2020) explore the use of kirigami techniques to create deployable structures. The method involves cutting and folding flat sheet material to form quad-based boxes that assemble into freeform shapes. The design focuses on creating desirable geometric and aesthetic quality of the designed structures, utilizes smooth curve networks to define cuts and folds.

The structures are deployed by folding the pre-cut sheet material along the designated lines, guided by the quad-based box pattern. The final 3D shape is achieved through the geometric arrangement and connections of the folded elements

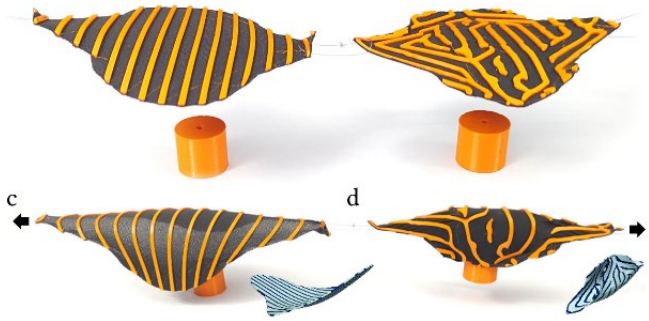

Figure 17: *Differentiable Stripe Patterns (Maestre et al., 2023)*

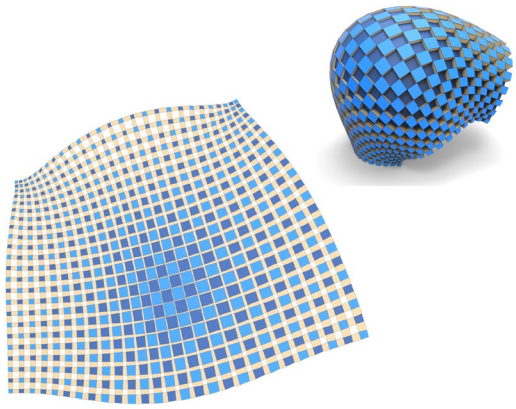

Figure 16: *Freeform Quad-Based Kirigami (Jiang et al., 2020)*

Programmable Auxetics

Konaković et al. (2018) leverages spatially graded auxetic metamaterials to create deployable structures that can approximate doubly curved surfaces. The structures are actuated from a flat initial state via inflation or gravitational loading, achieving maximal expansion in the deployed state. The structures are deployed by either inflating the auxetic material or subjecting it to gravitational loading. Both methods achieve maximal expansion, ensuring that the final shape is determined by the pre-programmed geometry of the material.

Elastic Umbrella Mechanisms

Ren et al. (2022) introduce a new type of volumetric deployable structure called an umbrella mesh, which consists of elastic beams, rigid plates, and hinge joints. The structures are fabricated in a compact, zero-energy rest state and deploy into bending-active 3D target surfaces. During deployment, the elastic beams rotate from vertical to horizontal configurations, transforming the compact structure into a curved surface. Deployment is achieved by pushing or pulling the triangular plates of the umbrella cells towards each other, causing the elastic beams to rotate from vertical to horizontal configurations. The differing heights of the cells create kinematic incompatibilities, forcing the structure to buckle into the desired curved shape.

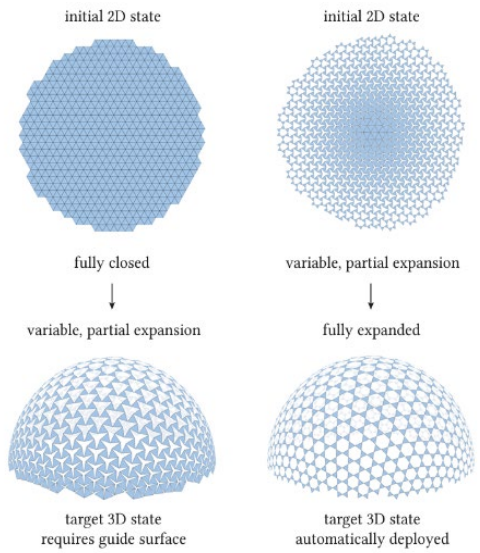

Figure 18: *Programmable Auxetics (Konaković et al., 2018)*

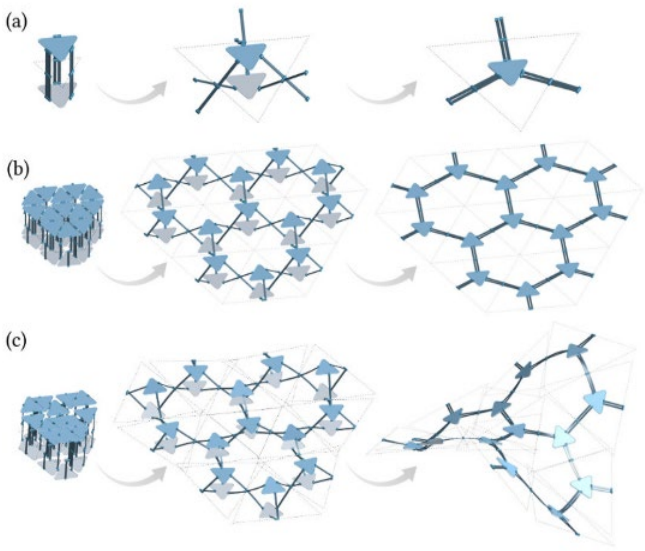

Figure 19: *Elastic Umbrella Mechanisms (Ren et al., 2022)*

Tension-Actuated Shaping Objects

Guseinov et al. (2017) present a method for creating self-actuated, smooth, three-dimensional shells from an initially flat state. The structures are made of flat, rigid tiles connected by thin, pre-stretched elastic sheets. When released, the elastic sheets exert contraction forces that shape the assembly into a stable 3D configuration.

The structures are deployed by releasing the pre-stretched elastic sheets, allowing them to contract and exert forces on the rigid tiles. The contraction forces, combined with the contact forces between the tiles, shape the assembly into the desired stable 3D configuration.

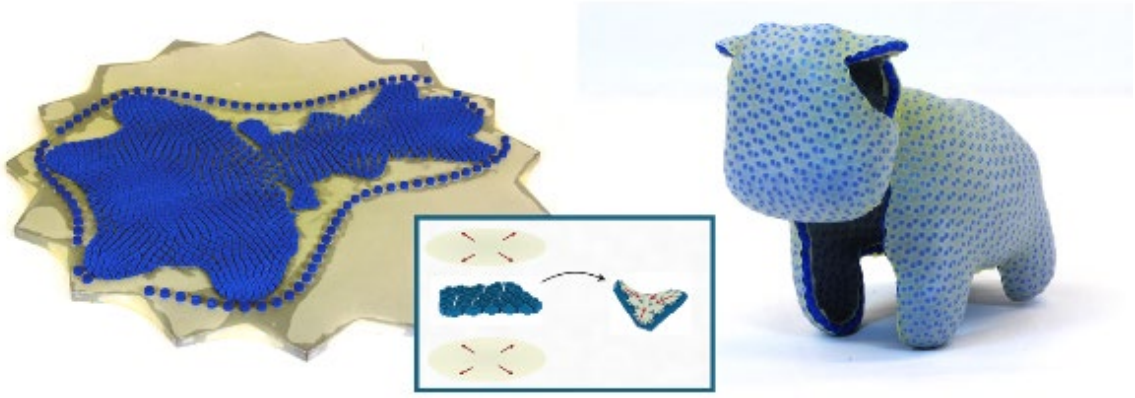

Figure 20: *Tension-Actuated Shaping Objects (Guseinov et al., 2017)*

3.2.2 Comparison of Methods Structure Transformation

Auxetic Applications

The following projects each incorporate some form of auxetics to enable shape transformation and deployment, but they differ significantly in their approaches and outcomes.

Konaković et al. (2016) developed a homogeneous auxetic pattern consisting of identical triangular tiles. This pattern facilitates the creation of double-curved surfaces from flat, flexible materials. However, the uniformity of the pattern limits the variety of achievable shapes, necessitating the use of guide surfaces to ensure precise deployment.

Building on the previous work, Konaković-Luković et al. (2018) introduced a spatially graded auxetic pattern where triangle sizes vary to encode specific expansion factors. This innovation expands the range of shapes that can be achieved and enables automatic deployment through inflation or gravity, removing the dependency on guide surfaces. The material's flat configuration inherently encodes the target shape, simplifying the deployment process.

Chen et al. (2021) focused on bistable auxetic cells that feature two stable states: a flat fabrication state and an expanded deployed state. Their approach leverages a precomputed library of optimized bistable cells and employs metric distortion analysis to achieve desired shapes. The deployed configurations are stable equilibria, requiring no continuous external forces to maintain their form, making this method particularly efficient.

Ou et al. (2018) takes inspiration from auxetic mechanisms, particularly the Rotating Polygon structure. Rather than relying solely on intrinsic material properties, KinetiX employs a parametric design approach to expand transformation possibilities. By adjusting hinge positions and incorporating both in-plane and out-of-plane rotations, KinetiX achieves transformations such as uniform scaling, shearing, bending, and twisting, surpassing the conventional expansion and contraction behaviors typical of auxetic materials.

Elastic Bending for Deployment

Both Pillwein et al. (2020) and Ren et al. (2022) employ elastic bending as a mechanism for deployment. However, their methods differ significantly in structure and approach.

Pillwein et al. (2020) utilize a grid-like structure composed of a basic four-bar linkage system with rigid members, rotating joints, and a single degree of freedom. By adjusting the angle of the linkage, the system buckles out of plane to maintain its length, enabling deployment.

In contrast, Ren et al. (2022) employ a network of scissor mechanisms integrated within individual umbrella cells. The variation in heights between neighbouring umbrella cells creates geometric incompatibilities during deployment, inducing out-of-plane buckling to achieve the desired surface configuration.

Inflation for Deployment

Both Konaković et al. (2018) and Panetta et al. (2021) leverage inflation as a mechanism for deployment, but their methods utilize distinct structural designs.

Konaković et al. (2018) develop an auxetic pattern tailored to a desired target shape. This pattern is deployed using an inflatable balloon placed beneath it. The auxetic structure constrains the balloon, shaping its expansion during deployment.

Panetta et al. (2021) fabricate a structure by bonding two layers of inextensible sheet material along curves, forming a network of tubular channels. These channels are inflated with air or fluids, enabling the surface to deploy effectively.

Common Challenges:

Accurate Shape Approximation: A key challenge is ensuring the deployed structure accurately approximates the desired 3D target shape. Factors like material properties, hinge design, and the complexity of the target geometry can affect the final shape fidelity. Achieving a balance between the desired shape and the constraints imposed by the material system is crucial for all these projects. (Pillwein et al., 2020; Pillwein & Musialski, 2021; Chen et al., 2021; Konaković et al., 2016; Panetta et al., 2021; Maestre et al., 2023; Jiang et al., 2020; Ou et al., 2018; Konaković et al., 2018; Ren et al., 2022; Guseinov et al., 2017)

Robust and Predictable Deployment: Ensuring reliable and predictable deployment from the compact state to the final shape is another common hurdle. Issues like self-intersections, buckling, or getting stuck in local energy minima during deployment need to be addressed for practical applications. These projects utilize various strategies, like spatially graded patterns, bistable mechanisms, or guide surfaces, to enhance the robustness of the deployment process. (Ibid)

Computational Design Complexity: Designing these structures involves solving complex optimization problems considering material behavior, geometric constraints, and kinematic limitations. Developing efficient and robust computational tools to navigate this design space and optimize for specific performance criteria is crucial for the

conclusion. (Pillwein et al., 2020; Pillwein & Musialski, 2021; Chen et al., 2021; Konaković et al., 2016; Panetta et al., 2021; Maestre et al., 2023; Jiang et al., 2020; Konaković et al., 2018; Ren et al., 2022; Guseinov et al., 2017)

Conclusion

The reviewed projects demonstrate the diverse approaches and advancements in utilizing auxetics and other mechanisms for shape transformation and deployable structures. While methods such as homogeneous and spatially graded auxetic patterns, bistable cells, elastic bending, and inflation highlight significant innovations, each approach balances unique trade-offs between deployment accuracy, robustness, and computational complexity. Challenges such as precise shape approximation, reliable deployment, and the development of efficient computational tools remain central to achieving practical and scalable applications.

3.3 Evaluation Criteria for Deployment Methods

The previous chapter discussed common challenges related to the design and fabrication of deployable structures, including:

- Accurate Shape Approximation: Achieving precise geometric configurations in both deployed and operational states.
- Robust and Predictable Deployment: Ensuring reliable transformation processes without damage or failure.
- Computational Design Complexity: Managing the intricate modeling and analysis required for these structures.

Among these, Accurate Shape Approximation and Robust and Predictable Deployment stand out as critical criteria for the success of deployable structures. Another significant aspect discussed was manufacturability, emphasizing the need to make these structures reliable and scalable for larger applications.

Research by S. Pellegrino (2001) and Fenci & Currie (2017) identifies key criteria for evaluating deployable structures:

1. Deployment and Retraction Process: The transformation must be autonomous, reliable, and damage-free. Deployment often represents the most challenging phase due to strict functional constraints. (Pellegrino, 2001)
2. Stiffness and Accuracy: Deployed structures must maintain precise operational functionality, such as providing shelter or forming reflective surfaces. Rigid elements must ensure stiffness, while elastic latching elements can enhance joint accuracy to mitigate potential weaknesses. (Pellegrino, 2001)
3. Material Efficiency and Weight: Lightweight materials with high strength-to-weight ratios are crucial for deployable structures. Compact packaging further enhances transportability and feasibility. (Pellegrino, 2001)
4. Stress and Strain Management: Components must withstand stress and strain across packaging, deployment, and operational states. Controlled release of elastic energy in structural elements (e.g., coiled rods) is essential. (Pellegrino, 2001)
5. Environmental and Operational Performance: Factors such as material choice, system configuration, control techniques, and cost significantly influence a structure's sustainability and functionality. (Fenci & Currie, 2017)

Conclusion

Based on these criteria, similar aspects have been merged for clarity and practicality:

1. Reliable Deployment and Retraction: Predictable transformation processes that ensure structural integrity.
2. Structural Integrity and Precision: Stiff, accurate configurations with robust joints to meet operational requirements.
3. Material Efficiency and Lightweight Design: Use of materials optimized for strength, weight, and compact packaging.

4. Stress and Energy Management: Effective handling of stress and strain during all operational phases.
5. Sustainability and Scalability: Environmentally conscious material choices and cost-effective designs for broader applicability.

3.4 Computational methods

3.4.1 Inverse design problem

The inverse design problem is the challenge of finding the optimal configuration of a structure so that, when deployed, it approximates a given target shape. This contrasts with forward design, where a structure's configuration is given, and its deployed shape is determined through simulation. (Panetta et al., 2021)

For example, in the research of Panetta et al. (2021), the goal is to find the optimal network of air channels so that the inflated surface conforms as closely as possible to a given 3D design surface. This problem is particularly challenging because the deployed state needs to satisfy static equilibrium conditions.

Another example is the research of Konaković et al. (2018) on auxetic materials, more specifically those based on a triangular linkage structure. In this case, the challenge is to determine the appropriate scaling of the triangular elements in the flat configuration so that the structure approximates a desired shape when expanded. The spatially varying maximal extension factor determines the fully expanded linkage's metric, which defines the deployed shape up to isometric deformation.

In the design research of Guseinov et al. (2017), they developed curvy shells formed from an initially flat state, the inverse design problem involves finding the optimal layout, shape, and attachment areas of the rigid tiles in the flat configuration so that the assembled structure closely matches the target shape when actuated by pre-stretched elastic sheets. The forces resulting from the contraction of the elastic sheet must balance the contact forces of the elements for the structure to be stable in its target configuration.

Several common challenges arise in these inverse design problems:

- Ensuring that the deployed shape conforms accurately to a target geometry.
- Satisfying equilibrium or stability conditions in the deployed state.
- Optimizing geometric parameters (such as scaling, tiling, or layout) in the flat state.
- Managing material behaviour and actuation forces during deployment.

3.4.2 Conformal mapping

Conformal mapping is a mathematical technique that preserves angles between curves when mapping a surface from one domain to another, for example, from a three-dimensional surface to a two-dimensional plane (Konaković et al., 2016). The amount of local scaling induced by the mapping is called the conformal scale factor. Conformal maps are particularly useful for understanding the design space of deployable structures because they provide a way to predict the relationship between the flattened configuration of a material and its deployed shape (Konaković et al., 2016).

Several studies utilize conformal mapping for the design of deployable structures (Guseinov et al., 2017; Ren et al., 2022; Panetta et al., 2021; Chen et al., 2021; Konaković et al., 2016, 2018), but each addresses specific challenges and limitations associated with the chosen material system:

- In the research of Konaković et al. (2016) conformal mapping with bounded scale factor is used to initialise a non-linear optimization process to simplify and adapt a 3D design surface with an auxetic linkage.
    - This method leverages the fact that the auxetic linkage, composed of rigid triangles connected by rotational joints, exhibits locally uniform scaling under deformation, similar to conformal maps. (Ibid)
    - However, the scale factor must be bounded between 1 and a material-dependent constant, limiting the achievable shapes. (Ibid)
    - To overcome this limitation, the authors suggest adding cone singularities—special points in the structure where the usual pattern is intentionally altered. These singularities help concentrate the distortion caused by stretching or compressing the material, making it possible to better approximate surfaces with higher curvature. (Ibid)

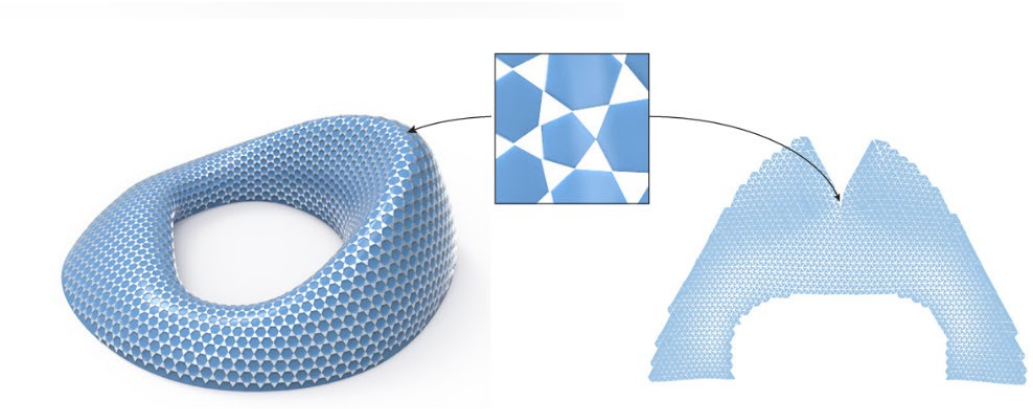

Figure 21: *Cone singularities (Konaković et al., 2018)*

- In other research of Konaković et al. (2018) they also employ conformal maps to understand the design space of deployable auxetic structures.
    - They show that surfaces created through inflation or gravitational loading must allow for conformal flattening with limited variation in scale. (Ibid)

- To make deployment easier, they propose spatially grading the auxetic linkage, which adjusts the linkage design to match the curvature of the target shape, enabling fast deployment without needing additional guide surfaces. (Ibid)

- Chen et al. (2021) uses conformal flattening as the first step in a design method for creating deployable surfaces with bistable auxetic cells.
    - Starting with a target surface, the algorithm flattens it to a plane and overlays a regular grid pattern.
    - The local scale factor for each cell is then used to pick the best-suited cell from a library, selecting the one with the highest stiffness in its second bistable state.

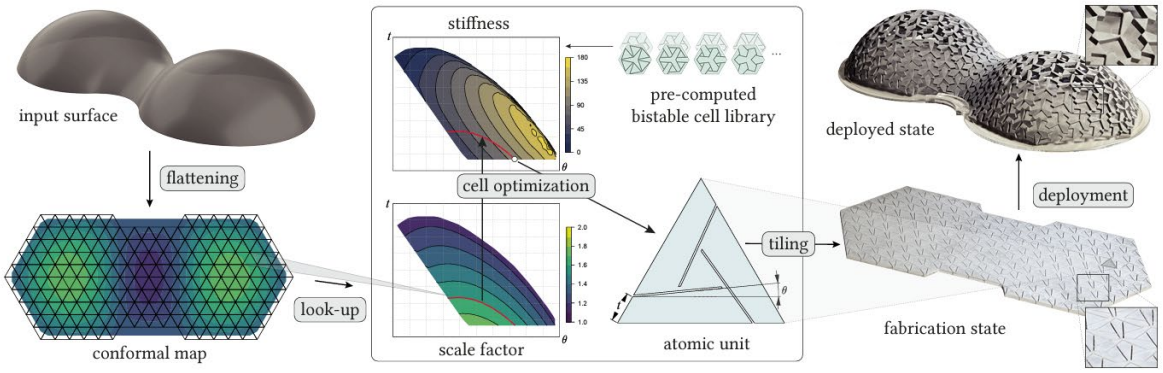

Figure 22: *Process (Chen et al., 2021)*

- Panetta et al. (2021) takes a different approach to conformal mapping for the inverse design of inflatables.
    - Instead of relying on traditional conformal mapping, the authors focus on anisotropic metric distortion, which accounts for how inflated air channels contract in different directions. (Ibid)
    - This method supports the design of more intricate inflatable shapes but requires a specialized optimization algorithm to handle the complexity of anisotropic behavior. (Ibid)

In summary, the sources demonstrate the utility of conformal mapping in understanding the relationship between a structure's flattened and deployed configurations, particularly for auxetic materials and inflatables. However, limitations such as restricted scale factors and the need to account for anisotropic material behaviour pose significant challenges. These constraints can limit the range of achievable shapes and require specialized computational methods, which may result in increased computational cost and reduced design flexibility.

3.4.3 Numerical optimization

Numerical optimization plays a crucial role in solving inverse design problems for deployable structures, as it provides a way to find optimal configurations that satisfy various constraints and objectives. The sources showcase different ways numerical optimization is applied to achieve specific design goals:

Konaković et al. (2016) utilizes numerical optimization for surface rationalization, aiming to approximate a given 3D design surface with an auxetic linkage. The authors employ a constrained-based optimization approach to:

- Ensure all triangles in the linkage maintain equal edge length.
- Prevent collisions between triangles.
- Minimize the distance between linkage vertices and the target surface.

They use conformal maps to initialize the optimization. The objective function is minimized using alternating minimization with auxiliary variables, an efficient method for handling large-scale optimization problems.

Konaković et al. (2018) employs numerical optimization to find the optimal scaling parameters and layout of a 2D auxetic linkage that approximates a target surface when deployed. The optimization process involves two steps:

1. **3D Linkage Optimization**: The linkage is optimized on the target surface to maximize surface expansion while maintaining connectivity and avoiding collisions.
2. **2D Linkage Optimization**: The optimized 3D linkage is flattened to a 2D plane, and the vertex positions are further optimized to ensure a valid planar configuration.

This two-step approach ensures that the deployed structure closely approximates the target surface while maintaining the structural integrity of the linkage.

Chen et al. (2021) focuses on optimizing the bistability and stiffness of individual auxetic cells to ensure robust deployment. They employ nonlinear periodic homogenization to simulate the mechanical properties of the cells and utilize a custom Newton solver to find cell parameters that maximize bistability and stiffness.

Panetta et al. (2021) introduce an algorithm that continuously adjusts the shape of air channel boundaries to closely match the inflated surface with the target design. The algorithm uses a simulation to predict how the structure will inflate, ensuring the final design is stable and balanced

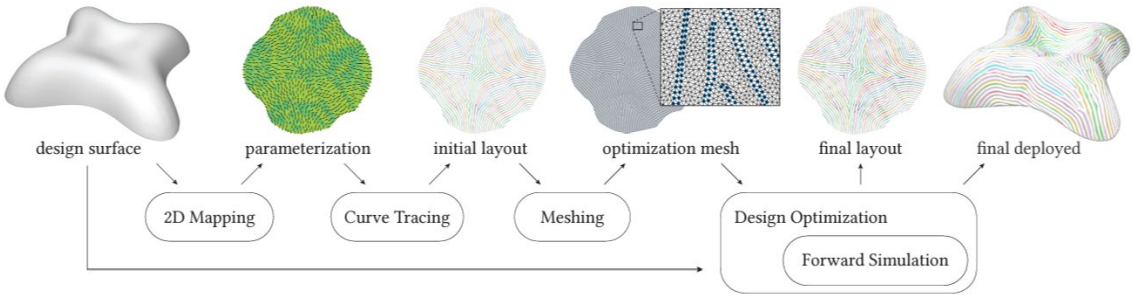

Figure 23: *Process (Panetta et al., 2021)*

Maestre et al. (2023) present a gradient-based optimization tool that automatically generates stripe patterns to achieve specific mechanical properties. The method uses advanced modeling techniques, including solid shell finite elements and XFEM, for precise simulations of elastic bi-material surfaces. By employing the adjoint method, the tool efficiently calculates gradients to optimize high-level design goals like overall stiffness.

Guseinov et al. (2017) features a two-step optimization procedure to approximate a 3D input model with a stable surface generated by tiles in an actuated configuration. First, a coarse optimization finds an approximate solution using a simplified energy model that avoids expensive force computations. Then, a local refinement step refines the solution using an accurate physics-based model and local optimization. This approach balances efficiency and accuracy in solving the complex layout and shape optimization problem.

3.4.4 Conclusion

The application of numerical optimization and conformal mapping techniques demonstrates significant progress in solving inverse design problems for deployable structures. Conformal mapping is often employed as a preliminary step to flatten a target surface while preserving local angles. For this, the conformal scale factor must not exceed the scale factor allowed by the material or mechanism. To address challenges associated with high curvature, cone singularities (cuts) can be introduced to reduce the maximum curvature, thereby lowering the conformal scale factor and enabling a better approximation of the target shape.

For structures with diverse mechanical properties, such as bistable auxetic cells, researchers can create a library of pre-simulated geometries by varying key parameters. This allows for the selection of cells that optimally balance multiple performance criteria, such as bistability and stiffness, during deployment.

Constraint-based optimization methods are also crucial in ensuring that initial mechanisms adhere to specific rules, such as preserving equal edge lengths in rigid elements or maintaining certain angles during deformation. These constraints are combined with objective functions to guide the optimization process toward a valid configuration.

Finally, simulation-based optimization methods, including finite element modelling (FEM), play a key role in predicting how structures will deploy. These simulations allow researchers to refine designs by adjusting variables to optimize deployment performance while maintaining structural stability. By leveraging these combined techniques, researchers have expanded the design space of deployable structures and enabled the development of highly intricate and functional configurations.

3.5 Conclusion Literature Review

Adaptive and deployable structures exist at the intersection of advanced engineering, material science, and design, combining expertise from these fields to create systems that transform according to user needs. However, designing these structures presents challenges. The most significant being the inverse design problem, determining the optimal initial configuration that accurately achieves a desired deployed shape.

Self-assembling structures are innovative due to their autonomous assembly capabilities; however, their practical implementation faces significant limitations. These structures require highly controlled environmental conditions, such as turbulent water or air, making them currently unsuitable for many real-world architectural or structural applications. Their primary applications remain limited to areas such as robotics and similar fields, and further research is essential to explore practical deployment scenarios in broader architectural contexts.

4D printing offers new opportunities by enabling materials to change shape in response to environmental stimuli. Despite its potential, a critical limitation is the lack of robust predictive modelling tools. The absence of these tools forces designers into inefficient trial-and-error methods, significantly slowing adoption for large-scale applications in fields like architecture and medicine.

Mechanical metamaterials demonstrate strong potential for practical use due to their precise deformability and adaptability. Their ability to scale to larger applications makes them particularly suitable for deployable structures. Programmable materials, designed with specific task-oriented units, further expand possibilities by enabling dynamic, shape-changing capabilities.

To successfully develop deployable structures, specific criteria must be addressed: reliable deployment, structural precision, material efficiency, stress management, and sustainability. Meeting these criteria ensures the structures are not only functional but also scalable and environmentally sustainable.

Various computational and optimization methods support deployable structure development. Conformal mapping is employed initially to produce a flattened yet geometrically accurate representation of the target shape. Optimization techniques such as constraint-based methods—maintaining specific design rules like consistent edge lengths or angles—and simulation-based methods, notably finite element modelling (FEM), are crucial. These simulations predict structural behaviour, enabling design refinement for enhanced performance.

By enhancing predictive modelling capabilities, refining materials, and advancing deployment methodologies, the practical realization of reliable, scalable, and efficient deployable structures can be achieved, significantly expanding their applicability in real-world scenarios.

4 METHODOLOGY

This research builds upon previous studies into auxetic structures, specifically focusing on the rotating polygon design, which is one of the most extensively investigated concepts in the field (Ou et al., 2018). This design consists of four rectangles connected at their corners, enabling dynamic shape transformations (see Figure 24).

In their work, Ou et al. (2018) demonstrated that by adjusting the hinge parameters of each unit cell, it is possible to control mechanical behaviours such as scaling, shearing, bending, and twisting. These unit cells can be assembled into larger structures capable of both planar (2D) and spatial (3D) transformations. This project takes inspiration from their approach and seeks to further develop and apply it to create deployable structures.

The objective of this research is to develop a method that can manipulate mechanical behaviour to design deployable structures. Ideally, the method should be applicable to any surface geometries and enable transformation between a compact, manufacturable state and a structurally stable deployed state.

3D printing was selected as the preferred manufacturing method because it allows for easy adjustment of local geometries, a key advantage for programmable metamaterials. Furthermore, manufacturing the structure in a flat state without the need for supports can significantly reduce material use, printing time, and post-processing efforts. A computational design tool based on this method would not only simplify fabrication but also enable the efficient production of large-scale, intricate deployable structures without requiring extensive manual assembly.

However, scaling up these concepts introduces its own set of challenges, which are discussed in further detail in chapter 6

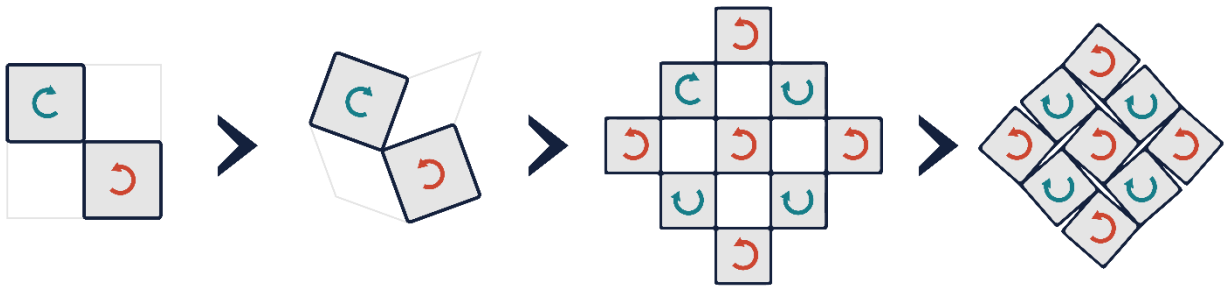

Figure 24: *rotating polygon design (own work)*

4.1 Exploration Phase

In the exploration phase, computational methods were explored and assessed to model rotating polygon structures and investigate how their behaviour can be controlled, similar to the approach taken by Ou et al. (2018). This was combined with the creation of physical prototypes, mainly to observe how the structures respond to applied forces, but also to gain a better understanding of the material properties and the detailing required to make the system function effectively.

At this stage, a forward design approach was still followed: designs were created and tested to observe their behaviour, to develop an understanding of how different parameters affect the system and how they might be used to control it.

4.1.1 Computational modelling

To model the rotating polygon structures, a Grasshopper script developed by Piker (2021) was used. This script translates any flat mesh geometry into a rotating polygon configuration and simulates its transformation.

The script performs the following operations:

- Converts the input mesh into a pattern of rotating polygons, using the mesh's diagonal lines as the basis for the transformation (see Figure 25).
- Simulates the transformation by rotating and scaling each panel simultaneously, ensuring that the panel corners remain connected throughout the motion.
- After the transformation, the entire structure is uniformly scaled so that each panel returns to its original size.

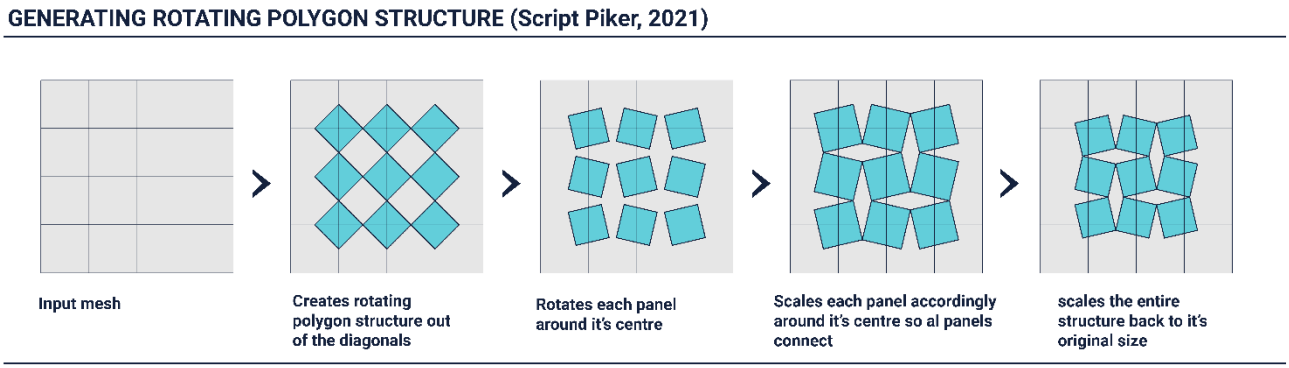

Figure 25: *Generating polygon structures as done in script from Piker (2021)*

Degree of Deployment

In this script you can control the amount each element rotates. This angle referred to as "**degree of deployment (DoD)**" can be used to define the amount a structure is deployed from its original configuration. in this script the original configuration with Degree of deployment of 0°, is open most expended configuration because this is how the grid is built, but it can also be measured from its closest configuration (in figure 26, 90° configuration).

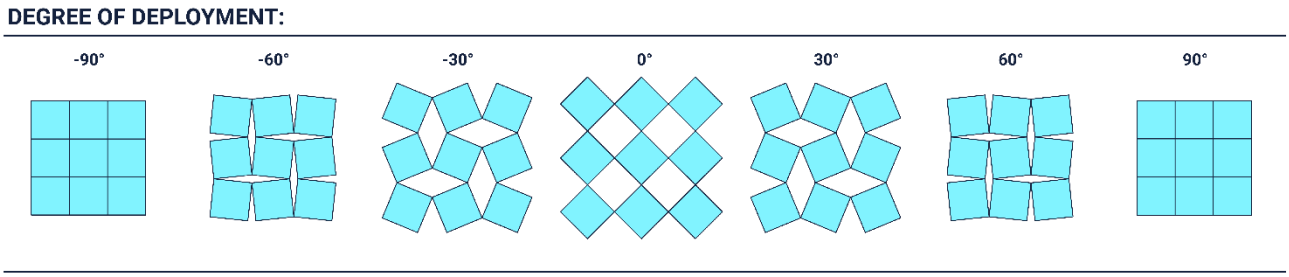

Figure 26: *degree of deployment rotating polygon structures*

4.1.2 Physical models

To better understand the structural behaviour and practical limitations of the system, a series of models was made.

Model 2 - Single-material compliant hinges

The first models replicated the bending-strip prototype described by Ou et al. (2018) to establish a basic printing workflow with thermoplastic polyurethane (TPU) and evaluate whether single-material, printed compliant hinges could replace the hinges used by Ou et al. In the original work, the authors either inserted conventional door hinges or produced dual material prints with stiff regions for the "rigid" parts and a softer material for the hinges.

The panels deformed as expected, but the assembly did not behave as a single mechanism; it had to be supported at several points to remain in its deployed state (see figure 27). This limitation was most likely due to:

1. **Non-ideal hinge behaviour** – the compliant hinges failed to deliver pure rotation, introducing unintended bending and shear.
2. **Flexure of nominally rigid segments** – regions meant to stay stiff also deformed, compromising the intended kinematics.

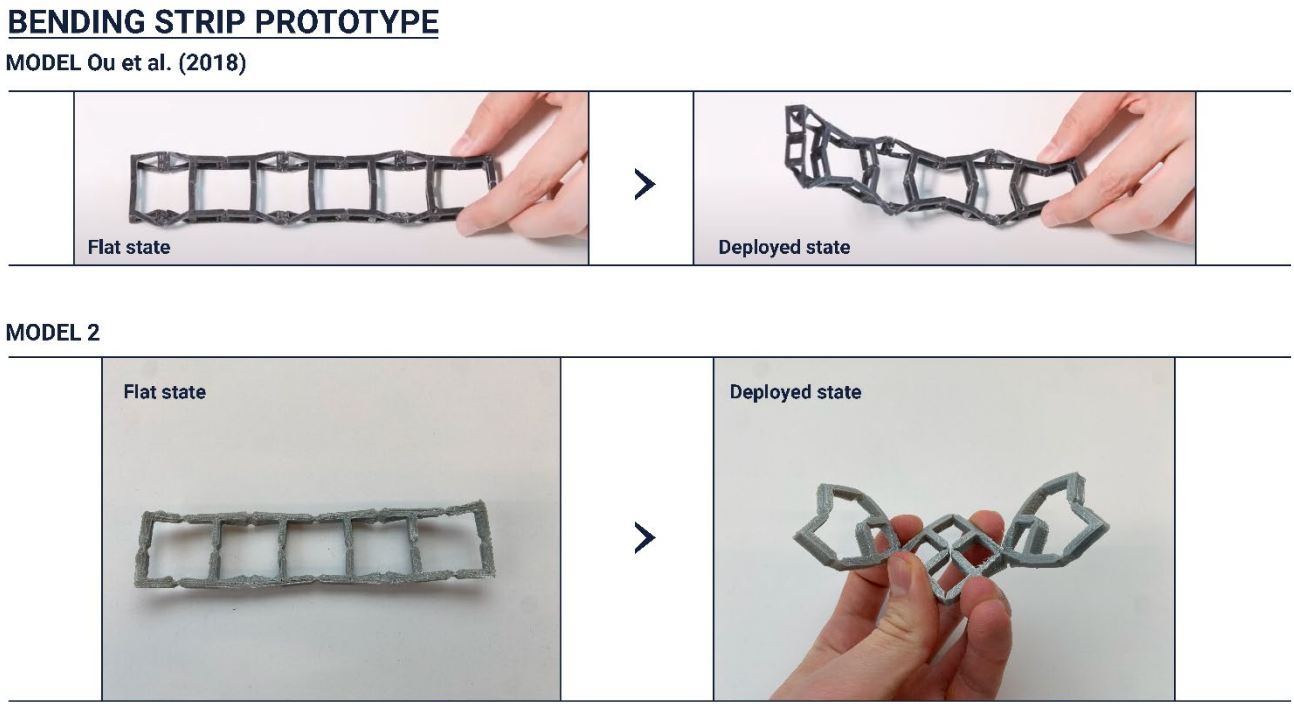

Figure 27: *Comparison model with Ou et al. (2018)*

Model 4 - Doubly curvature

The second set of models investigated whether the same kinematic system could produce *doubly curved* geometry. Although Ou et al. (2018) demonstrate a helmet-like prototype, that example appears to be assembled from strips that exhibit only single curvature (see figure 28). To achieve this *doubly curved* surfaces the following steps where taken:

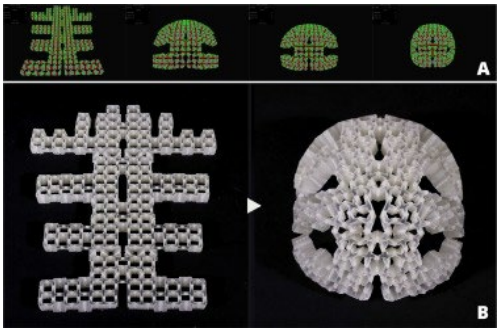

Figure 28: *prototype of foldable helmet (Ou et al. 2018)*

1. **Generating lattices.** The Grasshopper script by Piker (2021) was used to create auxetic *rotating-polygon* lattices in various shapes and to control their degree of deployment (creating more open or more closed structures).
2. **Layering lattices.** Two similar lattices were placed one above the other with coincident centroids, but each with at a different degree of deployment (one more open, the other more closed see figure 29).
3. **Lofting lattices.** Corresponding edges of the two lattices were lofted and their relative rotation constrained. Because the two layers expand or contract at different rates, the coupled assembly develops curvature in two principal directions, forming a doubly curved surface (see Figure 29).

Models 4 validate this approach and show that triangular polygons can be incorporated into the lattice without disrupting the kinematics.

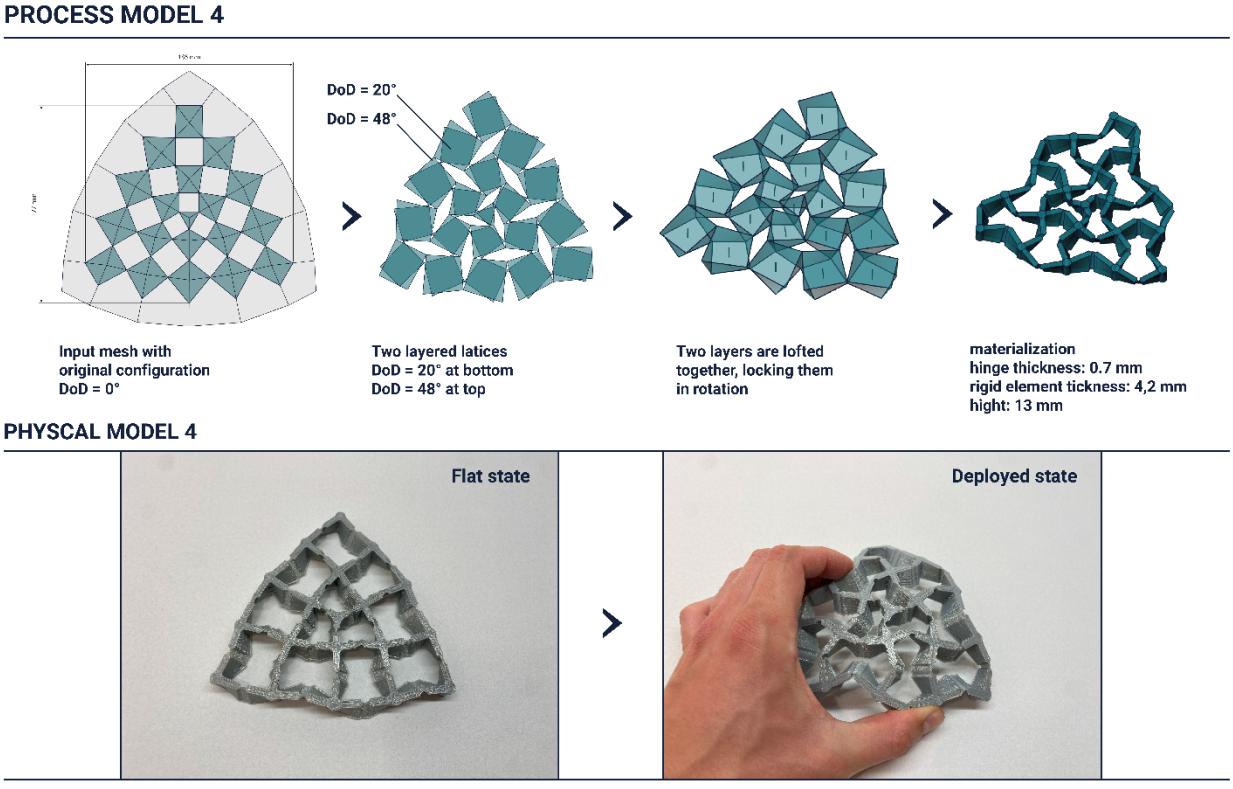

Figure 29: *process of the development of model 4*

Model 5 – unconstrained counter-rotation test

Model 5 was made with the same modified script by Piker (2021). This model explored the effect of removing the rotational constraint between the two stacked lattices (see figure 30). The layers were permitted to counter-rotate freely during deployment, with the intention of engaging a lock only after full extension. This configuration produced irregular, poorly coordinated motion; the structure felt flimsy and could not reach a stable deployed shape. The experiment therefore indicates that reliable operation requires the layers to be kinematically coupled throughout the deployment process.

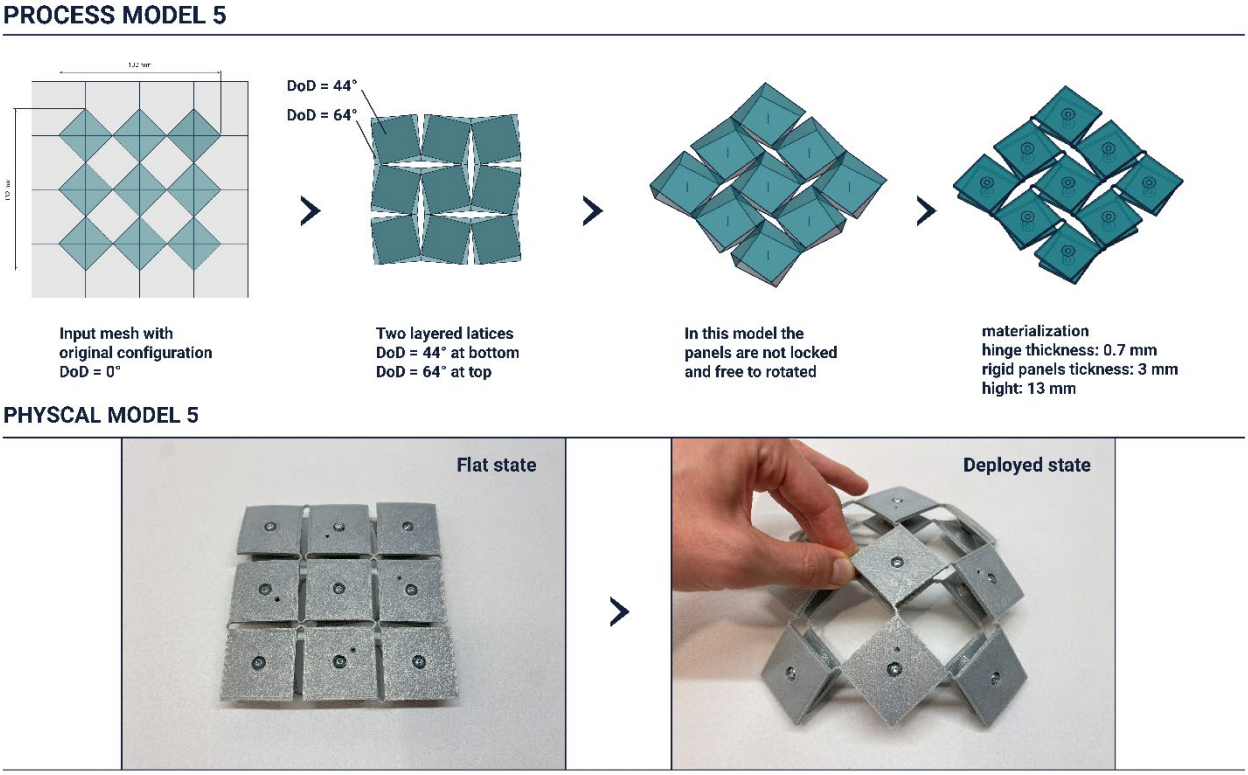

Figure 30: *process of the development of model 5*

4.2 Prototyping in TPU

Printing with thermoplastic polyurethane (TPU) proved challenging. Three different kinds of TPU were tested: TPU 45 D (≈ Shore 90 A), Ultrafuse TPU 85 A and Filaflex 60 A, each run with the supplier's recommended settings. Even so, persistent issues arose: rough surface finish, parts detaching from the build plate and occasional nozzle clogging. These difficulties were mostly caused by limitations in printing equipment and materials available at that time. In the end, all prototypes were fabricated with the 45 D grade, which provided the most reliable results.

4.3 Kinematic System

Of all the models, Model 4 showed the most promise. By layering two rotating polygon structures, each set to a different degree of deployment and locked in relative rotation, a three-dimensional, double-curved geometry was successfully created. Notably, this curvature is achieved and can be controlled by adjusting just two parameters in the modified script based on Piker's (2021) work: the Degree of Deployment (DoD) of each of the two rotating polygon layers (see Figure 31). The state of the created structure can also be described using this DoD parameter; in this case, the flat state corresponds to DoD = 0° (see Figure 32).

This kinematic system will serve as the foundation for the remainder of the research. The next step is to develop a script that allows the two lattice layers to vary locally, enabling fine-tuning of the curvature while maintaining the integrity of the rotating-polygon kinematics. This will be followed by testing whether the same approach can be applied to more complex target geometries. Achieving this will require a dedicated computational framework.

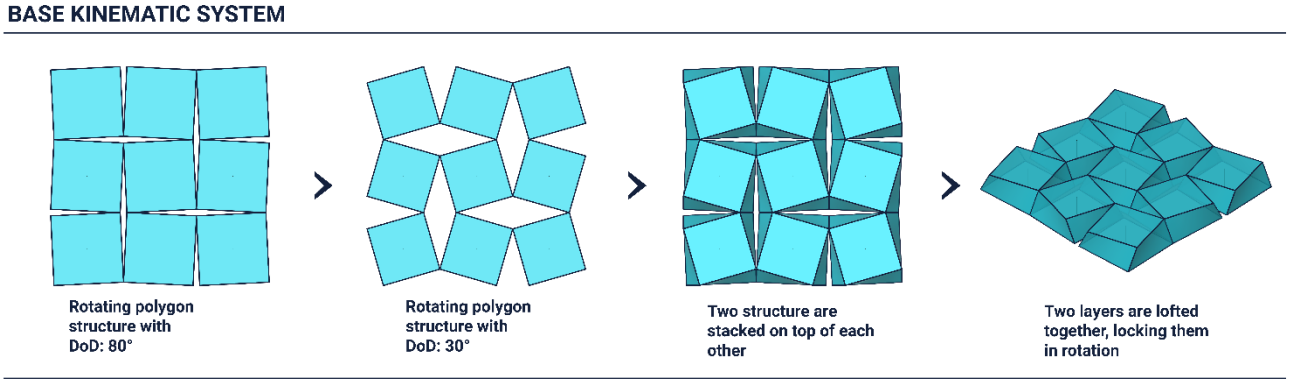

Figure 31: *Base kinematic system*

The script developed from Piker's (2021) example file shows that this method can create structures that either contract or expand to reach their three-dimensional deployed state (see Figure 32). This will be intergraded in the design tool as an option for the user.

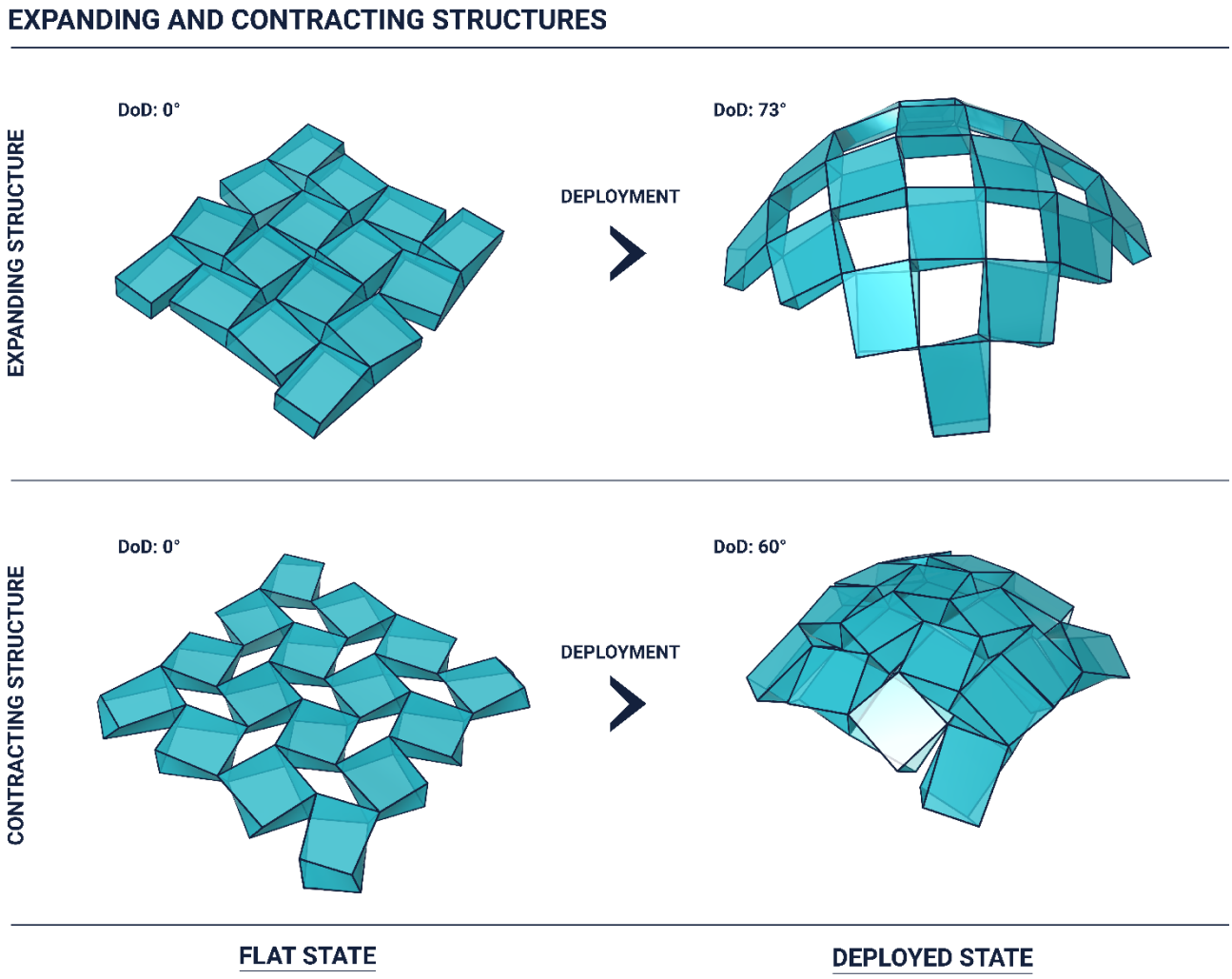

Figure 32: *kinematic system. Expanding & Contracting structure*

4.4 Change in Approach

After the exploration phase and looking into different grasshopper plugin options within Rhino3d a change in approach was developed.

Original approach

The literature study proposed the following workflow:

1. **Initial deployed grid**: Generate a reference grid directly on the target surface in its fully deployed state.
2. **Initial flat grid**: Flatten the deployed grid to obtain a planar layout that can be fabricated efficiently.
3. **Compare grids:** Compare the cells of the flat grid and the deployed grid to obtain the deformation needed for the shape to change from flat to deployed.
4. **Pre-compute kinematic system**: Determine the key variables of the kinematic system, generate all feasible variations within limits, simulate their deployment, and store both the variable sets and the resulting deformations.
5. **Adjust deployed grid:** Use the maximum deformation measured to adjust the deployed grid so that it can be realised from the flat grid with the kinematic system.
6. **Assembly**: For every cell in the grid, select the configuration that best satisfies the deformation required for deployment.
7. **Join elements**: Connect the configured cells to form a continuous, structurally coherent assembly.

Although the approach could be viable, it involves many sequential steps, each presenting its own challenges.

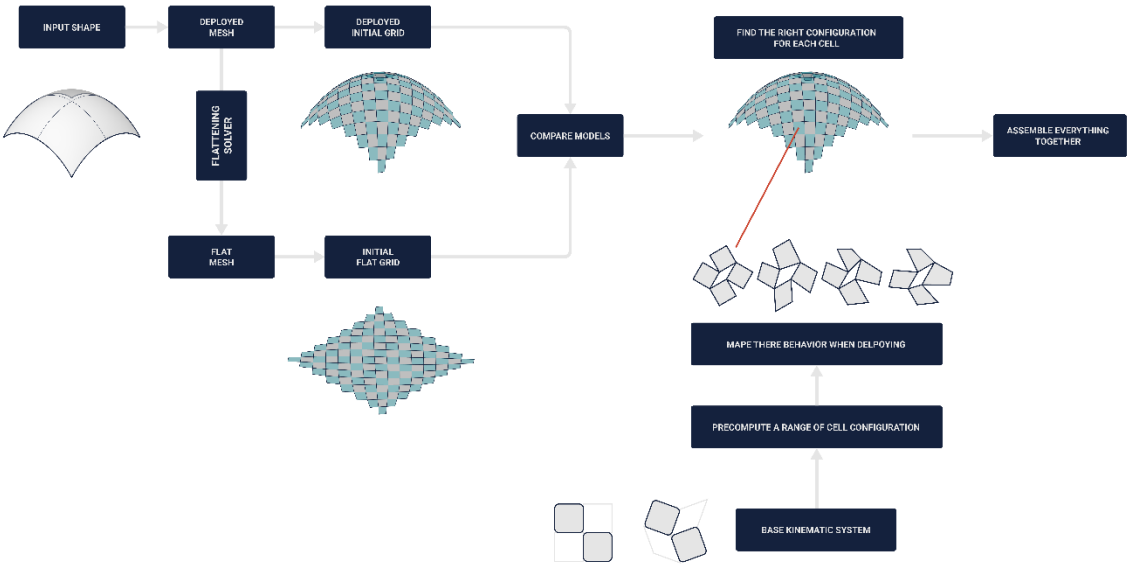

Figure 33: *Original approach*

New approach

A more compact workflow is possible by treating the problem as a form-finding task solved through dynamic relaxation. In Grasshopper, the Kangaroo physics engine is an interactive, constraint-based solver developed by Daniel Piker. This plugin provides this capability for this task. Kangaroo operates on simple geometric primitives (points, lines, meshes) and supports constraints such as fixed nodes, target lengths, target angles, and external loads. Each constraint carries a user-defined strength, allowing the simulation to balance competing requirements and converge on a feasible configuration (Piker, n.d.).

This approach requires the following steps:

1. **Initial deployed model** – Generate a reference grid on the target surface in the fully deployed state.
2. **Initial flat model** – Flatten the deployed grid to obtain a planar counterpart suitable for fabrication.
3. **Define constraints** – Assign constraints that preserve the intended kinematic behaviour while still permitting the required deformations elsewhere.
4. **Simultaneous form-finding** – Load both the flat and deployed models into a single Kangaroo solver and iteratively minimise the difference in corresponding element lengths between the two states.

Because the flat and deployed configurations are solved in a single optimisation loop, many challenges, such as finding the correct kinematic configuration for each cell, are resolved simultaneously. With an appropriate setup, the solver can adjust the deployed geometry whenever a target deformation exceeds the kinematic system's limits, resulting in a coherent final output and a fabricable assembly.

A drawback is that the most critical computations occur inside Kangaroo's solver, essentially a black box, so the method and its results depend heavily on providing accurate inputs and well-tuned constraints.

Alternative form-finding methods

During the development process, two alternative variations of the form-finding method were explored. Instead of using two models, one in a deployed state and one flat, the first variation involved starting with two flat models and pulling one into the desired shape. The second variation reversed this approach, starting with two deployed models and flattening one to simplify the overall procedure. However, experimentation showed that the reliability of results strongly depended on minimizing the required deformation within the solver. Therefore, providing inputs as close as possible to the desired outcome yielded the best results. As a result, the final approach uses one flat state and one deployed state as the starting inputs.

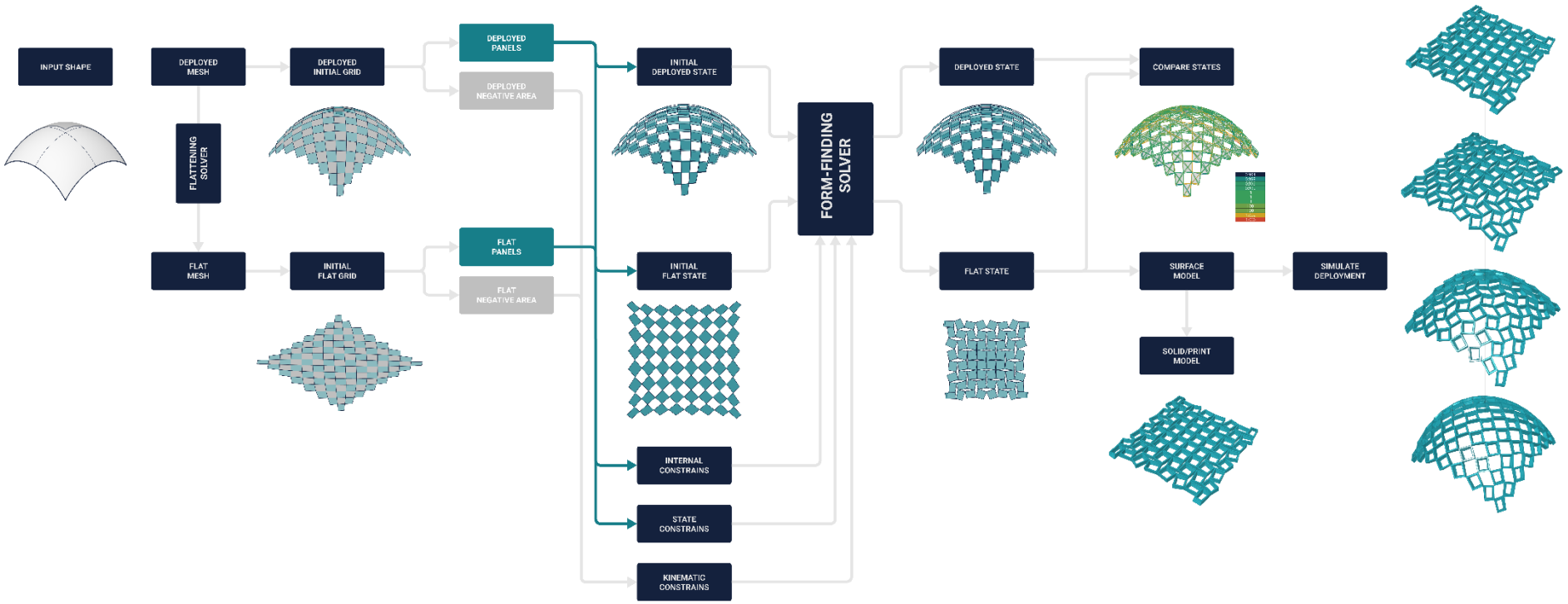

***Figure 34**: Flowchart approach*

5 DEVELOPMENT OF THE TOOL

To address the sub-research question: “Can a computational tool be developed to design adaptive deployable structures?” this study proposes a method that converts an input surface into a deployable structure able to approximate its form.

5.1 Test Shapes

The script was tested on three shapes with different curvatures (see figure 35), showing the tool can work for several kinds of geometry.

- **Monoclastic curvature** refers to surfaces that bend in only one main direction at a time, creating a singly curved shape (Whitehead, 2019).
- **Synclastic curvature** describes surfaces where both principal curvatures bend the same way, with the centers of curvature on the same side of the surface, like in a dome (Whitehead, 2019).
- **Anticlastic curvature** refers to surfaces where the principal curvatures bend in opposite directions, with the centers of curvature on opposite sides of the surface, forming saddle-like shapes (Whitehead, 2019).

Later in the research, the developed method will be applied to a case study with a more complex and unique shape, to further test how well it performs.

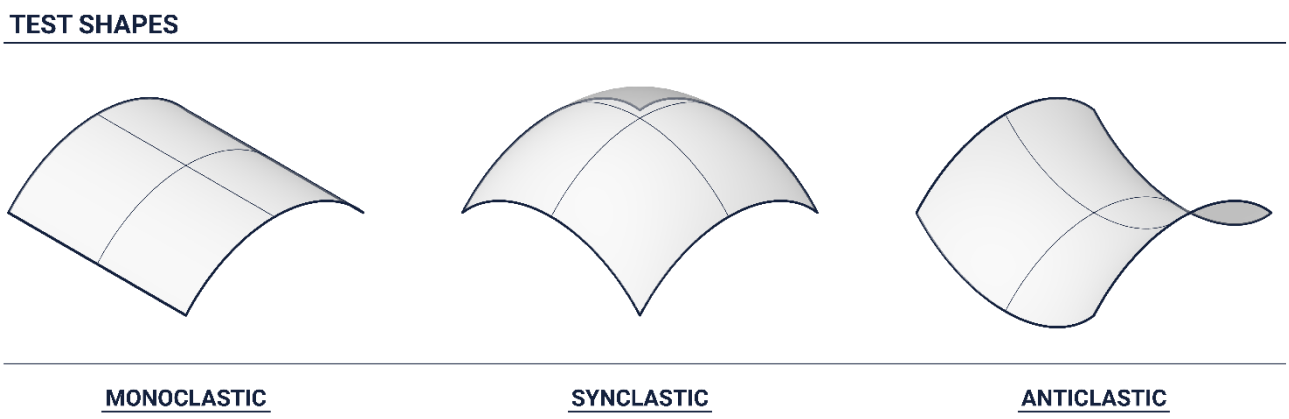

Figure 35: *three test shapes with different types of curvature: Monoclastic, Synclastic and Anticlastic.*

5.2 Data Structure

As discussed earlier, it is essential for the form-finding process to have a clearly structured data input, not only for defining the structure itself, but also for setting up the constraints defining its kinematic behaviour.

One effective method for constructing this kinematic structure is to apply a checkerboard pattern that divides a mesh into two distinct groups; a similar method was also demonstrated by Piker (2021) in his example script. Using this approach, one group of mesh elements becomes the **Panels** from which the structure is built, while the other group forms the **Negative area** between these panels. This negative area is crucial for defining constraints, such as preventing collisions between elements, which will be explained in greater detail later. To successfully implement this method, it is necessary to begin with a well-defined mesh,

During the process, it was determined that creating the mesh diagonally, rather than aligned with the U/V directions of the input surface, leads to improved results. As shown in Figure 36a, a regular UV mesh causes corner elements to be connected to only one other element, leaving them under constrained and resulting in unpredictable behaviour.
This issue can be partially addressed by applying the inverse pattern and selecting an odd number of elements in both the U and V directions, as illustrated in Figure 36b.
Nevertheless, this approach still introduces unreliable results in the form-finding process: elements on the edge of the structure maintain two points on the boundary, leaving the link between them undefined and under constrained.

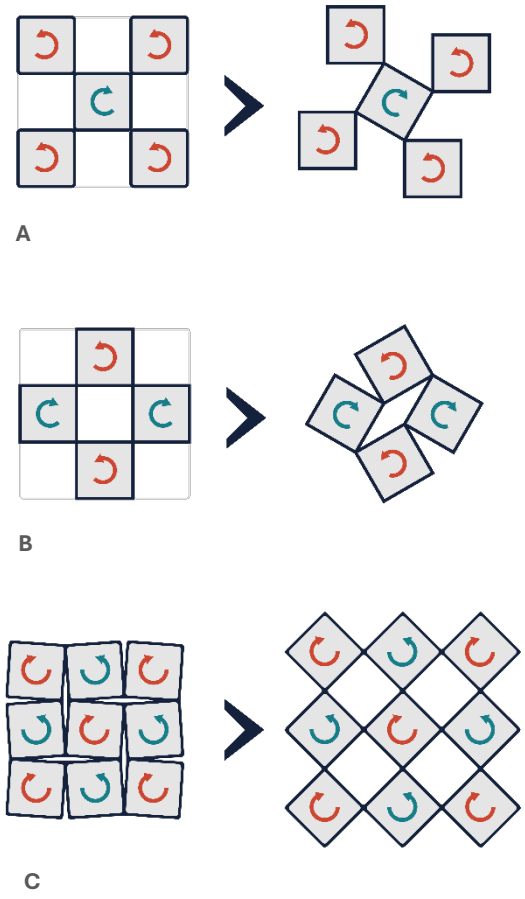

***Figure 36**: rotating polygon design. comparing horizontal/vertical grid (A & B) with diagonal grid (C)*

A diagonal mesh ensures that edge elements are always connected to three surrounding elements, leaving only one point on the boundary. Only the corner elements are connected to two surrounding elements, as depicted in Figure 36c. This configuration results in more stable and predictable behaviour during the simulation.

5.3 Grid

For the creation of the mesh, various mesh components from Grasshopper and its plugins were tested. However, these components did not provide the required level of control or were unable to generate a diagonal mesh as previously discussed. Therefore, a custom approach was developed, beginning with the creation of a grid of surface points within grasshopper, allowing flexibility to adjust the mesh density later in the process (discussed in more detail later). With a Python script within grasshopper, developed with support from ChatGPT.

This script first converts the list of surface points into a 2D grid and constructs a woven or diagonal quadrilateral mesh pattern. It first organizes the points into rows and columns based on given surface divisions (U and V), accounting for the relationship between spans and points. Then, it builds the mesh by connecting points in a specific pattern: for each row, depending on whether the row index is even or odd, the script selects groups of four points that form a diagonal diamond shape. Each group is added as a quad face to the mesh, ensuring all vertices are within valid grid bounds. (script can be found in the appendix)

The code is designed to handle both even and odd numbers of divisions, creating a consistent and visually structured weaving pattern. Its use of conditional looping and careful boundary checking ensures the creation of a clean mesh with aligned and consistently oriented faces, providing a reliable structure from which data can later be extracted and built upon in subsequent stages of the script.

Afterwards, the mesh is divided into two groups in a checkerboard pattern using a component from the Kangaroo Library (see Figure 37). This separation forms the "**Panels**," which serve as the basis for the structure, and the "**Negative space**" between them, which are necessary for establishing the kinematic constraints discussed later. The same operation is applied to an offset version of the mesh, which is required to create the layers that enable the base kinematic system.

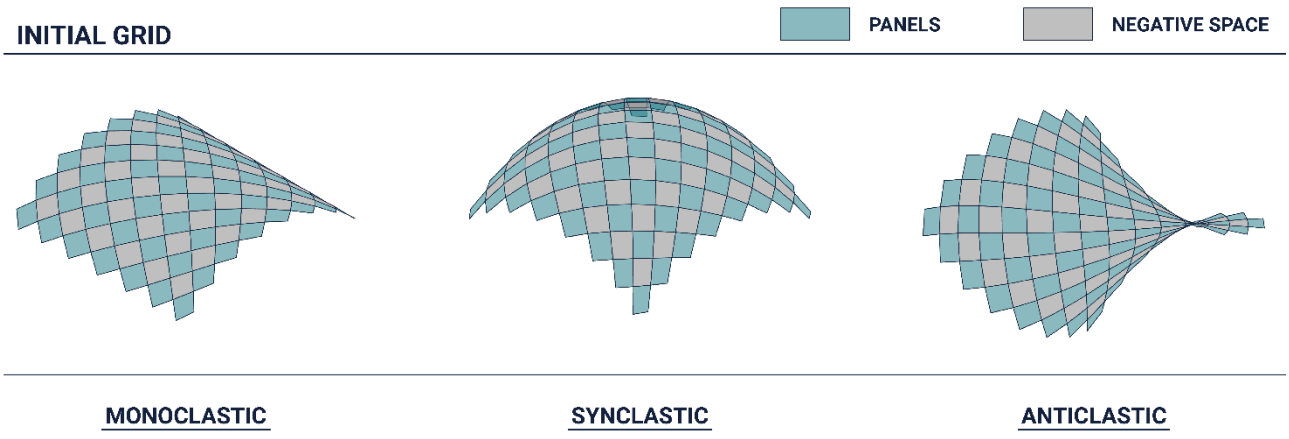

Figure 37: *initial grid of deployed state. Panels are divided in a checkerboard pattern into 2 groups: panels and negative space*

5.4 Flattening

The next step involves flattening the base mesh created from the input surface. The primary objective in this step is to ensure that the flattened mesh remains as close as possible to the original deployed mesh. Minimizing differences between the meshes reduces extreme deformations during the subsequent form-finding process, resulting in more reliable outcomes.

Kangaroo is also utilized for this flattening procedure, as it provides extensive control over the deformation in the model. The main constraint applied during this stage is ensuring all mesh planes remain on the XY-plane.

According to literature examined in the literature study, most related projects employ conformal mapping techniques for mesh flattening. Conformal mapping involves projecting a grid onto a flat surface while preserving angular relationships. However, these projects typically employ different kinematic systems and methods.

Preserving angles exclusively, as done in conformal mapping, can lead to significant length deformation in the mesh edges. To prevent this, constrains to equally preserve angles, edge lengths, and rectangle diagonals were implemented, each assigned the same constraint strength (weight) within Kangaroo.

After the flattening prosses the mesh is offset by a set distance to creating the two layers and both layers are divided in the checkerboard pattern to create the "**Panels**" and "**Negative space**" just like the Deployed Grid (see figure 38).

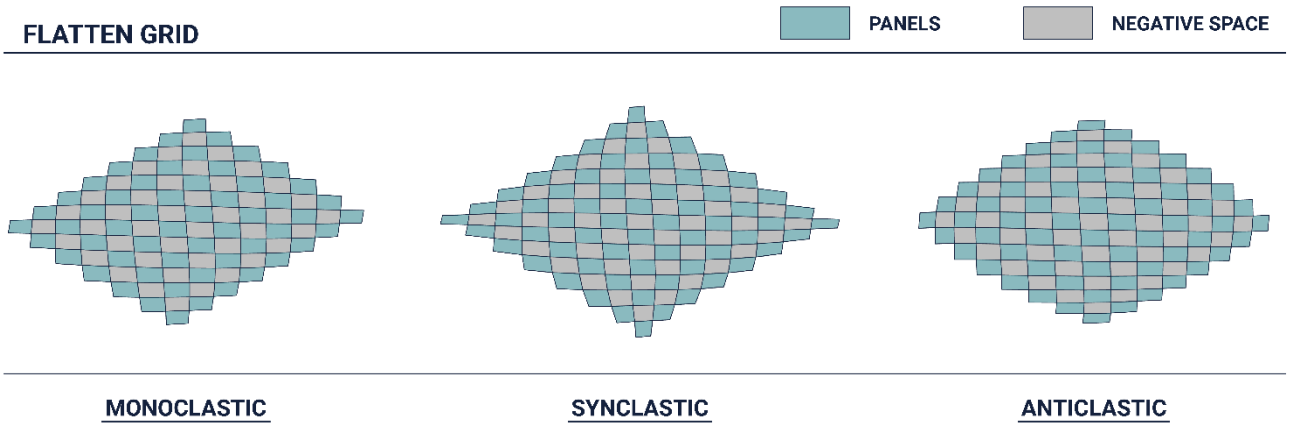

Figure 38: *Initial grid of flat state. Panels are divided in a checkerboard pattern into 2 groups: panels and negative space*

5.5 Constrains

Setting up the Constrains starts by defining the base kinematic system, then marking which elements may move or deform and which must remain fixed. Correct strength values are essential for a stable solution, and they are usually found through an iterative process of testing and adjustment until the relative influence of all constraints is balanced.

For clarity the constraints used here are grouped into four categories:

- **Global Equal length Constraint (GEC)** – couples corresponding elements in State 1 and State 2 so that their lengths remain identical.
- **Internal Constraints** – maintain geometric relationships inside each element formed by the panels of the initial grid.
- **Kinematic Constraints** – these control relations between neighbouring elements, enforcing the kinematic system located in the negative space of the initial grid.
- **State Constraints** – describe additional requirements applied to the complete state of the structure (for example, overall boundary conditions or target positions).

The tool was originally designed to support both expanding and compressive structures. However, development shifted toward expanding structures due to their more reliable performance in the form-finding process. As a result, the following constraints are primarily focused on expanding structures, with adjustments for compressive structures discussed later.

5.5.1 Global Equal Length

What defines this approach is a single, global equal-length constraint linking two models with matching grids. These models are loaded into one solver and treated as **State 1** and **State 2** of the same deployable structure. The solver enforces the equal-length rule on every node-to-node link inside each element (see Figure 39). Because every link is length-matched, each element pair stays geometrically similar in both states.
When one state shifts into a new shape, two things happen:

1. Links inside each element search for a configuration that satisfies both states.

2. Elements re-arrange with respect to one another.

Applying the kinematic system described earlier should make the elements rotate rather than stretch. However, additional constraints are needed to guarantee this behaviour across the whole structure.

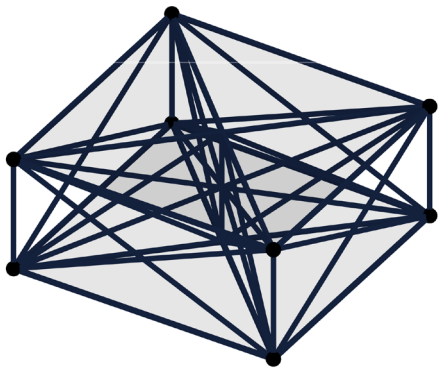

Figure 39: *every node-to-node link within an element*

5.5.2 Internal Constrains

The desired deformation behaviour for the internal elements requires that the paired panels remain parallel to each other, maintaining a consistent offset distance constrained by a central axis, while still allowing rotation around this axis.

The internal constraints applied to achieve this are visualized by colour in Figure 40.

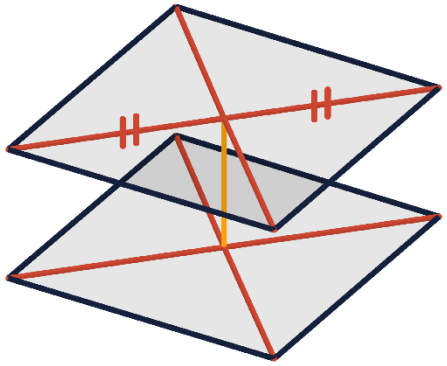

Figure 40: *Internal constrains that maintain the kinematic system. Centre axis (yellow), Diagonals (red), edges (dark blue)*

Centre axis

The panels should be allowed to rotate relative to each other to achieve the effect described in the base kinematic system section. To ensure the panels remain centred above each other during rotation, the central axis is constrained to maintain its original length using a high-strength (weight) constraint. Additionally, the central axis is constrained to remain perpendicular (at a 90-degree angle) to the diagonals.

Diagonals

The diagonal edges maintain the position of the central axis and prevent excessive deformation of the panels. Each diagonal is divided at the midpoint, with both resulting segments constrained to remain colinear. Additionally, an equal-length constraint is applied to both halves to ensure the midpoint remains centred.

An equal-length constraint is also applied between the perpendicular diagonals. While this constraint is not strictly necessary, it improves the uniformity and reliability of the resulting structure.

Panel edges

The panel edges should be allowed to deform to determine the optimal configuration in both states. However, it is also important that these edges remain close to their original lengths while retaining freedom of movement. Therefore, a length constraint with a low strength (weight) is applied.

All these internal constraints are applied only in state 1; however, due to the global equal-length constraint, they also indirectly influence state 2. The panels remain parallel through the application of a state constraint, which will be explained in more detail later.

5.5.3 Kinematic constrains

The kinematic constraints control the structure's movement, encourage the transition towards a desired state (such as contracting), and prevent collisions between elements. These constraints are defined using the negative panels, establishing spatial relationships between the panels (see Figure 41).

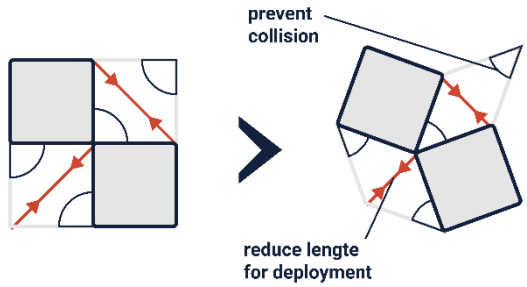

Figure 41: *kinematic constrains*

Implementing these constraints was challenging because the requirements for encouraging panels to fold together and simultaneously preventing collisions often conflicted. Even minor collisions caused significant problems later in the form-finding process.

Angle constraints proved to be less effective when applied directly to a 3D structure. Moreover, the negative panels required to be split in two groups because these needed constrained in different corners (see Figure 41for angles within the negative space).

Ultimately, collision prevention was effectively achieved using a component called "no fold-through." To actively encourage contraction, a constant tension force was applied, which could be toggled on or off depending on the scenario. Additionally, an equal-edge-length constraint was implemented between panels to ensure the structure could fully close (see Figure 41 for further explanation).

5.5.4 State Constrains

In this project, Case 1 represents the flat state, intended primarily to facilitate ease of manufacturing. Ideally, this state should also have a minimal footprint to reduce the required size of the print bed. To achieve this, the panel vertices are constrained to remain on their original plane without any additional boundary constraints.

Case 2 corresponds to the deployed state, designed to approximate the desired target shape. In this state, panel vertices are constrained to lie precisely on the input surface. Additionally, vertices located along the structure’s boundary edges are constrained to remain on the boundary to maintain the deployed configuration.

To ensure that the structure prioritizes flatness when required, the constraint enforcing the flatness state (Case 1) was assigned a higher strength (weight) compared to the constraints defining the deployed shape (Case 2). Consequently, if the target shape cannot be fully realized due to kinematic limitations, the form-finding process will automatically adjust the deployed configuration accordingly.

5.6 Results Form-Finding

The three test shapes are input into Kangaroo with all the previously discussed constraints to assess how well the developed computational method could approximate these surfaces. The outcomes reveal successful transformation of all three geometries into deployable structures with distinct degrees of deployment (DoD): 68° for monoclastic, 78° for synclastic, and 121° for anticlastic. These values represent the angular difference of the elements between the flat and deployed states.

The synclastic geometry stands out due to its relatively high DoD. This suggests that a greater portion of the available kinematic transformation potential is utilized to reach the deployed form. As a result, the grid lines in the synclastic structure are less straight and exhibit more pronounced angular deviations or "kinks." This deviation from geometric regularity indicates that the synclastic shape is more challenging to realize with the current kinematic system and may have implications for structural performance, particularly in terms of stiffness and load distribution.

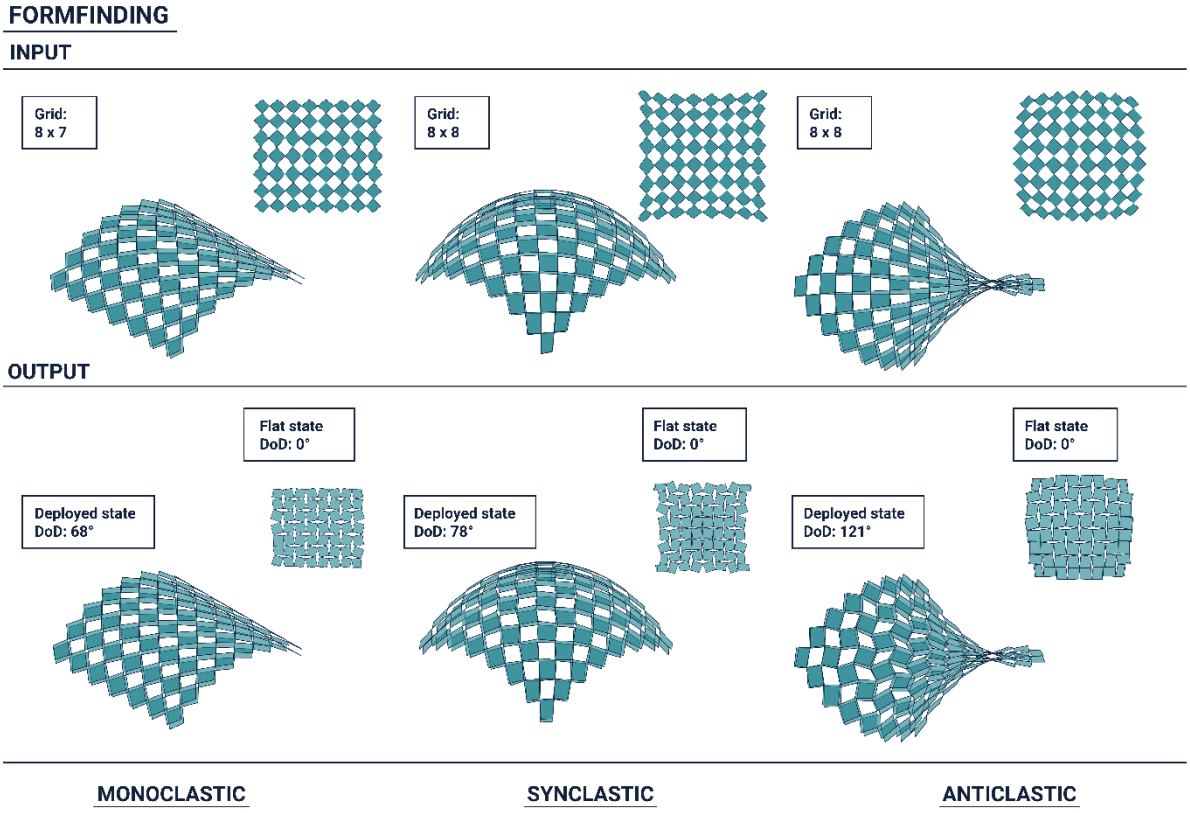

Figure 42: *Form-finding process of the three test shapes*

5.7 Compressive Structure

Initially, the computational tool was intended to accommodate both compressive and expanding structures. However, during its development, the focus gradually shifted towards expanding structures, as these consistently produced better results in the form-finding process. Additionally, compressive structures were preferred because they allowed larger deployed shapes to be realized using smaller print bed sizes.

For compressive structures, the constraints applied differ slightly from those used for expanding structures. Specifically, the fixation of boundary points described in the state constraints is reversed. Instead of constraining boundary points in the deployed state, boundary points are fixed in the flat state. This reversal causes the structure to contract when transitioning from flat to deployed.

However, releasing the boundary constraints in the deployed state led to the structure only partially covering the intended target shape. An attempt was made to resolve this issue by scaling up the flat state and subsequently fixing the boundary points. Unfortunately, this approach introduced larger discrepancies between the initial flat and deployed grids, resulting in less reliable outcomes during the form-finding process.

The option to switch to a compressive structure remains available. However, due to the increased deformation and reduced accuracy in matching the target shape, it is considered less reliable within the current setup.

5.8 Validation Form-finding

To verify whether the output geometries are valid, the different states are compared to evaluate the amount of deformation between them. This is done by drawing and measuring all possible connections (lines) between the vertices of each rigid element and comparing them to their counterparts in the other state (see figure 43).

If the scale difference between corresponding elements is too large, adjustments must be made to the constraints or the input surface. During constraint development, the goal was to keep the scale difference within 1% (between 0.99 and 1.01).

The validation results show that all three geometries remain within acceptable deformation limits, with scale differences of 0.6% for monoclastic and synclastic, and 0.9% for anticlastic shapes (see figure 43). The higher deviation in the anticlastic configuration indicates increased strain due to its complex curvature, but all remain feasible for production using flexible materials like TPU. However, with hinges that do not allow for any tolerance, excessive deformation could result in a structure that is unable to fully deploy.

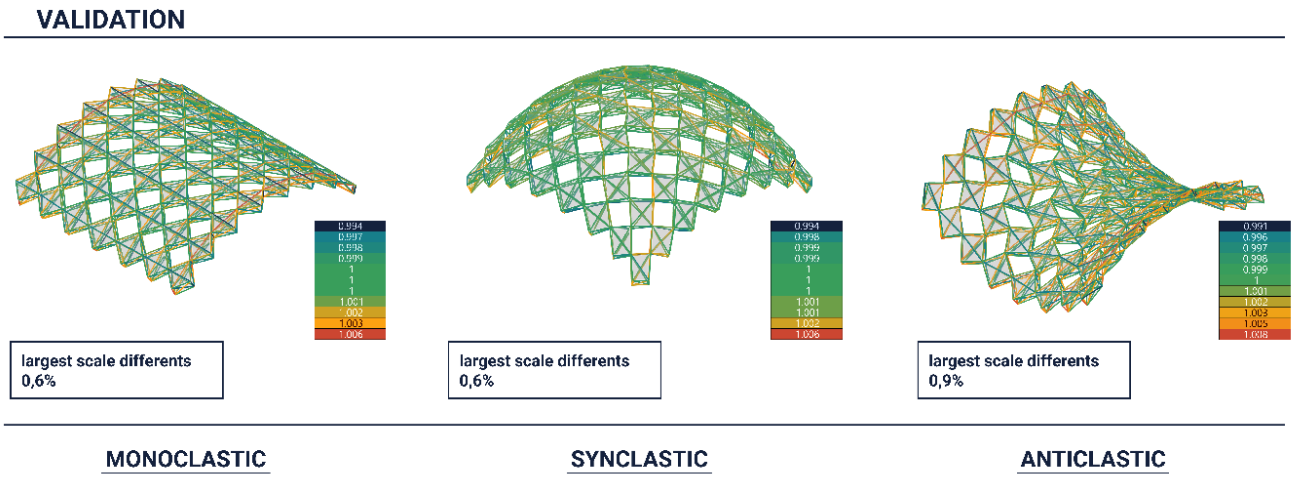

Figure 43: *validation output form-finding process. Measuring the scale differents between the each link of both states*

5.9 Simulation of Deployment

After the form-finding process, the deployment of the geometry from its flat state to the deployed state can be simulated.

This is done by feeding the flat panels from the form-finding stage back into a Kangaroo solver. A high-strength length constraint is applied to every node-to-node connection within each element, causing the elements to behave as rigid bodies. To initiate the transition toward the deployed shape, length constraints are applied to the diagonals within the negative space, not with their original lengths, but with the target lengths from the deployed state (see Figure 44).

It should be noted that this simulation does not account for material properties or hinge tolerances. It serves solely as a visual confirmation that, under ideal conditions, the structure behaves as expected.

CASESTUDY CURVATURE

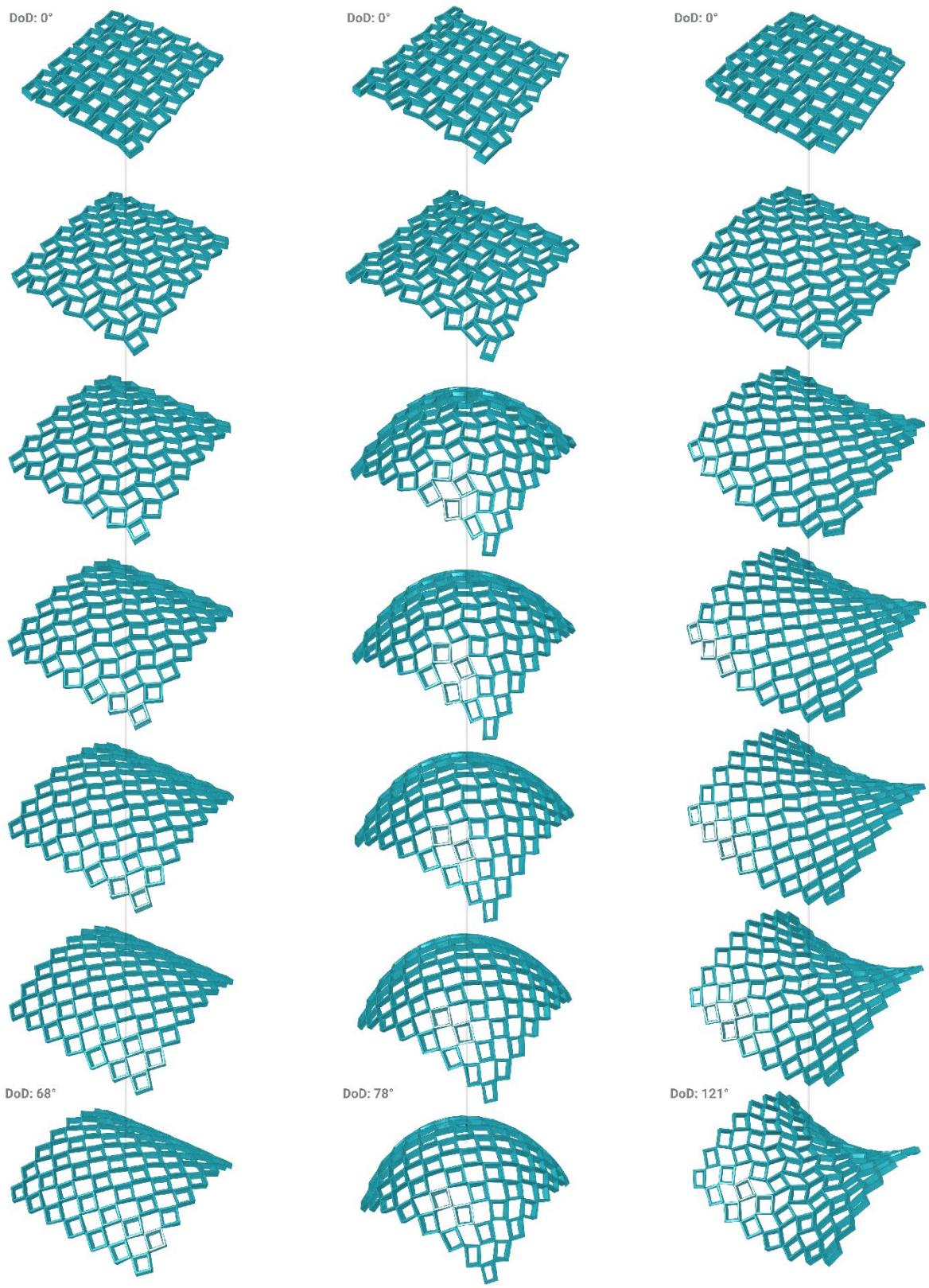

MONOCLASTIC | SYNCLASTIC | ANTICLASTIC

Figure 44: *models test shapes*

5.10 Physical Models

To demonstrate the effectiveness of the proposed method, two of the test models were fabricated: the synclastic and anticlastic shapes. These were selected because they presented the greatest challenge, as both are doubly curved surfaces.

A new material, TPU Foamy 95A, was used for printing. This filament expands when heated, and the degree of foaming can be adjusted slightly through print settings. When foamed, less material is used, which in turn allows partial control over the flexibility of the printed structures (Recreus, 2024).

The combination of this material and a new printer led to improved print quality and enabled the production of larger prototypes.

Both models use five keystones to maintain their deployed state. These keystones were custom-designed blocks that fit into the negative spaces of the deployed structure, preventing it from collapsing back into its flat form.

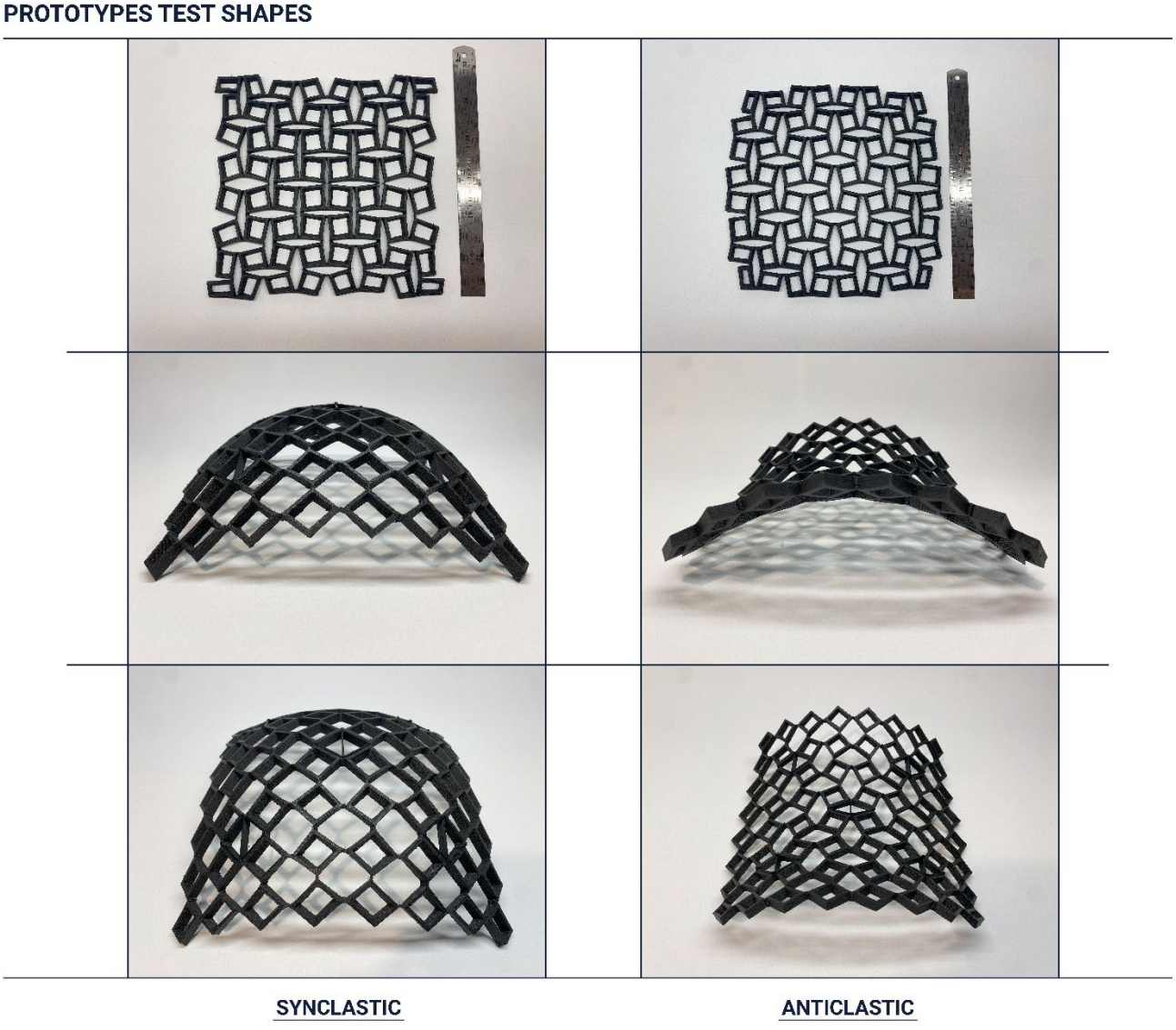

Figure 45: *models test shapes*

5.11 Conclusion

In summary, the developed script translates a target surface into a deployable auxetic lattice through form-finding based on dynamic relaxation. This process involves the creation of two models: a flat model and a deployed model. Both models are constructed using a grid derived from a kinematic system. Constraints are assigned to preserve the intended kinematic behaviour while allowing the necessary deformations elsewhere in the structure.

Both the flat and deployed models are loaded into a single Kangaroo solver, where an iterative process minimizes the differences in corresponding element lengths between the two states. Validation is achieved by comparing the elements of the two models and animating the deployment sequence.

Tests conducted on synclastic, anticlastic, and monoclastic surfaces confirmed that the script can approximate a variety of surfaces with different curvature types. Additionally, physical prototypes produced from TPU demonstrated that the method is feasible at a smaller scale. These prototypes were maintained in their deployed state through keystone locking of the kinematic mechanism. However, when scaling up, an alternative deployment support system will be necessary.

Further improvement remains, particularly in the mesh generation, the flattening process, and the assignment of constraints, especially along the edges. Improving these aspects would result in an overall more efficient and reliable script.

6 SCALING UP

This paragraph addresses the sub-research question: *Can programmable mechanical metamaterials be scaled up to create larger, safe, and stable structures?* Several key factors are examined to explore this question, including material selection, manufacturing methods, and joint design. These aspects are closely interconnected, as decisions in one area often impose constraints or create opportunities in others. The discussion covers the limitations of large-scale additive manufacturing, compares various material options, and explores deployment strategies. Additionally, it considers opportunities for structural optimization and introduces methods for structural analysis.

Industry experts were consulted to review the design, address potential challenges, and suggest solutions. Two companies were contacted for this purpose:

- **BouwLab/3DMZ** is an innovation hub focused on advancing digital construction techniques, including 3D printing, robotics, and sustainable building methods. It serves as a collaborative environment where companies, researchers, and startups develop and test new technologies for the construction sector (BouwLab, n.d.).
- **CEAD Group** is a technology company specializing in large-scale 3D printing solutions, particularly for industrial applications using composite materials. It is known for developing innovative additive manufacturing systems, such as robotic arms and gantry-based printers, aimed at efficient and sustainable production (CEAD Group, n.d.).

BouwLab was sufficiently interested in the project to offer hands-on support with material selection and large-scale testing. They provided access to their robotic arm 3D printer to assist in evaluating the printability of flexible thermoplastic materials. Together, preliminary tests were conducted to assess print quality, hinge performance, and interlayer bonding. Based on the results, a suitable material was selected and two full-scale (1:1) prototype segments were fabricated.

6.1 Deployment Methode

A secondary system is required to enable controlled deployment and stabilization of the structure. This system is essential to allow on-site assembly without the need for heavy machinery such as cranes. Once the structure is fixed to its anchor points, it should be able to stand independently.

A cable-based system was considered as a potential solution. Cables offer flexibility in adapting to different configurations and require minimal assembly after the structure is produced. By tensioning the cables during deployment and securing them afterward, the structure could be stabilized in its deployed state.

Four cable systems were evaluated:

Cable System 1: Potentially functional for compressive structures but would require the cable to slide through the structure during deployment. Since the project involves an expanding structure, this option was disregarded.

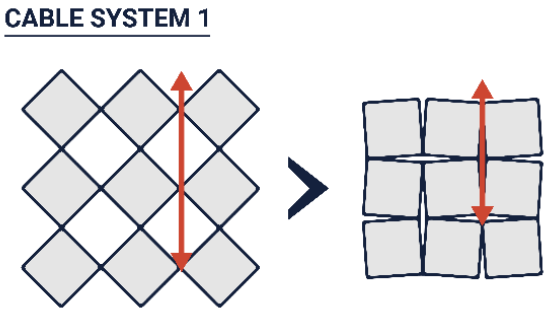

Figure 46: Cable System 1

Cable System 2: Theoretically possible. As the cable path does not shorten during deployment, stability would rely on the cable naturally following the load path. However, during physical testing, this system did not perform well and appeared to require higher tension, making it less feasible.

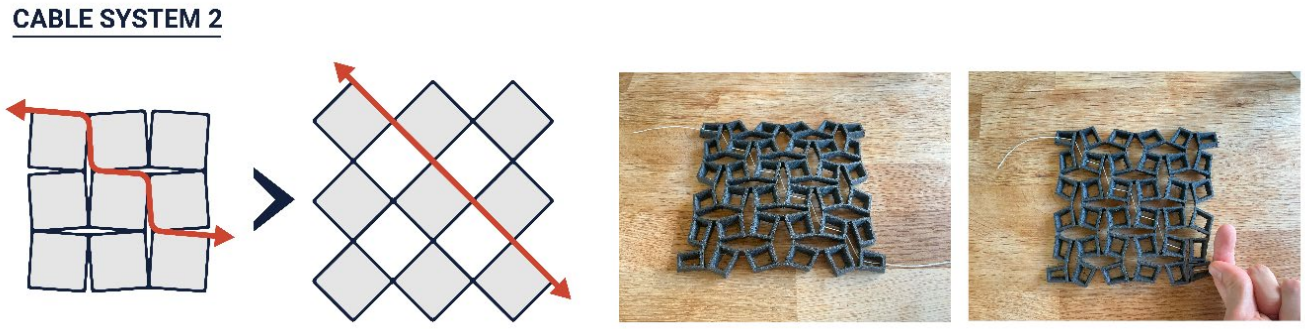

Figure 47: Cable System 1

Cable System 3: Showed the most potential. In this case, the cable path shortens during deployment, allowing compatibility with expanding structures. An additional cable might be necessary to prevent the elements from rotating too far. However, testing with a scale model revealed that high friction between the cable and the soft material caused significant issues. For this system to function properly, the cable must be able to slide through the structure with minimal friction.

CABLE SYSTEM 3

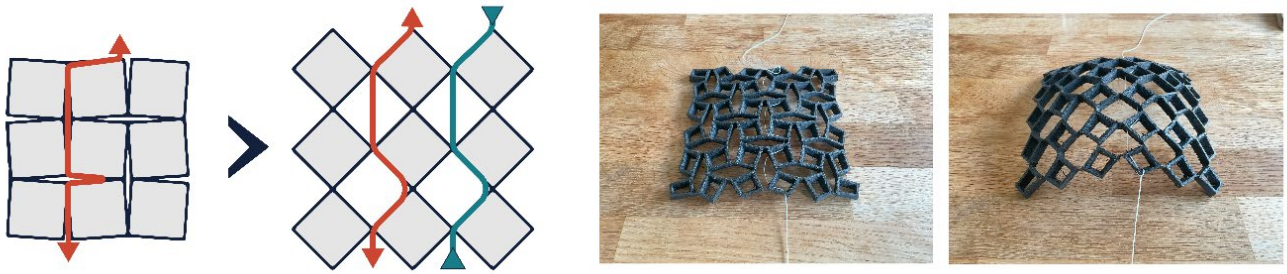

Figure 48: *Cable System 3*

Cable System 4: Developed through observations of the test models: synclastic and anticlastic. It was noted that clamping the models at specific points allowed for easier deployment into their final configurations. These critical points were later used to position keystone elements to lock the structure in place.
For the case study, these tension points could, for example, be placed only around the edges, at every other element (see Figure 49).
Cable System 4 appeared to be the most feasible option for smaller-scale structures like the case study. Its main drawback is that it requires multiple tension points throughout the structure. For larger structures with more elements, this could become a limiting factor, and a different deployment method might be necessary.

CABLE SYSTEM 4

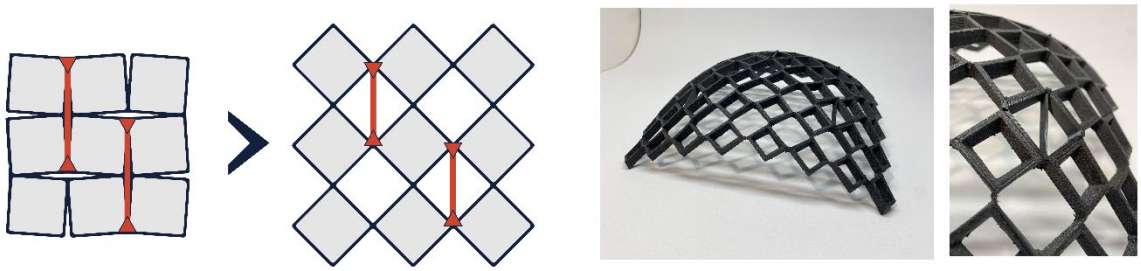

Figure 49: *Cable System 4*

To tension the cables, two products can be used depending on the force requirements:

- **Tension straps**: A cheaper and smaller option, but with a shorter lever arm, requiring more force from the operator.
- **Cable pullers**: Slightly larger and more expensive but equipped with a longer lever arm, allowing easier tensioning.

In practice, multiple people would likely need to operate the ratchets simultaneously to gradually bring the structure into its deployed configuration. This gradual process is important to avoid introducing high stresses into the structure during deployment.

TENSION STRAP	CABLE PULLER
	

Figure 50: *tension systems*

6.2 Large Format Additive Manufacturing

Large-scale 3D printing differs significantly from the desktop 3D printers commonly used for smaller projects. While the core principles of additive manufacturing remain the same, large-format processes introduce unique limitations and requirements that must be considered during the design phase. To better understand these factors, CEAD Group provided a set of design guidelines outlining key constraints and best practices specific to Large Format Additive Manufacturing (LFAM) (CEAD Group, 2025).

Design Requirements and Limitations

1. Geometry and Bead Dimensions

LFAM uses nozzles significantly larger than those in desktop 3D printing. Nozzle sizes typically range from 2 mm to 26 mm. The bead width (the width of a single extruded line) is usually calculated as 1.5 times the nozzle diameter. This results in bead widths ranging from 3 mm to 39 mm.

While the absolute minimum bead width is equal to the nozzle diameter (a 1.0 ratio), this is not recommended due to potential extrusion instability and poor layer bonding. The 1.5 ratio is considered the standard for consistent quality and structural integrity.

Layer height, another critical dimension, is constrained by the width of the bead. The maximum layer height should not exceed 50% of the bead width to ensure proper adhesion between layers. Using too small a layer height relative to the extrusion rate can cause over-extrusion, leading to a wrinkling effect on the surface of the print.

The bead width range is important for determining the minimum thickness of the compliant hinge parts, which are expected to be around two times the bead width to ensure a continuous path.

2. Structural and Wall Design

LFAM typically avoids using infill due to the large amount of material required and the significant increase in print time and weight. Instead, most parts rely on strong outer walls. When thicker walls or multi-bead structures are necessary, a calculation known as the CAD offset is used to ensure proper bonding between adjacent beads. The CAD offset is defined as:

CAD offset = (Bead Width × 2) × 0.95

This results in a 5% overlap between adjacent beads, ensuring sufficient fusion without excessive material buildup.

Overhangs are limited to a maximum of 45 degrees from vertical. Exceeding this angle risks bead slippage or collapse due to insufficient support from the layer below. Designers are advised to use CAD draft or overhang analysis tools to identify areas that exceed this limit.

3. Toolpath Design and Movement

Continuous toolpaths are strongly preferred in LFAM to minimize defects caused by travel moves and start-stop operations. Start-stops are challenging in large-format systems due to the pressure and flow characteristics of molten pellets. These interruptions can cause drooling, uneven surfaces, and weak points in the part.

Designers should aim for toolpaths that begin and end at the same point and avoid self-intersections. Simple visualization techniques, like tracing the path with a pen without lifting it, can help identify discontinuities in the design.

Continuous toolpaths are critical for producing functional compliant hinges without start-stop defects, which could introduce weak points in the movement of the deployable structures.

4. Layer Time and Cooling

LFAM prioritizes **layer time**—the time between depositing successive layers in the same location—over traditional print speed metrics. Proper layer time ensures that each layer has cooled sufficiently to support the next, while still retaining enough heat to bond properly.

Insufficient layer time results in deformation and sagging as soft layers cannot support the structure above. Conversely, excessive layer time can cause layers to cool too much, leading to poor adhesion or delamination.

Layer time varies by material and geometry. Manufacturers like CEAD provide material-specific guidelines known as "layer time sheets" to assist with proper configuration. Additional adjustments may be required based on ambient conditions or complex geometries.

5. Heat Management

Heat plays a central role in LFAM print quality. The large volume of extruded material means that internal and external cooling must be carefully managed.

Key heat-related challenges include:

- **Warping due to thermal contraction**: As layers cool, they shrink, which can lead to deformation. This is especially problematic in long, continuous toolpaths.
- **Heat buildup in enclosed sections**: When printing closed geometries, hot air may become trapped inside the part, slowing cooling and causing sagging or distortion.
- **Hot pockets**: Regions where multiple beads are concentrated in a small area retain heat longer, often requiring increased layer times to avoid deformation.

Environmental temperature also influences heat management. Colder surroundings accelerate cooling and may require slower print speeds or a heated print bed to maintain quality.

6. Design Detail and Resolution

Compared to desktop 3D printing, LFAM is limited in the level of fine detail it can achieve due to the large nozzle and bead sizes. Very small features, sharp corners, or intricate surface textures may not print accurately and should either be simplified or handled through secondary processes like CNC milling.

Sharp corners are discouraged as they can cause material accumulation, over-extrusion, and dragging. Smooth transitions are preferred for consistent bead flow and accuracy.

7. Printing Orientation and Slicing Strategy

Standard LFAM printing is performed with 90-degree planar slicing. However, when geometries are not printable using this method—especially those with significant overhangs or closed tops—alternative strategies can be used.

One such method is **45-degree printing**, where layers are deposited at an angle, allowing for overhangs and tops to be printed without additional support. Designers must be aware of the challenges this poses, including visualizing the design at an angle and accounting for recessed features that may become unsupported.

More advanced slicing methods include **multi-planar**, **non-planar**, and **segmented slicing**, which allow for greater flexibility in printing complex geometries. These techniques often require customized toolpath generation and careful planning.

8. Machine and Material Constraints

The maximum size of a printable part is constrained by the build volume of the LFAM machine, which may span several feet or meters. However, even if a part fits within the build volume, its layer size must be compatible with the maximum material output of the extruder.

If the layer is too large and the extruder cannot deposit material fast enough, the lower layers may cool excessively before the upper layers are applied, leading to poor bonding and structural weaknesses. As a result, print sizes must be evaluated against both machine volume and material throughput.

So, the size of each panel in the deployable structure is not only limited by the build volume of the LFAM machine but also by the maximum material output of the extruder

Flexible materials

In discussions with BouwLab and CEAD Group, it was confirmed that printing flexible materials like TPU is technically possible but not recommended. Both companies reported little to no practical experience with flexible filament at large scales and highlighted additional risks such as warping due to thermal contraction. Nevertheless, they acknowledged that, under the right conditions, it could be achieved (BouwLab, n.d.) (CEAD Group, n.d.).

6.3 Hinges

The most crucial part in this concept is the hinges. This Detail could make or break the project

Several options exist for implementing hinge mechanisms in deployable 3D-printed structures. Each approach presents specific benefits and challenges, particularly when scaled for large-format printing.

- **Separate components**: This approach involves printing each component individually and assembling the structure afterward. The hinges in this case are mechanical door hinges, with elements connected using metal pins.
  While this is a realistic and feasible method, it requires manual assembly, which undermines the goal of creating a fully integrated, self-deployable structure (see Figure 51a).
- **Printing mechanical hinges in place**: This method also relies on mechanical door hinges but involves printing multiple elements already assembled, with only the pins added afterward.
  Although this technique is used in small-scale 3D printing, it becomes challenging at larger scales due to the difficulty of maintaining separation between components. Additionally, the printing process would involve frequent starts and stops, making continuous path printing impossible.
- **Single-material compliant hinges**: This option connects rigid elements with thin strips of the same material, acting as flexible hinges.
  While these are not perfect hinges and can lead to unwanted deformation, they can offer high reliability and may outlast mechanical hinges (source needed).
  All previous prototypes have used this approach.
  The main challenge lies in selecting a material that is stiff enough for the rigid elements while remaining flexible at the hinge locations.

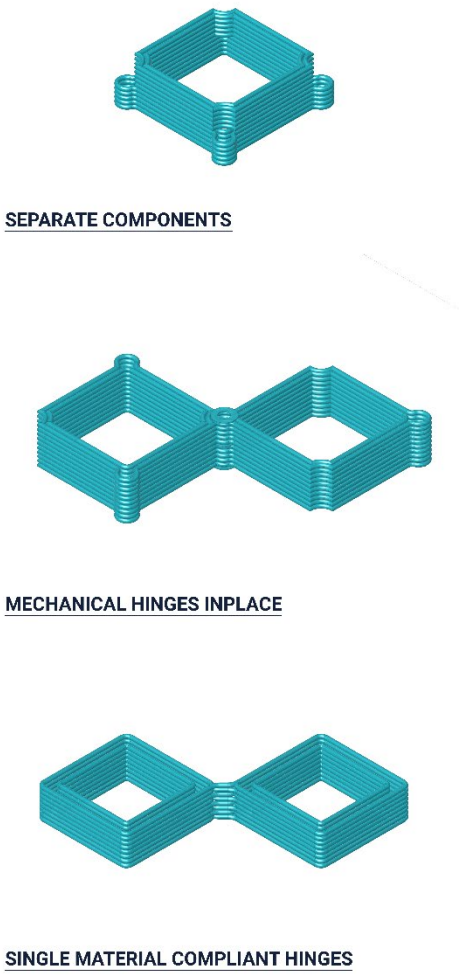

Figure 51: *hinge options*

These hinge implementation options were discussed with two industry partners: Bouwlab and CEAD Group. Their feedback is summarized as follows:

- Both parties considered the option of printing separate components as the most realistic and feasible for current large-scale 3D printing capabilities.
- The method of printing mechanical hinges in place was disregarded due to the need for frequent starting and stopping during the printing process, which prevents a continuous printing path and increases complexity.
- The option of single-material compliant hinges would require printing in a flexible material. Both companies had limited to no experience with such materials and, while they did not consider it impossible, they did not recommend it.

Bouw Lab agreed that the use of single-material compliant hinges would be the most promising approach for this application. They considered the concept sufficiently interesting and innovative to assist in producing a 1:1 scale prototype segment to test the material behaviour in relation to a compliant hinge (see Figure 52).

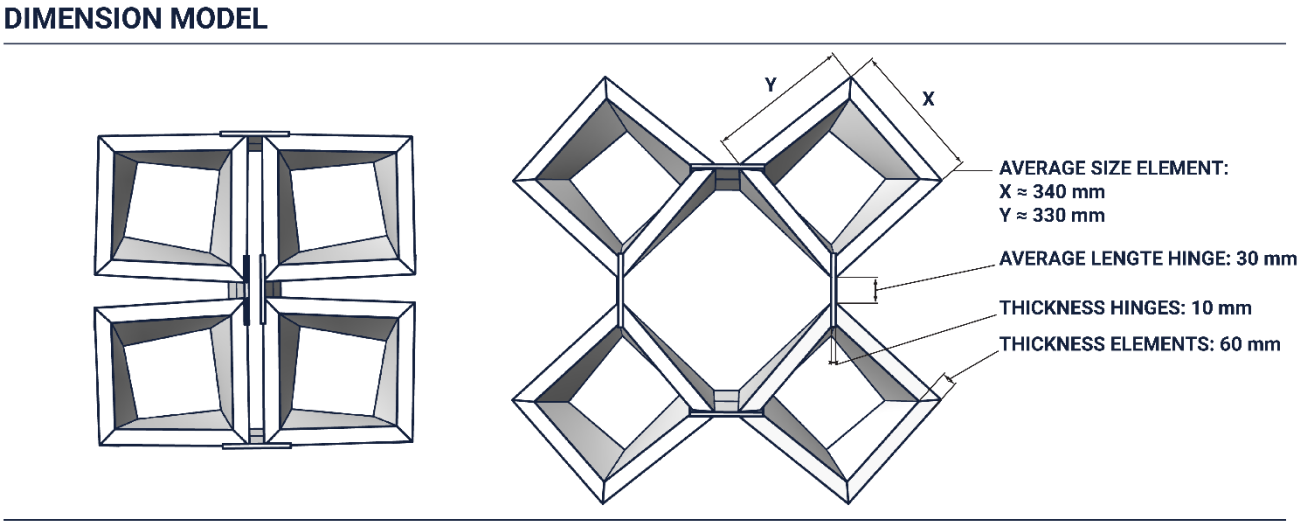

Figure 52: *proposed 1:1 Detail*

6.4 Material

Scale Prototypes

During the development of small-scale prototypes for this project, several challenges associated with printing TPU were encountered. These challenges provided valuable insights into the material behaviour and print process constraints. Key observations included:

- **Absence of Cooling Fan Usage**: Printing TPU without active cooling was necessary to prevent layer delamination and to maintain interlayer adhesion.
- **Reduced Printing Speed**: Slower print speeds were required to ensure consistent material deposition and to avoid defects associated with filament elasticity.
- **Material Preparation**: Proper drying of TPU filament was critical, as moisture absorption led to printing inconsistencies and structural weaknesses.

Issues experienced during the printing process included:

- **Warping and Bed Adhesion Failures**: TPU prints frequently detached from the print bed, causing warping and deformation.
- **Poor Surface Finish**: Surface quality was adversely affected by material properties and print parameters, leading to rough and inconsistent textures.
- **Nozzle Clogging**: TPU's softness and tendency to expand under heat often resulted in nozzle blockages, necessitating frequent maintenance.

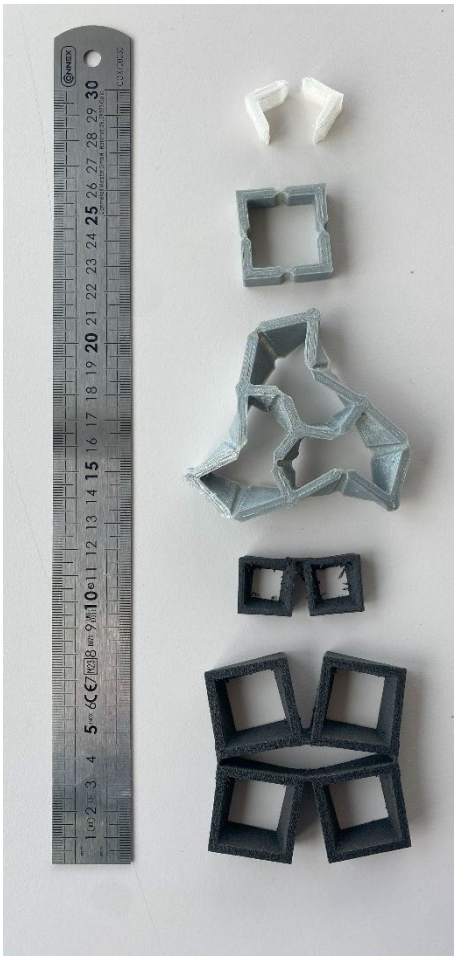

Figure 53: *test prints compliant hinge*

For each material tested an initial test print was done to assess the quality of compliant hinges, a critical feature for deployable structures.

Through iterative testing, foaming TPU emerged as a promising material solution. Specifically, **TPU Foamy 95A** was utilized (Recreus, 2024). This material exhibits the ability to expand when heated, with the degree of foaming adjustable through print settings. The foaming process reduces material density, thereby offering partial control over the flexibility of the printed structures. This characteristic enables not only global but also potential localized tuning of mechanical properties. (Recreus, 2024)

The application of foaming TPU presents significant opportunities for Large Format Additive Manufacturing (LFAM). The material's lower density reduces the overall weight of printed parts, which can mitigate issues such as sagging during printing. Additionally, the decreased material volume may lessen the dependency on active cooling, a common bottleneck in LFAM processes.

However, the use of foaming materials in LFAM remains an open research topic. Further investigation is required to fully understand the behaviour, reliability, and scalability of foamed TPU structures in large-scale manufacturing contexts.

LFAM

For scaling up the concept of deployable structures, the material requirements may differ from those suitable for small-scale prototypes. A material with a higher Young's modulus is beneficial for maintaining structural integrity and stability in larger, self-supporting structures. Without sufficient stiffness, such structures are prone to excessive deformation under their own weight, potentially leading to functional failure or compromised performance. However, if the material is too stiff, it can negatively affect the performance of compliant hinges by increasing the force required for deployment. Therefore, a balance must be achieved between overall structural stiffness and hinge flexibility.

To identify suitable candidate materials, a comparative analysis was conducted using Granta Edupack (Ansys Granta EduPack, 2024). In this analysis:

- The X-axis represents price per volume, as material cost significantly impacts the financial feasibility of large-scale production.
- The Y-axis represents the Young's modulus, providing an indication of material stiffness.

A material selection filter was applied based on the following criteria:

- **Thermoplastic elastomers** were selected, as these materials exhibit flexible, rubber-like properties, important for the complain hinges while remaining processable through heating, making them generally viable for 3D printing.
- **Young's modulus range** was set between 0.01 GPa and 5 GPa, based on observations made during the prototyping phase regarding acceptable levels of flexibility and stiffness. The lower bound corresponds to the modulus of the material used in initial prototypes, while the upper bound was selected to approximate the stiffness of softwood (Ansys Granta EduPack, 2024).

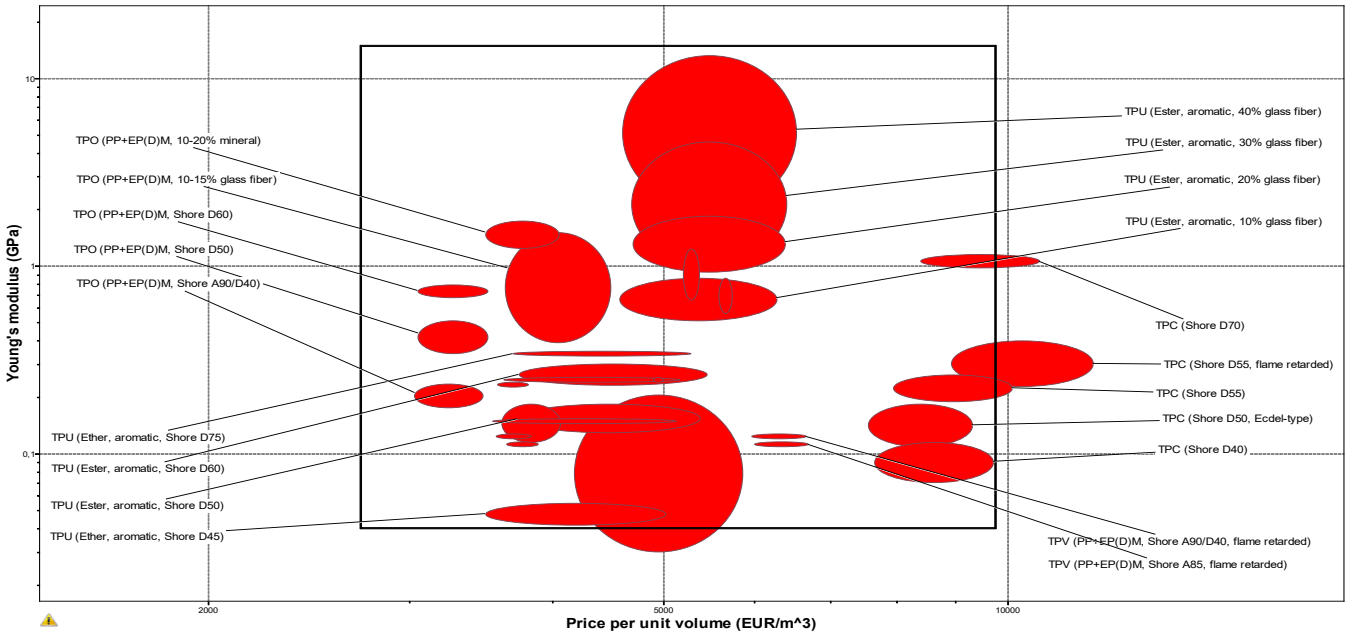

Figure 54: *graph material comparison (Ansys Granta EduPack, 2024).*

Key Observations from the Material Comparison:

- At the lower end of the graph, TPU 45D, the material predominantly used for the original scale prototypes, exhibited a Young's modulus of approximately 0.05 GPa.
- Higher Shore hardness variants of TPU, up to 75D, demonstrated an increased Young's modulus, reaching approximately 0.34 GPa.
- To achieve even higher stiffness within TPU materials, glass fiber reinforcement is necessary. The data shows that:
    - 10% glass fiber TPU achieves ~0.5 GPa,
    - 20% glass fiber TPU achieves ~1.2 GPa,
    - 30% glass fiber TPU achieves ~4.7 GPa, and
    - 40% glass fiber TPU achieves ~13.2 GPa.
- Another promising material family identified is Thermoplastic Copolyester (TPC):
    - Available in Shore hardness values of 50D and 70D.
    - Exhibits a Young's modulus range of 0.23–1.16 GPa.
    - While more expensive than standard TPU, TPC offers advantages such as lower water absorption over time, potentially enhancing outdoor durability. However, the extent to which these benefits large-scale structures require further investigation.
- Other material types such as TPO (Thermoplastic Polyolefin) and TPV (Thermoplastic Vulcanizate) were also identified. However, limited information regarding their suitability for 3D printing led to their exclusion from further consideration, in order to avoid introducing additional uncertainties into the research.

Responds bouwLab

According to Bouwlab, materials with a Shore hardness of 75D would likely be too stiff and lack the necessary flexibility for the hinges, based on the wall thicknesses in the current design. Instead, they recommended a material with a Shore hardness of 90A, which demonstrated promising flexibility in samples with thicknesses of 10–15 mm. However, at greater thicknesses (30–40 mm), the material exhibited reduced flexibility (BouwLab, n.d.).

They also emphasized that materials listed in databases such as EduPack typically represent general material properties and do not necessarily correspond to printable compounds. Specialized formulations are usually required for robotic 3D printing, and the development of such compounds is generally only feasible at industrial scales involving large material volumes. As a result, Bouwlab is limited to using commercially available materials from their suppliers and cannot request custom material mixes for small-scale applications (BouwLab, n.d.).

Bouwlab recommended the following materials:

1. **TPU F98A** – Lubrizol ESTANE® 3D TPU F98A-030
   This thermoplastic polyurethane exhibits high flexibility and durability, suitable for various additive manufacturing applications. (Lubrizol Corporation, n.d.)
2. **TPU C88A** – BASF Elastollan® C 88 A
   A versatile TPU compound with balanced stiffness and elasticity, often used for industrial prototyping. (BASF Polyurethanes GmbH, n.d.)
3. **TPU C78A** – BASF Elastollan® C 78 A
   A slightly softer alternative to C88A, offering increased flexibility while maintaining mechanical stability. (BASF Polyurethanes GmbH, n.d.)
4. **TPE00VEPv1** – Caracol ENSOFT SO-161-70A
   A polyolefin-based thermoplastic elastomer with a Shore hardness of 90A, known for its printability in large-scale robotic 3D printing and a favorable balance of strength and flexibility. (Caracol S.r.l., 2023)

The stiffest of the recommended materials, TPU F98A, was selected for further investigation in the structural analysis. To perform this analysis, detailed mechanical properties were required. However, as not all necessary material properties were available from the datasheet, several assumptions had to be made. These assumptions are outlined in the table below.

ESTANE® 3D TPU F98A-030 CR HC PL

Property	Value	Basis
Young's (Elastic) Modulus	**35 kN / cm^2** ≈ 350 MPa	Extrapolated from the BASF Elastollan® stiffness chart for 95 Sh A polyester TPUs, adjusted to 98 Sh A (BASF, 2018).
In-plane Shear Modulus	**12 kN / cm^2** ≈ 120 MPa	G = E / 2(1 + ν) with ν ≈ 0.47 for rubber-like TPUs (BASF, 2018).
Transverse Shear Modulus	**4.8 kN / cm^2** ≈ 48 MPa	Reduced to 40 % of in-plane G to reflect typical XY/Z tensile-strength ratios for printed TPUs (MatWeb, n.d.-b).
Specific Weight γ	**10.7 kN / m^3**	Density ρ = 1.09 g / cm^3 from the Lubrizol technical data sheet; γ = ρ g (Lubrizol, 2019).
Coefficient of Thermal Expansion (linear)	**0.9 – 1.1 × 10^{-4} / °C**	Typical unfilled TPU band 80–120 µm m^{-1} °C^{-1}; mid-range adopted (MatWeb, n.d.-c).
Tensile Strength (XY build)	**2.8 kN / cm^2** ≈ 28 MPa	Direct value from Lubrizol TDS (Lubrizol, 2019).
Compressive Strength (yield)	**1.5 kN / cm^2** ≈ 15 MPa *est.*	Average compressive yield for very-hard TPUs of similar hardness (MatWeb, n.d.-d).

Additives

In discussions with the CEAD Group, it was noted that additives are commonly added into filaments to enhance specific material properties. Additives are used to:

- Improve fire resistance to meet Eurocode standards for architectural applications.
- Enhance UV resistance, thereby increasing the material's durability in outdoor environments.

At this stage, it remains unclear which specific additives are used, whether they are compatible with the materials identified in this study, and what effects they might have on mechanical properties or printability. These factors would require further investigation to determine their feasibility and impact on performance.

For this research, it is assumed that similar additives could be incorporated into the selected materials without significantly compromising the intended mechanical behaviour or print quality.

Summary

Material selection for scaling up deployable structures requires balancing structural stiffness with flexibility in the hinges. To identify suitable candidates, a comparative analysis was conducted using Granta EduPack, focusing on thermoplastic elastomers (TPEs) within a defined stiffness range. Materials such as TPU in various hardness levels, glass fiber-reinforced TPU, and Thermoplastic Copolyester (TPC) were examined.

However, Bouwlab highlighted the limitations of database-listed properties and emphasized the need for application-specific printable compounds. They recommended four commercially viable materials for robotic 3D printing: TPU F98A, TPU C88A, TPU C78A, and Caracol's TPE00VEPv1. TPU F98A, the stiffest among them, was selected for further structural analysis., was selected for structural analysis.

6.5 Prototype 1:1

To better understand how these materials perform at lager scale, support was provided by BouwLab, which facilitated large-format printing tests using their in-house robotic arm printer. Two prototypes were produced using ENSOFT SO-161-70A, a polyolefin-based thermoplastic elastomer with a Shore hardness of 90A. This material, previously used in robotic printing by other companies, is softer than initially anticipated but available in stiffer variants, which could be considered for future prototypes.

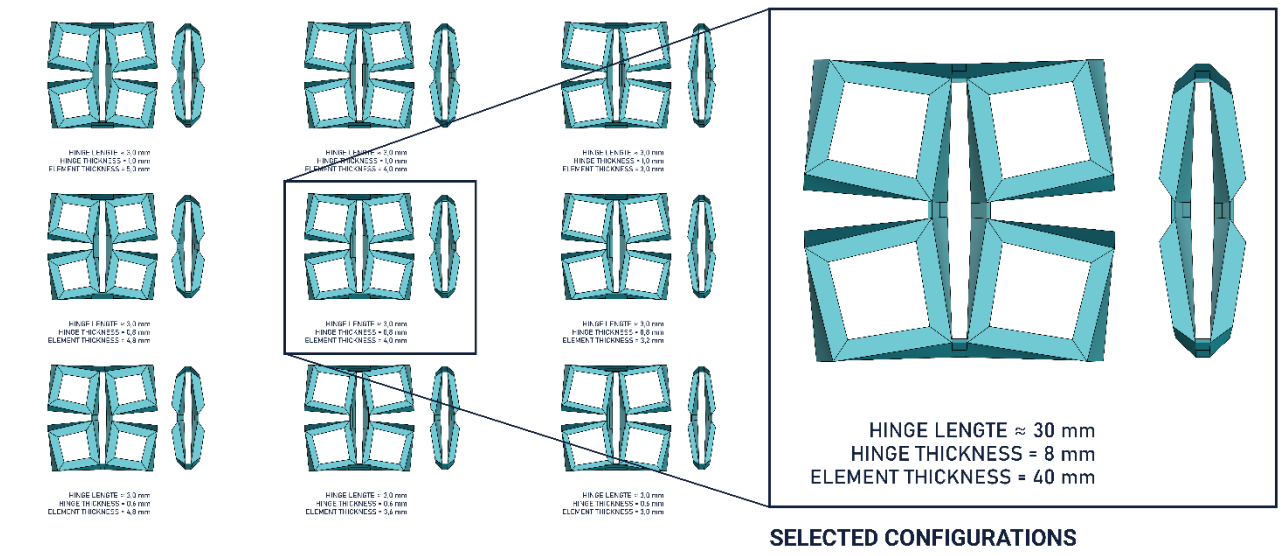

Figure 55: *Proposed model for 1:1 prototype*

As this was also BouwLab's first experience printing with thermoplastic elastomers, preliminary test prints were conducted to explore how extrusion flow and bead width influence interlayer bonding. In these tests, different toolpath settings were also evaluated in the robotic arm slicer to improve print quality and consistency. These tests focused on:

- Minimising starting and stopping points to promote a continuous extrusion path.
- Controlling seam placement to prevent weak points from occurring at critical locations, such as hinge lines.

However, controlling start-stop behaviour proved to be a trade-off within the slicing software used for robotic printing. To gain more precise control, future iterations could benefit from a custom toolpath developed in Grasshopper, allowing targeted manipulation of extrusion behaviour.

Ultimately, two full-scale prototypes were printed using identical dimensions (see Figure 55). The first prototype served to evaluate hinge performance and overall flexibility. Following successful results, the second prototype incorporated four fully connected elements using the same design parameters.

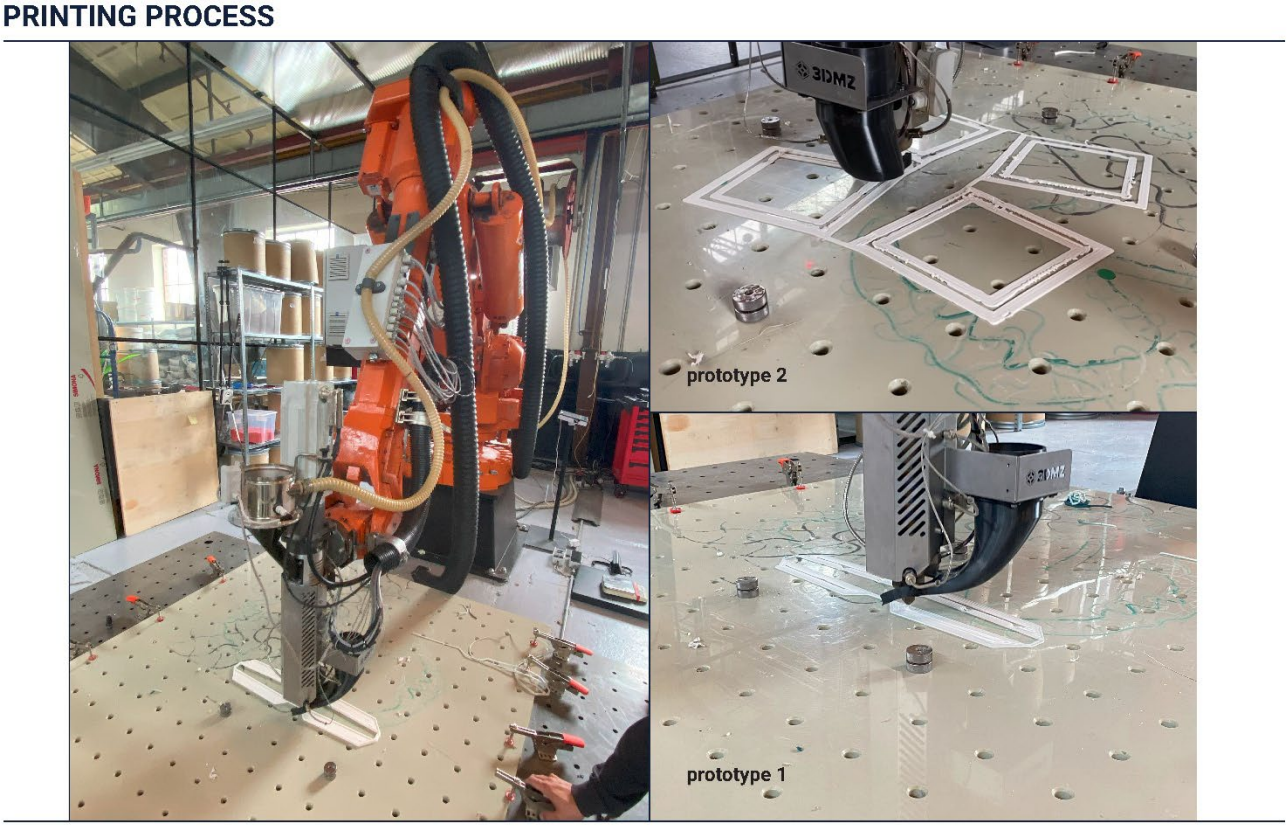

Figure 57: *Printing process 1:1 prototype*

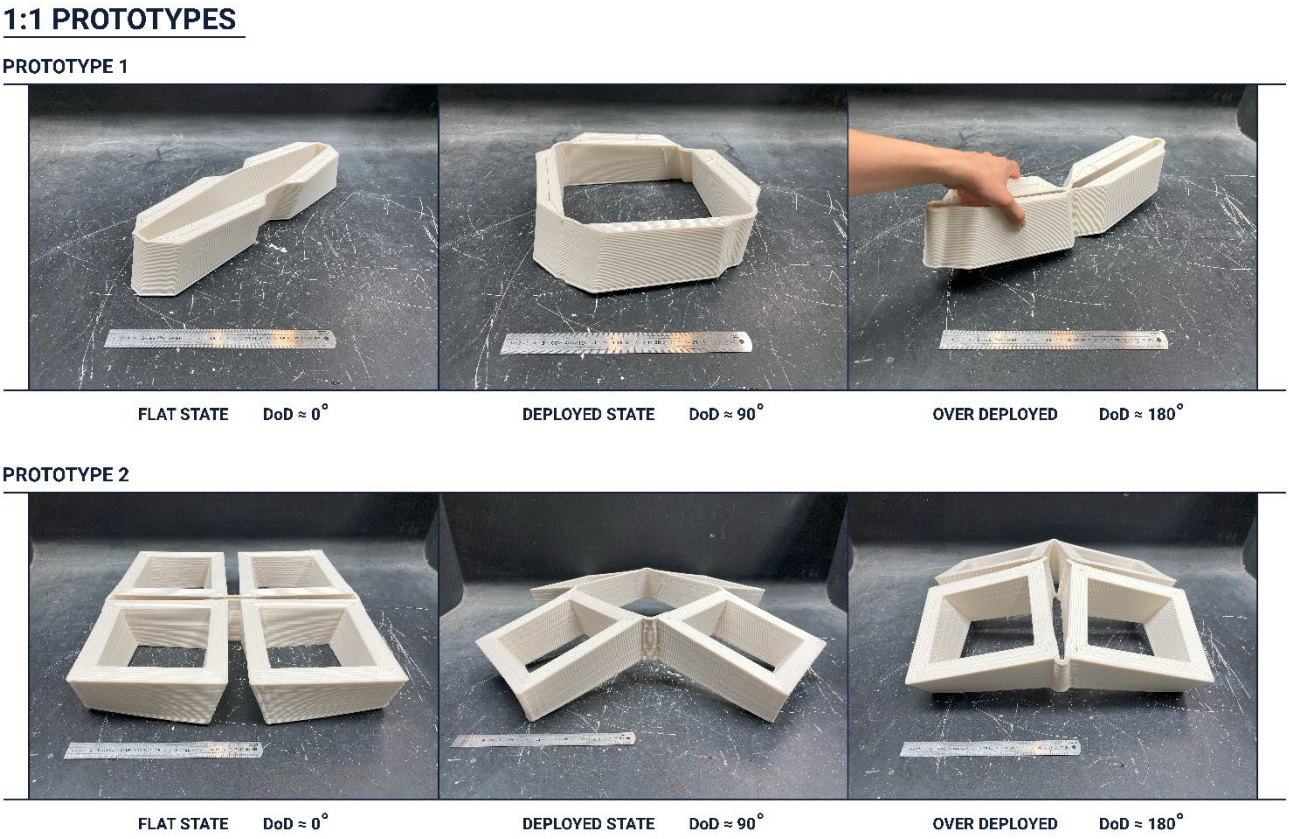

Figure 56: *Prototypes 1:1*

6.6 Alternative hinge details

The full-scale prototype highlights that weight is a significant issue. This is primarily due to two factors:

- The prototypes were fabricated using a softer material than originally intended. The design initially specified TPU with a Shore hardness of 90A, which also has a higher Young's modulus. However, the prototypes were printed using TPU with a Shore hardness of 70A, which has significantly lower stiffness. As a result, more material had to be added to the rigid elements to maintain structural integrity, which substantially increased the overall weight.
- A balanced relationship must be established between the selected material and the thickness ratio of the hinge and the rigid elements. To optimize material use, the rigid elements could also be printed with internal infill structures rather than as solid volumes.

Nonetheless, the rigid elements are primarily dimensioned to meet the stiffness requirements of the deployment phase. Once the structure is fully deployed, this level of stiffness is no longer necessary. This discrepancy between the structural demands during deployment and those in the deployed state is discussed further in Chapter 7.2.2. In the deployed configuration, the compliant hinges become the most critical detail of the structure.

To address this, two alternative hinge details were developed with the aim of reducing material use and improving structural performance:

- **Dual material printing**
  This approach involves using a stiffer material such as PLA, PETG with fibre reinforcement for the rigid elements, combined with a flexible material such as TPU for the compliant hinges. This would significantly reduce overall weight and minimize unwanted deformation during deployment. However, it requires a printer capable of multi-material printing, ideally equipped with dual nozzles. While feasible at small scales, this technology is not yet widely available for large-format 3D printing.
- **Stiffening panels**
  This alternative reduces the wall thickness of printed elements and incorporates stiffening panels made from higher-stiffness materials such as wood, acrylic, or polycarbonate. In this scenario, the printed structure acts as a formwork or housing for the panels, maintaining a consistent overall thickness. This approach could significantly reduce both material consumption and print time. However, it introduces additional steps in the production process, including post-print installation of the panels.

Both solutions require further investigation and prototyping to evaluate their structural performance and practical feasibility.

ALTERNATIVE HINGE DETAILS

DUAL MATERIAL 3D PRINTING

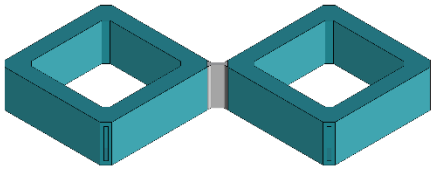

Structure 3D printed in two different materials. Requires dual nozzle

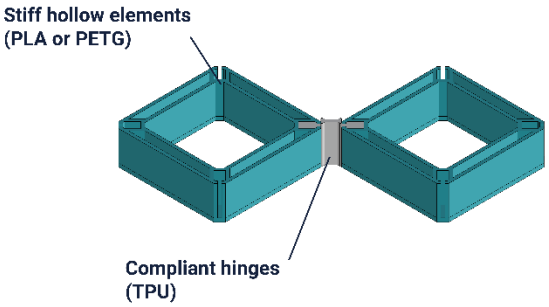

STIFFENING BY PANELS

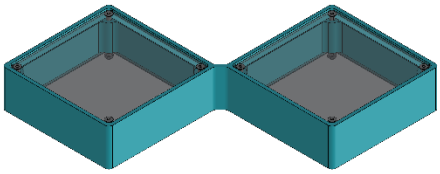

Thin printed elements stiffened by panels of a stiff light weight material

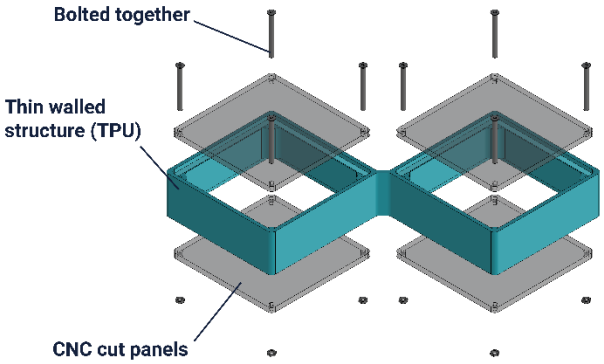

Figure 58: *Alternative Hinge Details*

7 CASE STUDY

The goal of this case study was to design a structure that could be manufactured using currently available materials and 3D printing technologies and prove that this method can be scaled up

The chosen application for the case study is a small shelter intended for use at events and festivals. The prototype is intended to:

- Demonstrate the ability to span a small structural distance
- Evaluate whether the system can be deployed quickly and easily
- If physically constructed, illustrate the potential of this method for designing and developing 3D structures

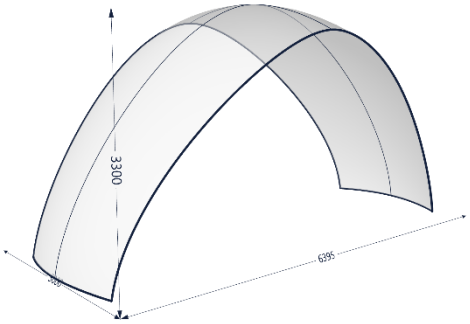

Figure 59: *Dimension case study*

The resulting structure, shown in Figure 60, is a simple form that can accommodate various functions such as a bar, information desk, exhibition stand, or standing desk for networking events, making it suitable for multiple use cases.

APPLICATION

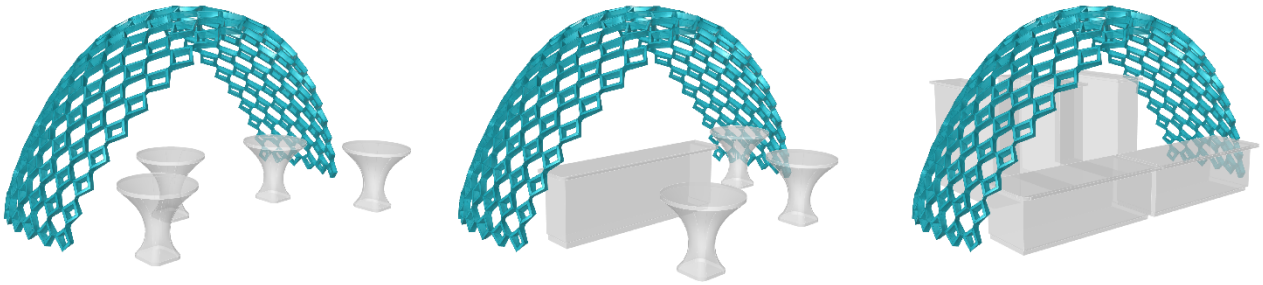

Figure 60: *possible scenarios/application*

Although the method can theoretically be applied to almost any surface geometry (within certain limits), it is of particular interest to observe how different curvatures affect the structural behaviour. To explore this, the shelter was designed using a parametric script that allows curvature to be adjusted in both principal directions. These parameters can later be integrated into the optimization process described in a subsequent section.

To ensure consistent and comparable results during optimization, the overall shape was kept symmetric along two axes. Additionally, the geometry was given a wider base to better distribute the resulting forces. Which was a clear issue in earlier test shapes.

CASE STUDY VARIATIONS

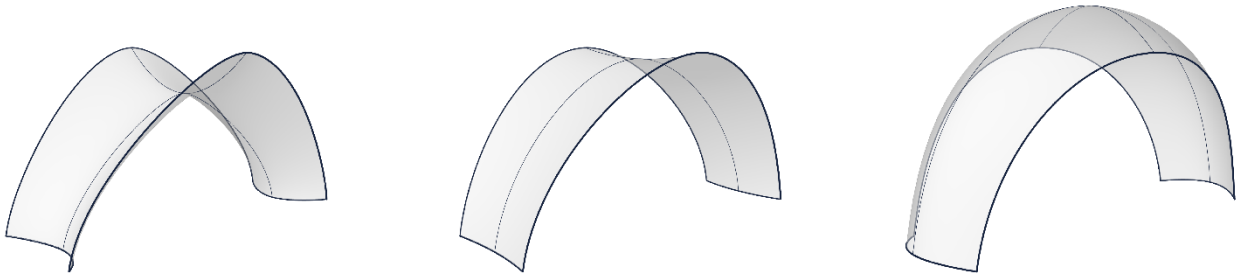

Figure 61: *Case study Geometry variations*

During the project, contact was established with representatives from the Highlight Festival, who expressed potential interest in exhibiting the case study. As the focus would be on showcasing the structure rather than its practical application, most of the requirements provided were related to thematic relevance and safety.

1. Thematic Relevance – Robotics
The project must align with the 2026 Highlight Delft theme of "Robotics." As 2026 has been designated the "Robot Year" in Delft, projects are expected to connect to robotic technologies or themes. Since this structure is entirely produced and 3D printed by robots, it fits particularly well within this theme.

2. Fire Safety of Materials
Materials used must comply with fire safety regulations. For plastic-based constructions, it is critical to ensure that materials are flame-retardant and do not melt or drip when exposed to fire. This is an important material requirement, which will be further discussed in the sub-paragraph "Materials."

3. Weight and Ballast
The weight of the final structure must be taken into account, as overhead structures are particularly susceptible to upward wind loads. For instance, a standard 3x3m event tent typically requires approximately 500 kg of ballast to meet safety standards. Although this requirement is important, it has no significant impact on the structure itself.

4. Assembly and Transport
Quick assembly and disassembly are major advantages in event production. The design must facilitate easy transport and setup, preferably with minimal parts and tools. Ideally, the packed structure should also be forklift accessible. Deployment strategies will be discussed later.

5. Scalability and Modularity
The structure should be scalable and modular to allow the linking of multiple units for larger applications. Plug-and-play functionality or a connectable system is preferred to enable flexibility during events. Given that the geometry of the case study is a portal, it can easily be repeated and connected. Additionally, the system allows for the development of custom connecting parts if needed.

7.1 Structural Optimisation

The Grasshopper script developed for form-finding contains multiple parameters and objectives that can be used/improved by optimisation. Ideally, the process should be optimised by:

- Finding the optimum geometry for the case study.
- Adjusting the density and size of the elements locally.
- Finding the optimum offset between layers for the most material-efficient structure.
- Balancing the strengths for each constraint in the form-finding process to gain the most reliable results.
- Simulating the deployment from its flat state, accounting for material deformation and hinge tolerances.
- Finding the minimum and best locations for the cables to tension the structure into its shape.
- Minimizing material thickness while ensuring the structure still meets operational load cases and conditions.
- Simulating the deployment to the deployed configuration, accounting for material deformation and hinge tolerances and measuring how closely it approximates the target shape.

However, because the Grasshopper script for form-finding is already computationally intensive, by adding a full Karamba structural analysis would push the run-time per design well beyond what is practical for iterative optimisation.

Therefore, we decided to focus solely on the first two objectives: finding the optimal geometry for the case study and adjusting the element density and size locally. With the deformation of the structure under vertical loading as the objective.

To calculate deformation, Karamba3D was used an engineering tool that integrates with Grasshopper for Rhino and enables interactive, real-time Finite Element Analysis of spatial trusses, frames, and shells within a visual programming environment (Karamba3D, n.d.).

We use a highly simplified structural model in Karamba (see Figure 64): a coarse mesh, idealised line hinges, and intentionally over-stiffened members. This lets us compare alternative geometries during optimisation without accounting for material grades, section thicknesses, or hinge detailing. Every candidate is subjected to the same vertical load case with supports at the corners. The deformation is measured as objective.

Instead of applying a population-based genetic algorithm such as Galapagos to optimise the structure, a simplified grid search method was used to explore the design space. This approach samples the fitness landscape by varying only two design parameters at a time. While not an optimization algorithm in the strict sense, grid search allows for direct visualization of the fitness landscape. By analysing the resulting deformation values across a limited set of parameter combinations, a near-optimal design region can be identified with significantly fewer configurations. However, this method does not guarantee a global optimum, can be computationally inefficient for high-dimensional problems, and is limited by the resolution of the chosen parameter grid.

Two such fitness landscapes were generated and analysed in the case study:

- One examining the influence of curvature variations on structural deformation.
- One examining the influence of mesh density variations on structural deformation.

Fitness Landscape Geometry

As discussed earlier in the "Case Study" section, the development of the geometry for the case study initially involved creating several parameters to control the curvature, which could then be used to identify an optimal design. These parameters are (see Figure 62):

- **Curvature in the U direction**: This corresponds to the width, or the short span. The parameter ranges from 0 to 1, with 0 representing negative curvature, 0.5 a flat geometry, and 1 a positive curvature.
- **Curvature in the V direction**: This corresponds to the length, or the long span. The parameter also ranges from 0 to 1, with sharper shapes occurring as the value approaches 0.

The maximum amount of curvature applied (i.e., the limits of these parameters) was largely determined by limitations and issues within the form-finding script. The most significant issue was overlapping during the flattening of the geometry.

Although it would have been possible to prevent overlaps by introducing additional constraints, thus allowing for a larger range of curvatures and more varied geometries. These measures could have compromised the reliability of the form-finding results. To avoid this risk, no additional constraints were implemented.

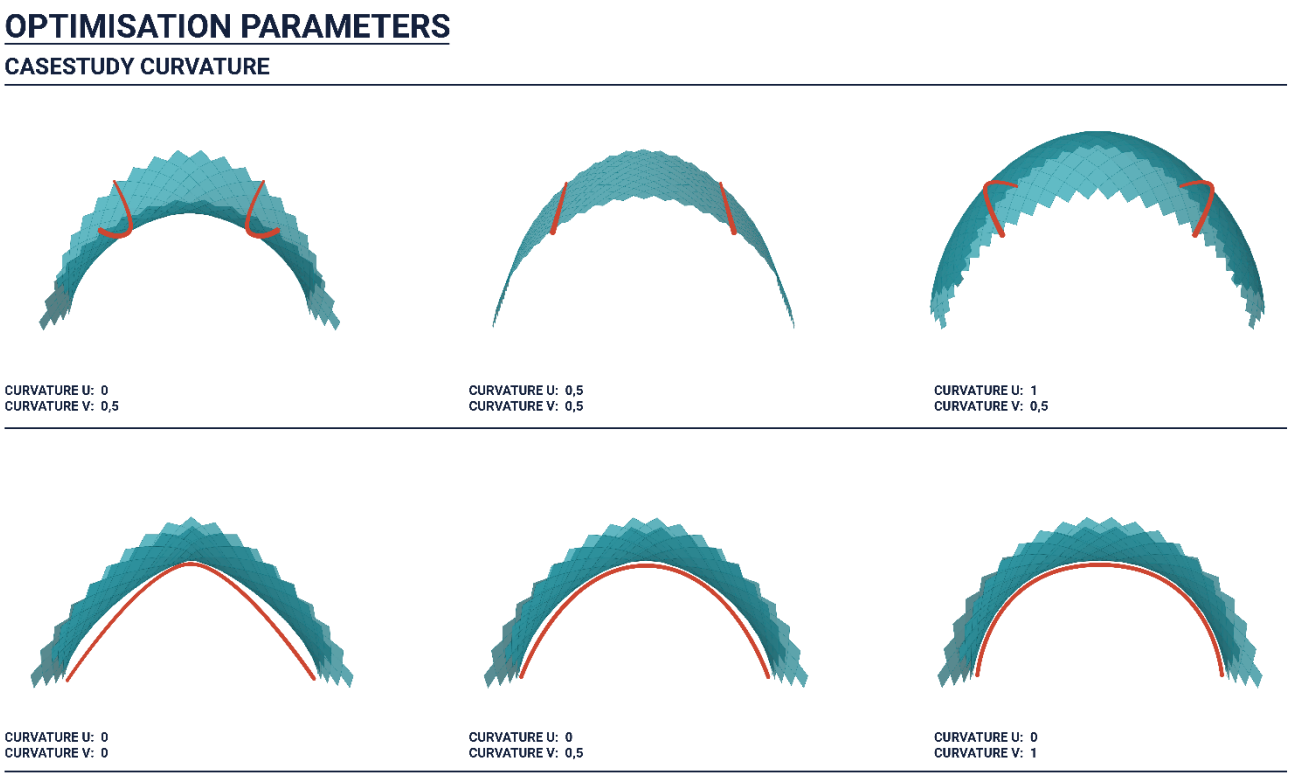

Figure 62: *parameters curvature case study*

To create the fitness landscape graph, all U-V curvature combinations were evaluated across a 10 by 10 grid, recording the input variables (U and V curvature) and the resulting deformation. The graph was mapped using the U and V values as the X and Y coordinates, and deformation as the objective in the Z direction (see Figure 63).

Additionally, images of all generated variations were saved, along with their corresponding parameters and resulting deformation values, to facilitate easier comparison of results and identification of potential issues.

Results

It is notable how little curvature in the U direction was present in the result with the lowest maximum displacement. Typically, a configuration with greater curvature would be expected to produce a stiffer overall geometry. This unexpected outcome may be attributed to the fact that the mesh density has not yet been adjusted.

Further investigation into the influence of mesh density on these results would be valuable. It is likely that changes in the mesh density would have a more impact on configurations with greater curvature.

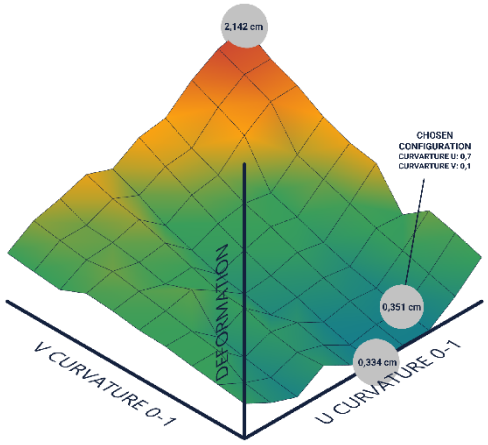

Figure 63: *fitness landscape curvature case study*

As expected, results with larger V values, leading to longer arch lengths, exhibit greater deformation, as shown in the graph.

An important note is that the element count in the V direction is based on the difference in length between the principal curves at the centre of the geometry. Consequently, structures with higher U and V values possess a larger element count in the V direction, and therefore a higher total element count overall. This variation likely influenced the deformation results. Although unintended, this approach was necessary to ensure that the elements remained as close to square as possible, thereby improving the reliability of the form-finding process.

It is also clear that configurations with high U and V values display increased deformation; however, these configurations provide the greatest usable space within the shelter. This represents a trade-off that could have been addressed through multi-objective optimization, though such an approach would have significantly increased computation time.

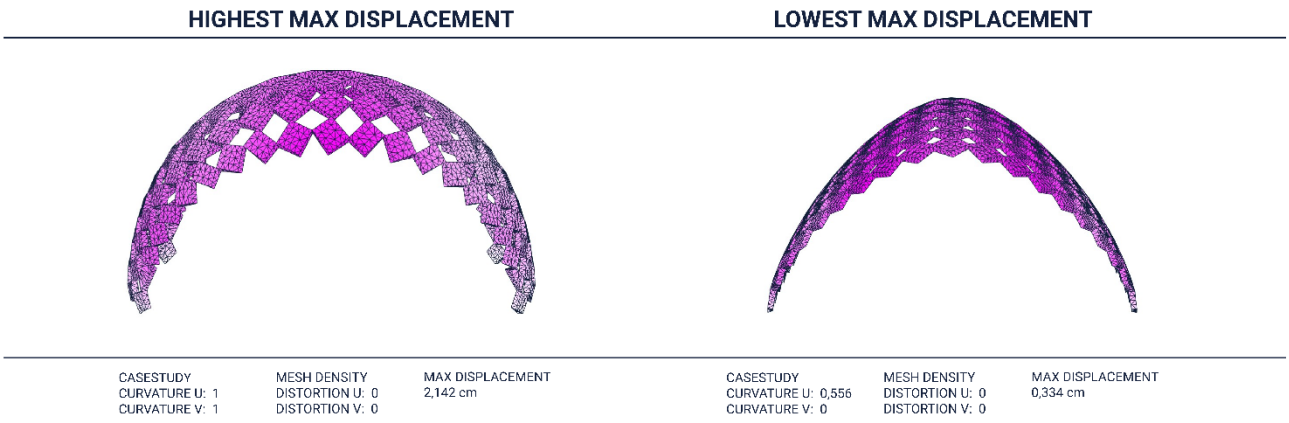

Figure 64: *configurations with the highest and lowest performance*

For the case study, the configuration with the best performance (lowest maximum displacement) was not chosen, as it presented an almost single curved geometry. To demonstrate double curved capabilities, a configuration with slightly more curvature, yet close to the best performing one, was selected. It is suspected that the configuration with more curvature will be more affected by the optimization in mesh density. There for, a configuration with increased curvature but still near-optimal performance was chosen for further optimisation.

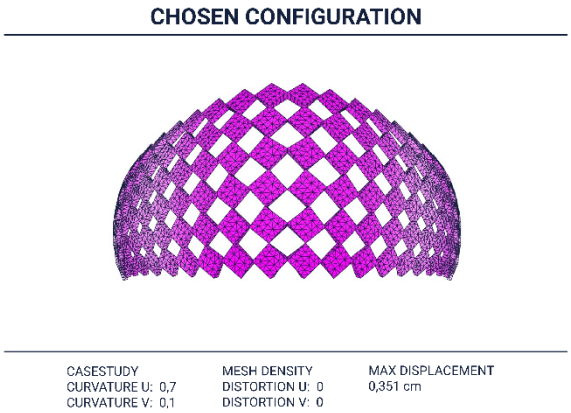

Figure 65: *chosen configuration*

Fitness Landscape Mesh Density

As mentioned in the "Creating the Mesh" section, the mesh is generated from a grid of points. The distances between these points are varied using consecutive domains to control the local mesh density across the surface.

To achieve this variation, a Gaussian function is applied to define the spacing between points:

$$y = \exp\left(\frac{(x-b)^2}{2c^2}\right)$$

In this function:

- **b** controls the location of the peak, which determines the position along the axis where the greatest stretching or compression of the mesh elements occurs.
- **c** controls the width (spread) of the peak, affecting how rapidly the element sizes change around the peak. A smaller c results in a sharper transition, while a larger c produces a more gradual change.

By adjusting the distances between points according to the values produced by this Gaussian function, the mesh density can be increased locally around the peak and decreased further away. This approach allows precise control over the distribution of elements in both the u and v directions.

The method provides control over local mesh density, enabling finer meshes where needed without globally increasing the total number of elements (see figure 66). Since the Gaussian function has only a single peak, it allows for the creation of one locally distorted area within the mesh, which is sufficient for the current case study being assessed.

For more complex geometries, with multiple changes in curvature or multiple local distortions are required, a different function (such as a sum of multiple Gaussians) would be necessary.

Because the geometry under consideration is symmetric along both axes, the **c** value can be disregarded. The spread of the distortion is assumed to be uniform in both directions, leaving only the b values to vary in both u and v direction. These two parameters, referred to as U distortion and V distortion (see Figure 66) are used to search for the near-optimal mesh configuration for the case study.

As before, a fitness landscape graph was generated by generating all combinations of U and V distortion across a 10×10 grid. The U and V distortion values were mapped to the X and Y axes, while the resulting deformation was plotted along the Z axis. Images of all variations were also saved, together with their corresponding input parameters and deformation values, to facilitate easy comparison and identification of potential issues.

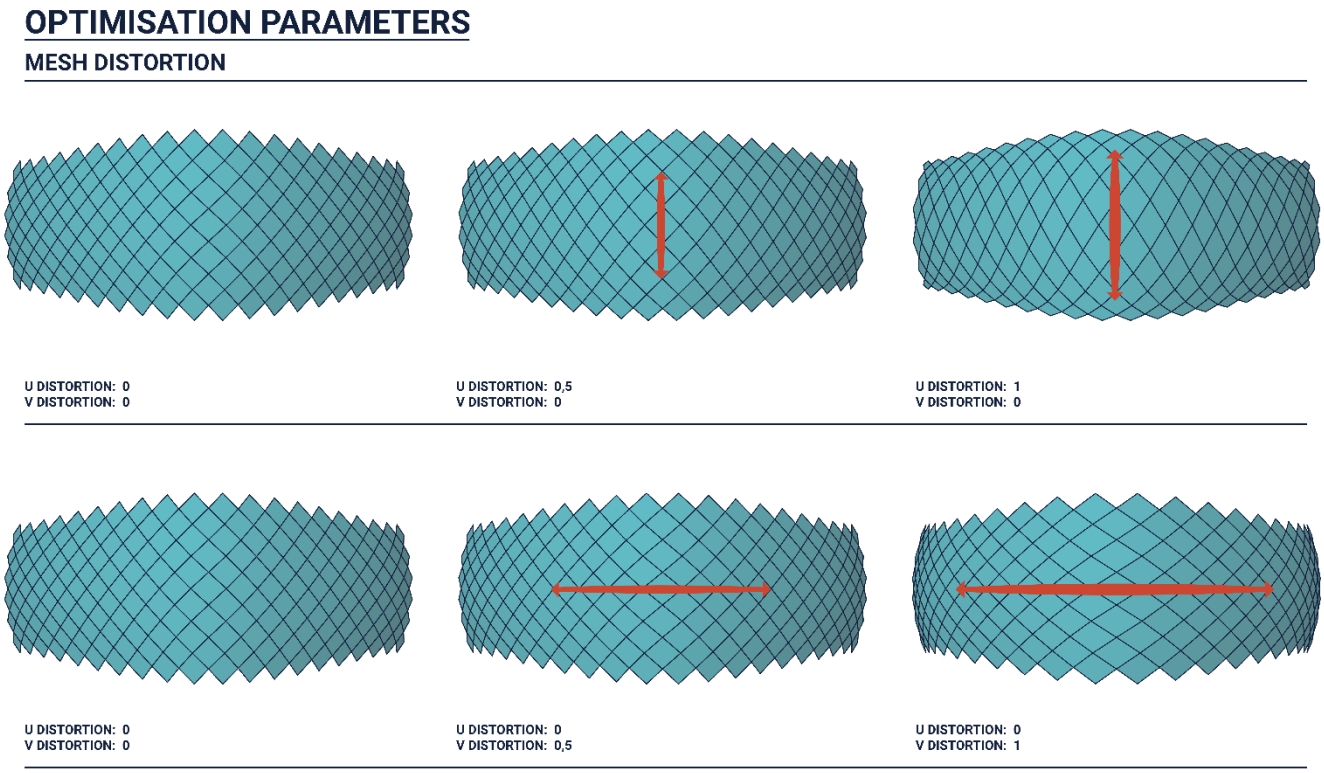

Figure 66: *parameters mesh distortion*

results

The optimum configuration, exhibiting the lowest maximum displacement, achieved a displacement of 0.334 cm. This represents a 5% improvement compared to the original configuration (U distortion = 0; V distortion = 0), making its performance comparable to the best-performing configuration identified in the curvature fitness landscape of the case study.

It is clearly visible that a high V-distortion leads to excessive mesh deformation, resulting in a more closed configuration and larger displacements (see Figure 67).

As previously mentioned, it is suspected that configurations with greater curvature could benefit more significantly from optimised mesh distortion. Further investigation of this hypothesis would be of interest.

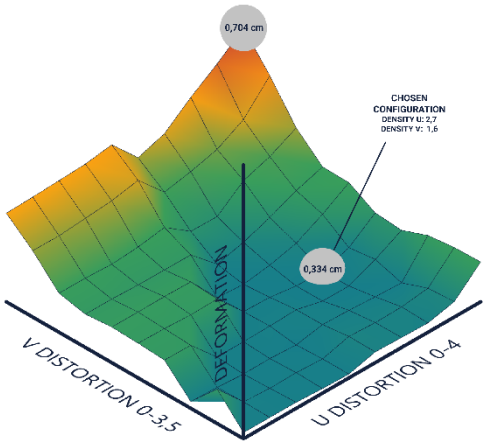

Figure 67: *fitness landscape mesh distortion*

The best-performing model, characterised by the lowest maximum displacement, will be further analysed using a more detailed structural model in the following section, *Structural Analysis*.

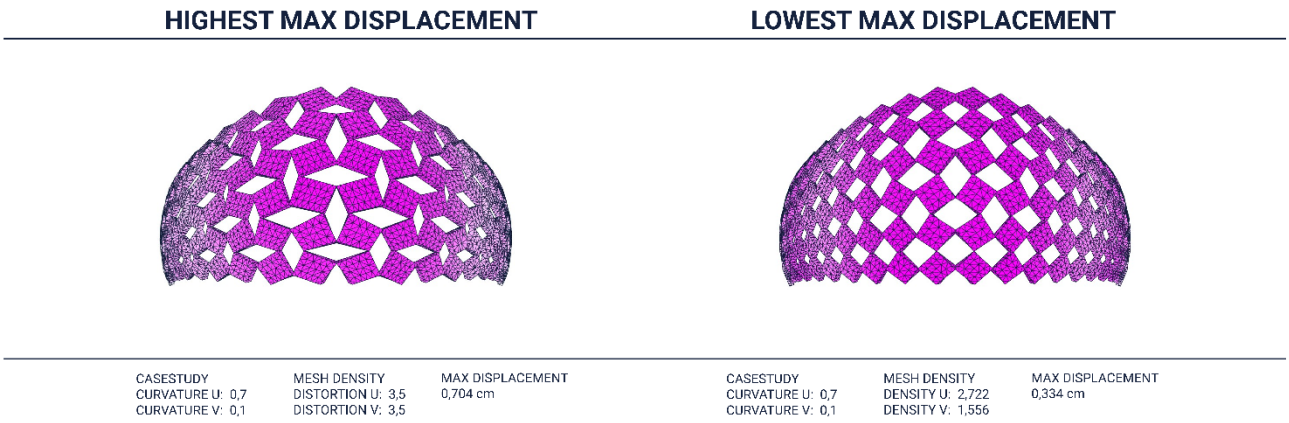

Figure 68: *configurations with the highest and lowest performance*

7.2 Structural Analysis

With the final geometry for the case study established, additional detail can now be added to the model to enable more advanced analyses. These analyses aim to assess how the added details affect the deployment, how much the structure deviates from the target shape, and whether it can withstand operational loads. They also help determine appropriate element and hinge thicknesses, as well as evaluate which material options meet the performance requirements.

Two types of Karamba analyses will be conducted:

- **Large Displacement Analysis** will be used to simulate the deployment process, analysing the transition from the flat, undeployed state to the fully deployed configuration.
- **Static Analysis** will be conducted on the deployed model under various load cases to evaluate whether the structure maintains stability and structural integrity under operational conditions.

Surface Model

The surface model serves as the input for the structural analysis. It is derived from the panels produced during the form-finding process, which are scaled to create space for the compliant hinges. These scaled panels are then lofted to form the shell of the rigid elements. Several key dimensions define the structural analysis:

- the average size of the elements
- the length of the compliant hinges
- the thickness of the rigid elements
- the thickness of the compliant hinges.

In Figure 69, the values used for the following analysis are shown.

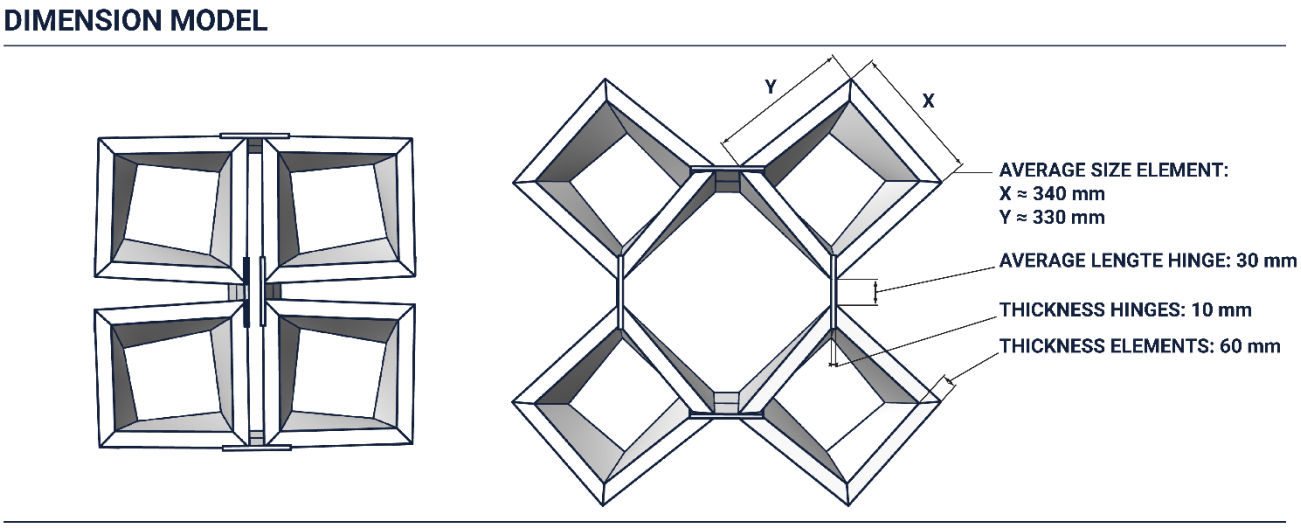

Figure 69: *Dimension of elements in the model*

7.2.1 Large Displacement Analysis

Large-deformation (geometrically nonlinear) analysis continuously updates the structure's stiffness matrix as it deforms, enforcing equilibrium on the changing geometry rather than on the initial shape. This allows the simulation to capture large member rotations, evolving load paths, and changes in stiffness that occur during motion.

These effects are critical for simulating deployment, as they reveal whether forces shift between elements as the form changes shape. In this analysis, the surface model is first meshed. Supports are defined as shown in Figure 70: one corner is fully fixed, one is fixed in two directions, and the remaining two corners are fixed only in the Z-direction. This setup allows those points to move within the plane during deployment.

The structure is deployed by tensioning cables (Figure 70, in red). Pretension in each cable is based on the following strain formula:

$$Strain\ (\varepsilon 0)\ = \frac{(cable\ lengte\ dep. - cable\ lengte\ flat)}{cable\ lengte\ flat}$$

The self-weight of the structure is also included in the analysis.

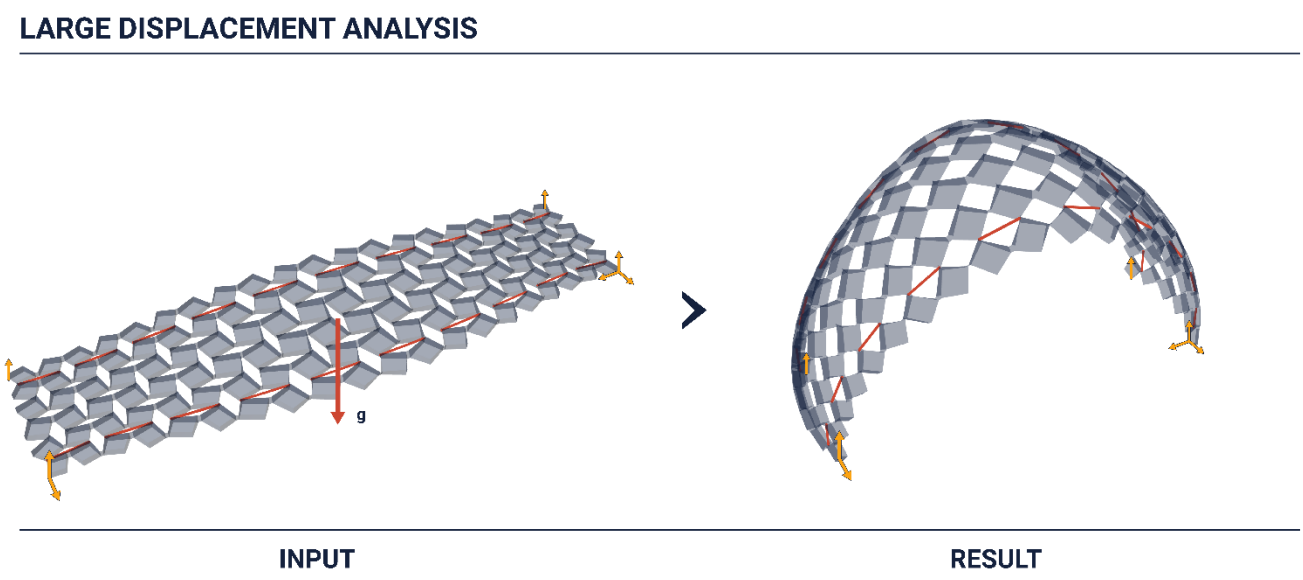

Figure 70: *results large displacement analysis considering deformations in the material during deployment*

To evaluate how closely the deformed model approximates the target shape, a contour plot is generated that measures the distance between the top panels of the deformed geometry (which serve as the loading surface) and the original input surface (see Figure 71).

This evaluation is performed for three different tension systems: one with 20 tension points, one with 10, and one with 5. The purpose is to assess how the number of tension points influences the accuracy of the deployed shape and to determine the minimum number of tension points required for effective deployment. Fewer tension points are preferred, as they simplify the assembly process.

The results show that all configurations exhibit regions of significant deviation from the target shape. However, the systems with 20 and 10 tension points still clearly approximate the desired geometry. In both cases, the largest deviations occur on the sides of the structure. For the model with 10 tension points, maximum deviations around 7.5 cm are observed, whereas the 20-point configuration exhibits deviations up to 10 cm in certain areas (see Figure 71).

The configuration with only 5 tension points did not fully deploy and is excluded from further analysis. Whether the system ultimately requires 10 or 20 tension points depends on the results of the structural analysis presented in the following chapter, particularly regarding the need for a secondary structure to support the lateral edges.

It is important to note that the large-deformation analysis only provides information about the final geometry. Any internal stresses induced during deployment are not included in this evaluation.

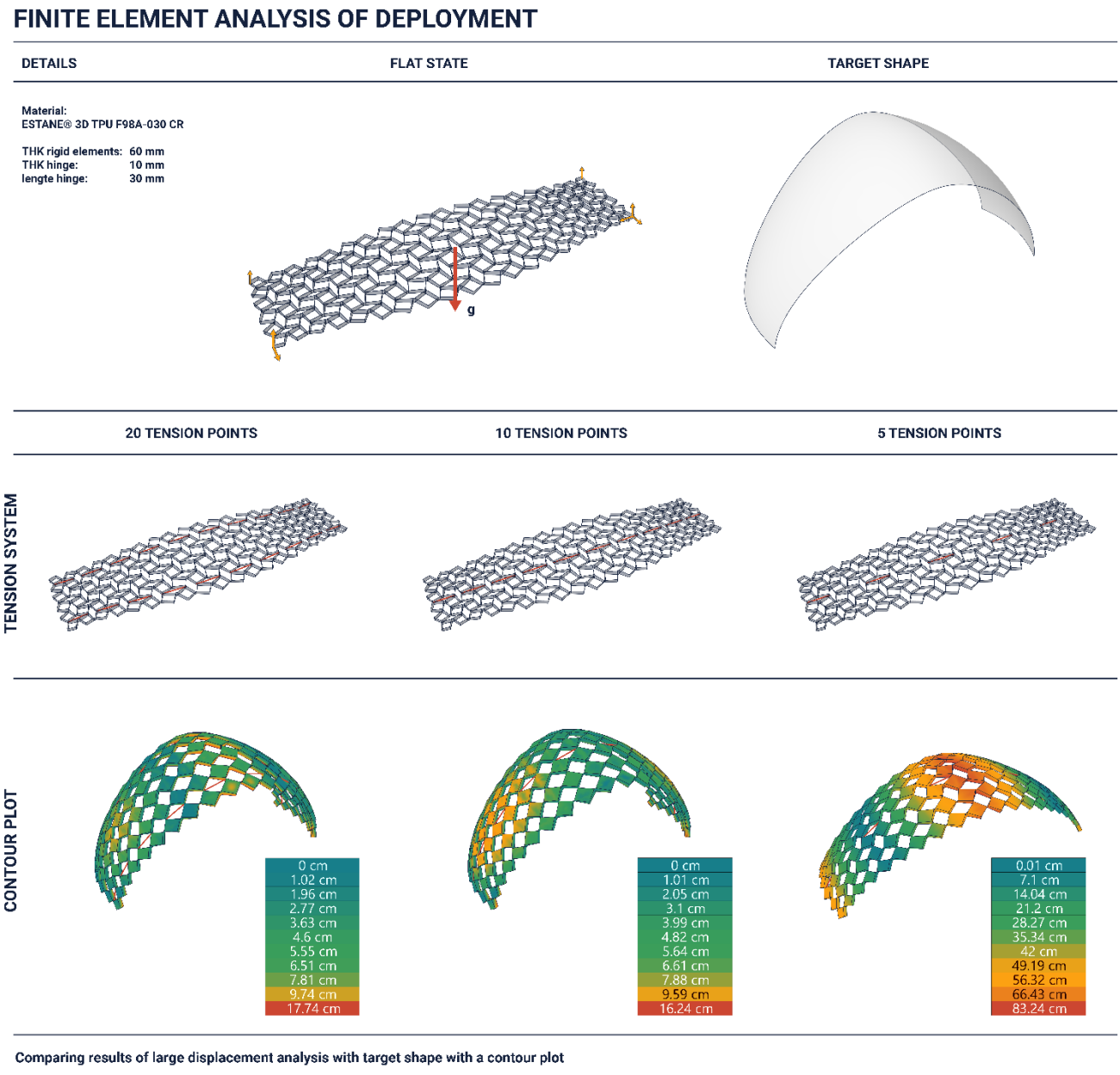

Figure 71: *Finite element analysis of deployment*

7.2.2 Static Analysis

The standard Analyse component in Karamba performs a linear-static check. It calculates displacements and internal forces under the assumption that the structure remains elastic. Since it evaluates the structure based on the original, undeformed geometry and does not account for geometric or material nonlinearities, the method is computationally efficient and reliable, provided that deformations remain small.

Boundary conditions

Initially, the structure was tested with supports only at the ground level, to investigate whether it could stand independently. However, this setup resulted in significant deformations under 90° wind loads, even when using stiffer materials such as TPC 70D or TPU reinforced with 20% glass fiber. These materials would also increase the force required for deployment. For this reason, the final configuration includes fixed supports along the entire boundary, as shown in Figure 72. This solution implies the need for an additional beam element on either side of the structure to accommodate the boundary fixation.

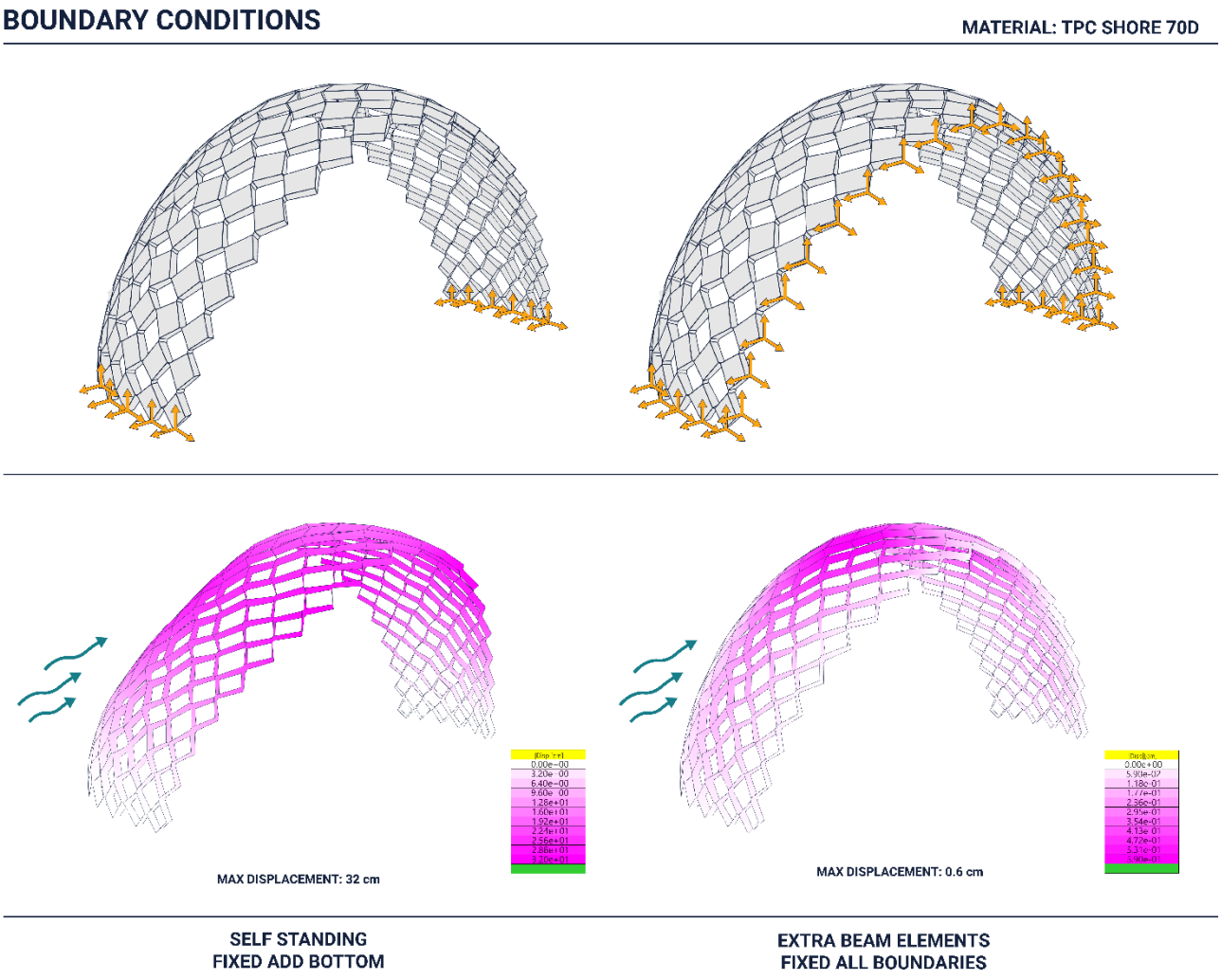

Figure 72: *Boundary conditions Finite element analysis Load cases*

Loads

For the applied wind load a simplified approach is used. A canopy with an arch shape and a free airflow is not well described in the Eurocodes (NEN, 2005). For this case study the Wind is simplified as acting on a two-sided sloping canopy with an inclination angle 30 degrees and free airflow. This results in differential pressure: a pushing force on the windward side and a suction (pulling) force on the leeward side.

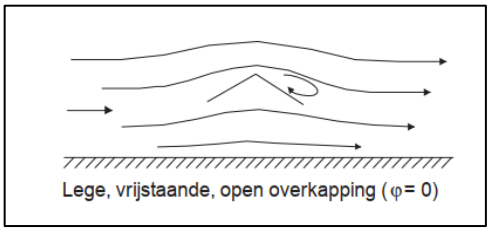

Figure 73: *two-sided slop with free airflow (NEN, 2005).*

The wind load value is based on the national annex to the Eurocode, specifically for Region II (*Gebied II*), which corresponds to unbuilt terrain and covers most of the Netherlands. According to this classification, a wind load of 0.6 kN/m^2 was used (see Table 1) (NEN, 2005).

Both the Ultimate Limit State (ULS) and Serviceability Limit State (SLS) calculations were performed assuming a Consequence Class CC1, as defined in the same standard (see table 2) (NEN, 2005).

Tabel NB.5 — Extreme stuwdruk in kN/m² als functie van de hoogte

Hoogte	Gebied I			Gebied II			Gebied III	
m	Kust	Onbebouwd	Bebouwd	Kust	Onbebouwd	Bebouwd	Onbebouwd	Bebouwd
1	0,93	0,71	0,69	0,78	0,60	0,58	0,49	0,48
2	1,11	0,71	0,69	0,93	0,60	0,58	0,49	0,48
3	1,22	0,71	0,69	1,02	0,60	0,58	0,49	0,48
4	1,30	0,71	0,69	1,09	0,60	0,58	0,49	0,48
5	1,37	0,78	0,69	1,14	0,66	0,58	0,54	0,48
6	1,42	0,84	0,69	1,19	0,71	0,58	0,58	0,48
7	1,47	0,89	0,69	1,23	0,75	0,58	0,62	0,48
8	1,51	0,94	0,73	1,26	0,79	0,62	0,65	0,51
9	1,55	0,98	0,77	1,29	0,82	0,65	0,68	0,53
10	1,58	1,02	0,81	1,32	0,85	0,68	0,70	0,56
15	1,71	1,16	0,96	1,43	0,98	0,80	0,80	0,66
20	1,80	1,27	1,07	1,51	1,07	0,90	0,88	0,74

Table 1: *Table wind loads (NEN, 2005).*

Combinations: assuming a consequence class CC1

Ultimate limit state:					
ULS 1	1,22	Self weight			
ULS 2	1,08	Self weight	+	1,35	Wind 0°
ULS 3	1,08	Self weight	+	1,35	Wind 90°
Serviceability limit state:					
SLS 1	1,0	Self weight			
SLS 2	1,0	Self weight	+	1,0	Wind 0°
SLS 3	1,0	Self weight	+	1,0	Wind 90°

Table 2: *Table Ultimate limit state and Serviceability limit state*

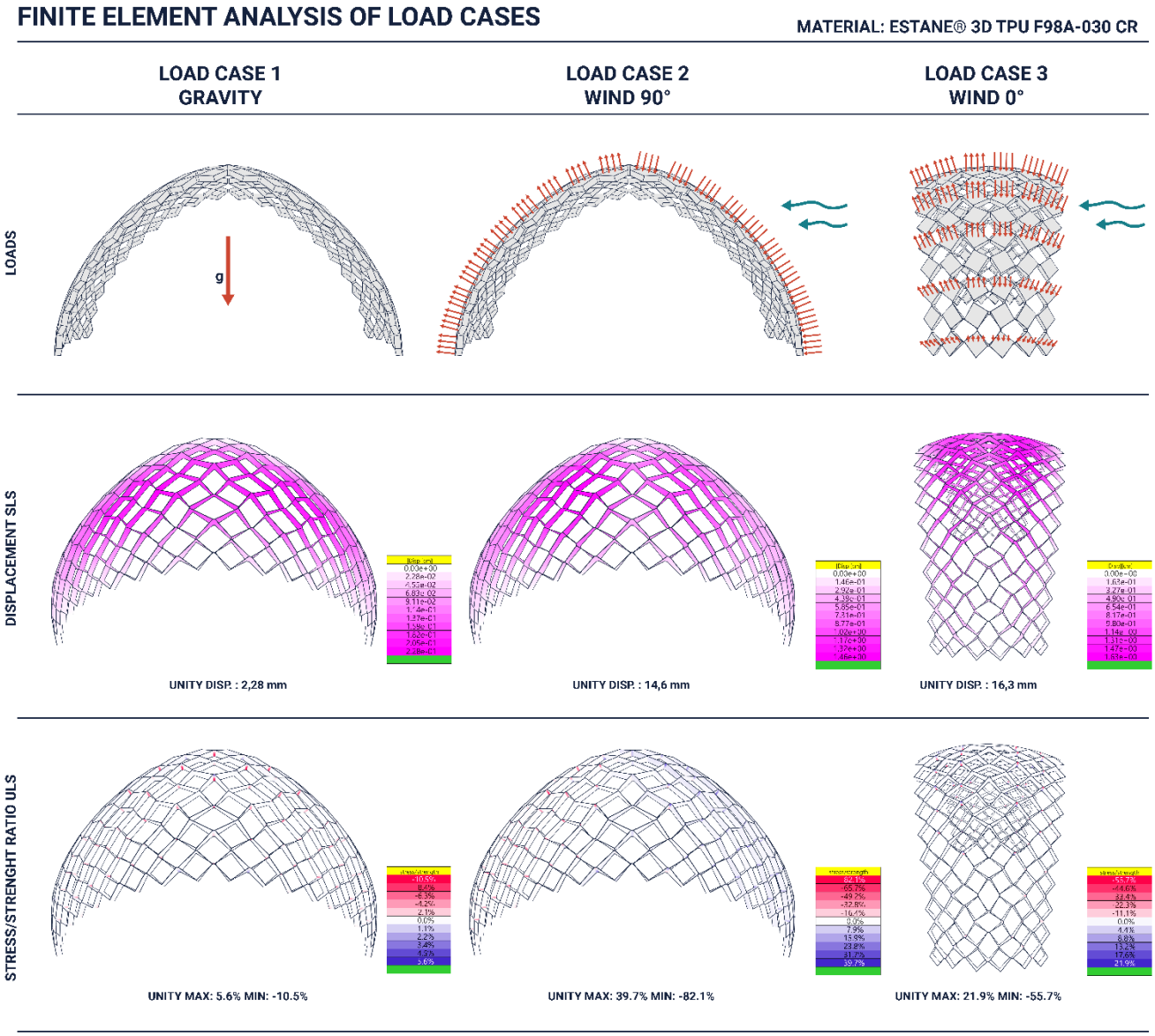

Figure 74: *Results finite element analysis load cases*

7.2.3 Results

The large-deformation analysis behaves as expected, with acceptable dimensions. While some areas show significant deviation from the target surface, the structure overall clearly resembles the desired shape.

With the structure supported at all boundary points, acceptable stress levels and deformations are achieved in all load cases when using the material suggested by BouwLab: ESTANE® 3D TPU F98A-030 CR HC PL. The maximum unity check is found for ULS of load case 2 and is equal to -82,1%. The maximum displacement is found for SLS of load case 3 and is equal to 1,63 cm.

However, this is in many respects a simplified analysis. The following important limitations should be noted:

- Any stresses in the material resulting from the deployment process are not taken into account.
- No material safety factors have been applied, as these do not yet exist for the selected material.
- The material is assumed to be isotropic, while 3D printed parts typically exhibit anisotropic behaviour.
- Creep in the material is not considered.
- Environmental factors such as heat and UV resistance are not included in the analysis.

In general, the compliant hinges require further detailed study. Their behaviour under compressive loads, their ability to prevent buckling, and risks such as delamination of print layers are all critical aspects that need to be addressed in future work.

7.3 Details

This chapter outlines the technical details developed for the case study. Based on the structural analysis, the structure requires a secondary stabilizing system in the form of an arched boundary beam. Anchoring is also necessary to ensure stability under wind loads. The structure must connect to these elements and incorporate tension points for the deployment process. The overall assembly and disassembly should be quick and straightforward.

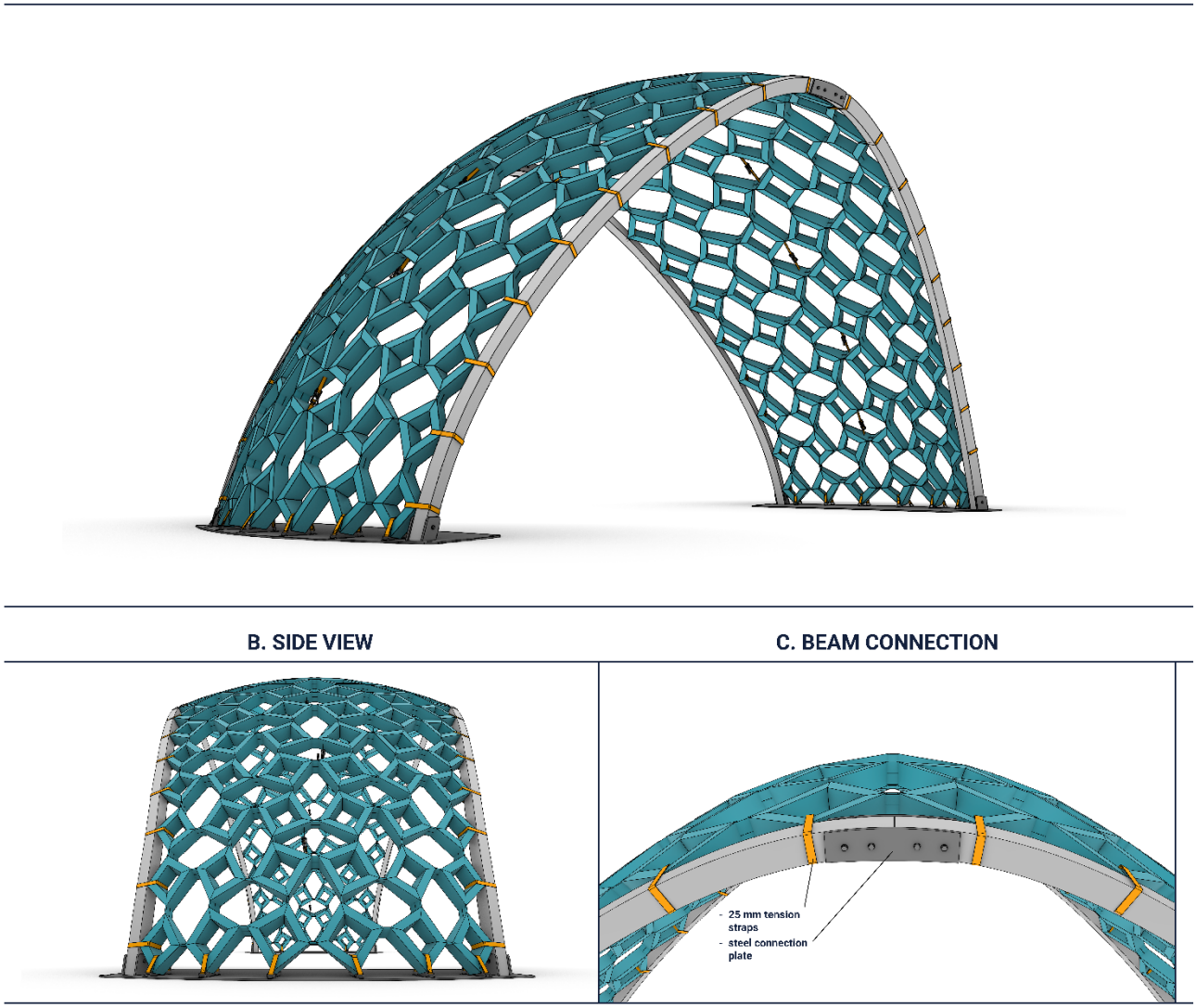

Figure 75: *Case study design/detials*

Boundary Beam

To provide lateral stiffness under wind loads (see Section 7.2.2), two steel profile beams are positioned along the edges of the structure. Each beam is divided into two segments to facilitate transport (see figure 75C). Once the structure is deployed, the beams can be installed adjacent to it.

Base Plate

To connect both the boundary beams and the structure to the ground, two custom base plates were designed (see figure 76F). These plates include fittings for the beams and integrated anchor points for the tension straps. The plates can be secured either by weighting them with concrete blocks or water reservoirs, or by bolting them directly to the ground. Each corner of the base plate includes a hole to allow for flexible anchoring options.

Connections

Given the structure's flexibility, connection details must accommodate deformation. Tension straps are used at each corner to fix the structure (see figure 76F). This method requires no tools and remains effective even if the structure has not fully reached its intended deployed shape. By tension these straps one by one the structure will get closer to its desired geometry.

Tension Points

As introduced in Section 6.1, deployment is achieved using ratcheting tension straps (see figure 76E). This system enables relatively higher pre-tension forces through manual operation and offer a low-cost, practical solution. A total of ten tension points is distributed around the structure, as analysed in the large displacement simulation (see Section 7.2.1).

To function as a shelter, a cover is still required. A lightweight solution is a tensile membrane, which can be attached around the edges and tensioned over the structure.

D. TOP VIEW

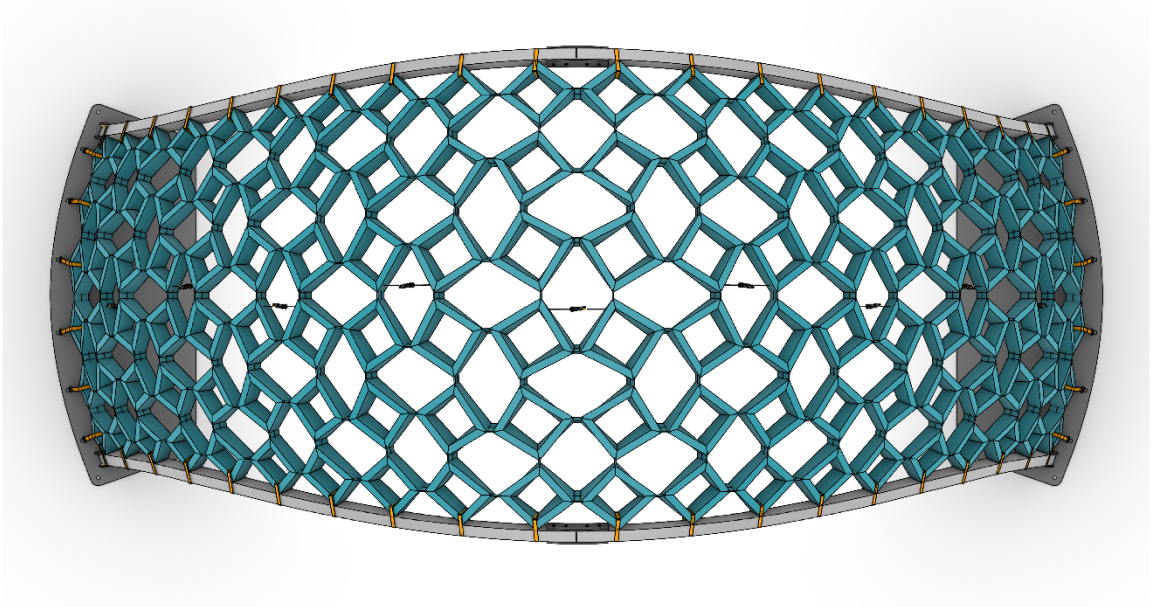

E. TENSION POINT

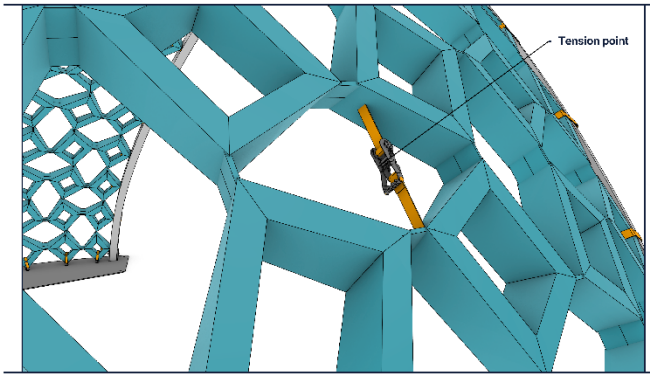

F. BASE PLATE

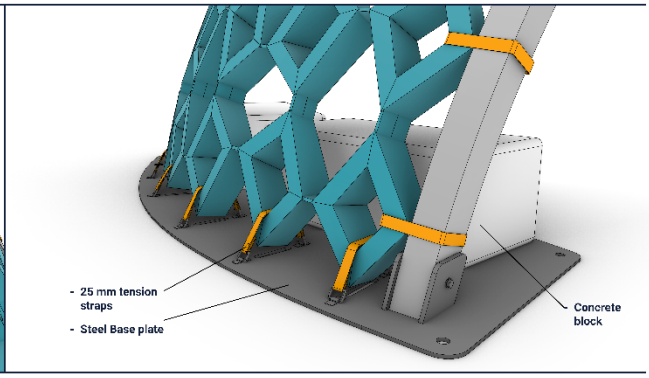

G. 1:2 DETAIL TENSION

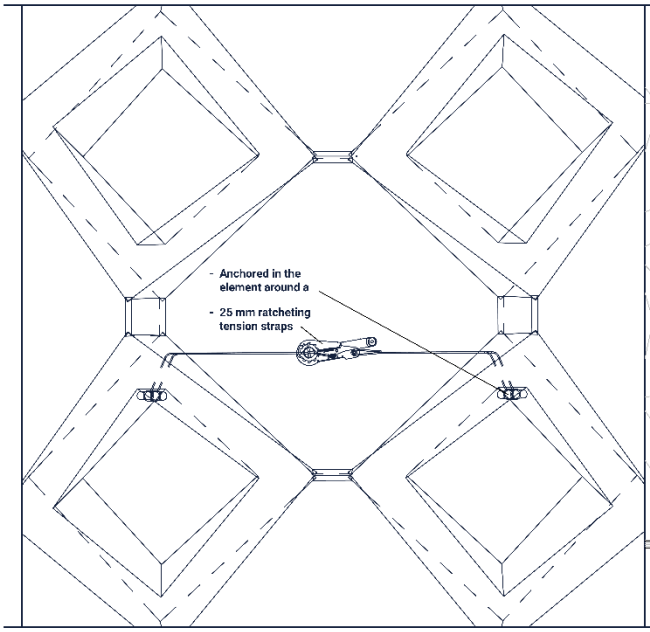

H. 1:2 DETAIL BASE

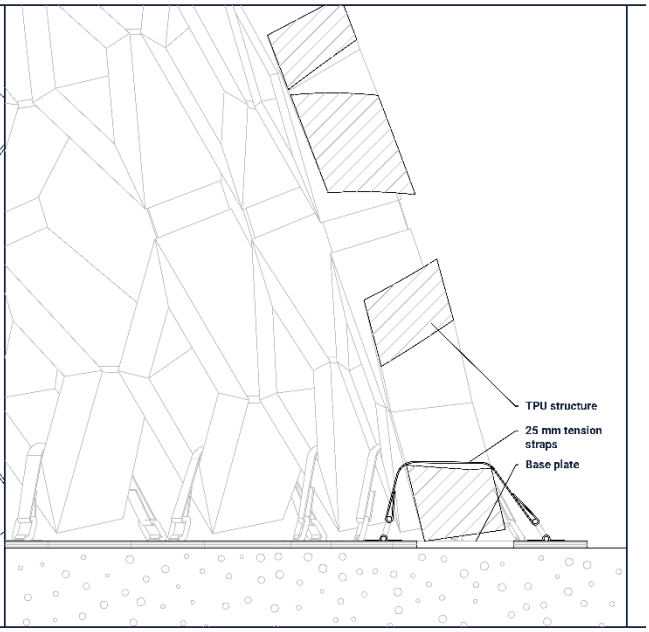

Figure 76: *Case study design/details part 2*

7.4 Panelling

To produce larger structures, such as the case study model, the geometry must be segmented into parts that fit within the build volume of the 3D printer. This is demonstrated using a 1:10 scale model.

The 1:10 scale model is fabricated using the Ender 3v3 Plus 3D printer, which has a bed size of 300 × 300 mm.

To reduce the surface area in the flat configuration, the form-finding parameters were slightly adjusted. This was achieved by reducing the length of the diagonals within the kinematic constraints (as described in chapter 4.5.3), effectively drawing the structure into a more compact configuration (see Figure 77). It should be noted that this adjustment may negatively affect the deployed configuration's structural performance, as the geometry in the deployed state is also altered.

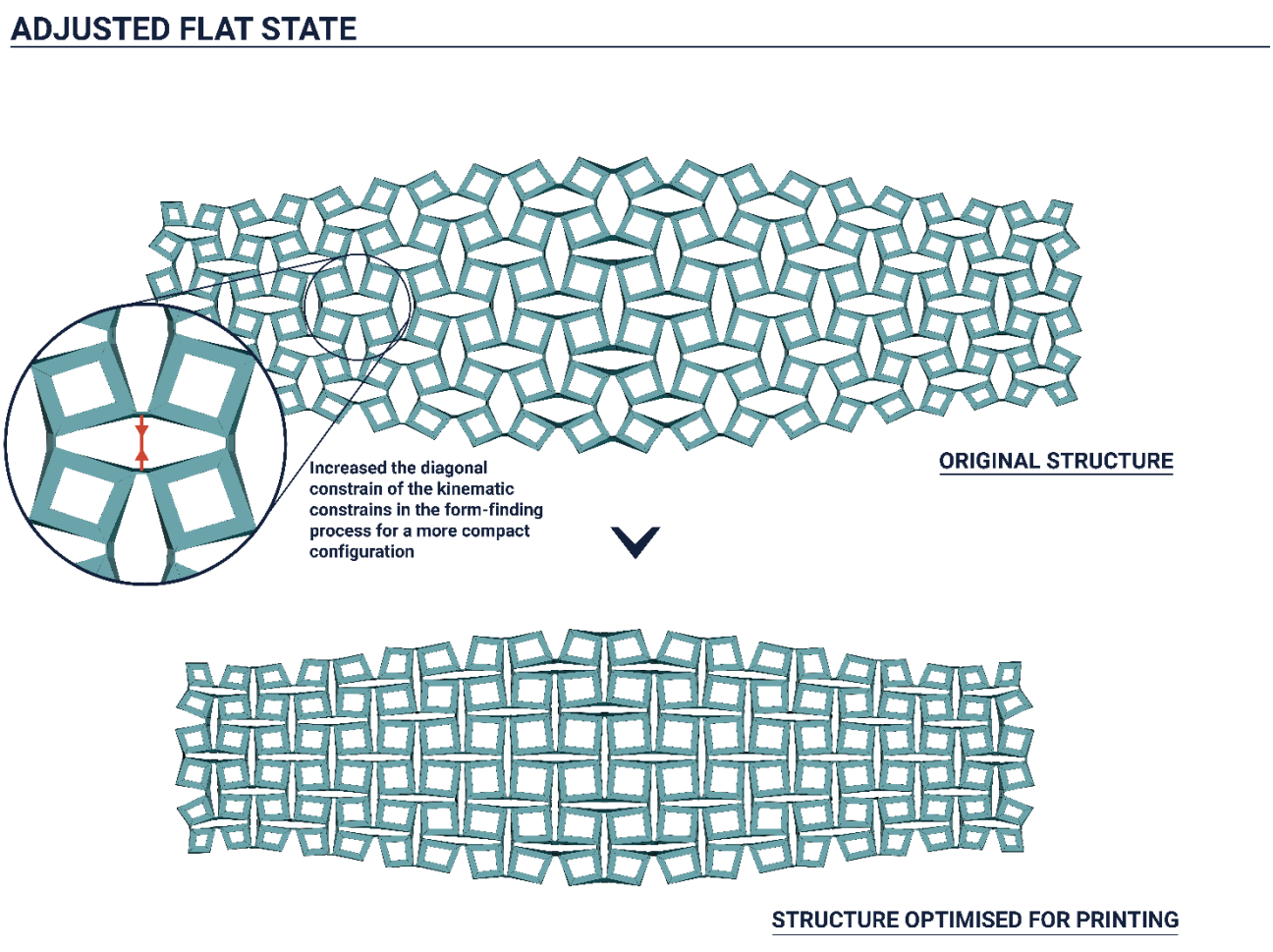

Figure 77: *Adjustment of the structure for more compact print panels*

As a result of this reduction in flat area, the structure was successfully divided into three segments, each fitting within the 300 × 300 mm bed (see Figure 78). Each segment includes an overlapping row to allow a physical connection with the next segment.

PANELIZATION 1:10 MODEL

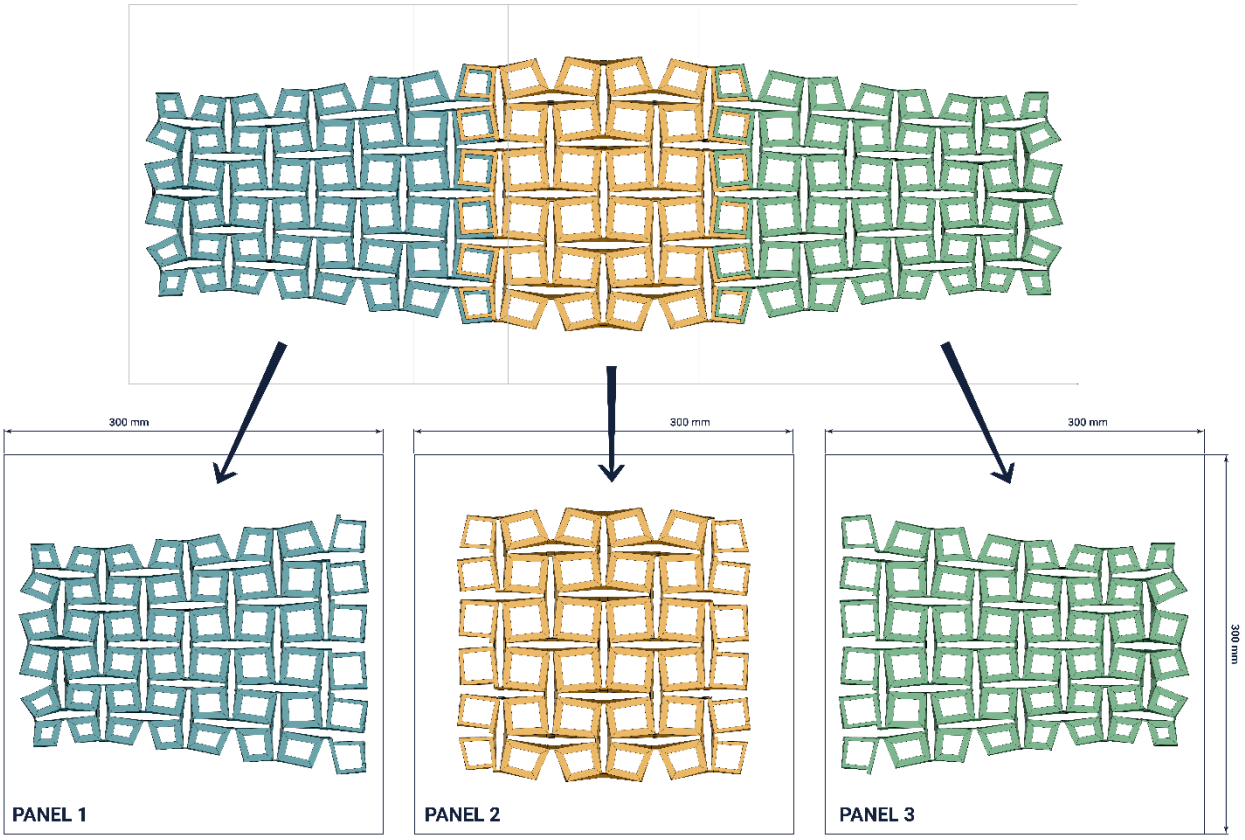

Figure 78: *Dividing the structure in 3 printable panels*

To connect the segments, a connection element was designed. This element consists of two parts and enables each component to connect with two adjacent elements within the same segment. The connection geometry is integrated into the overlapping panels of each segment (see Figure 79). For the real-life application these connections should be secured with bolts.

CONNECTION ELEMENT

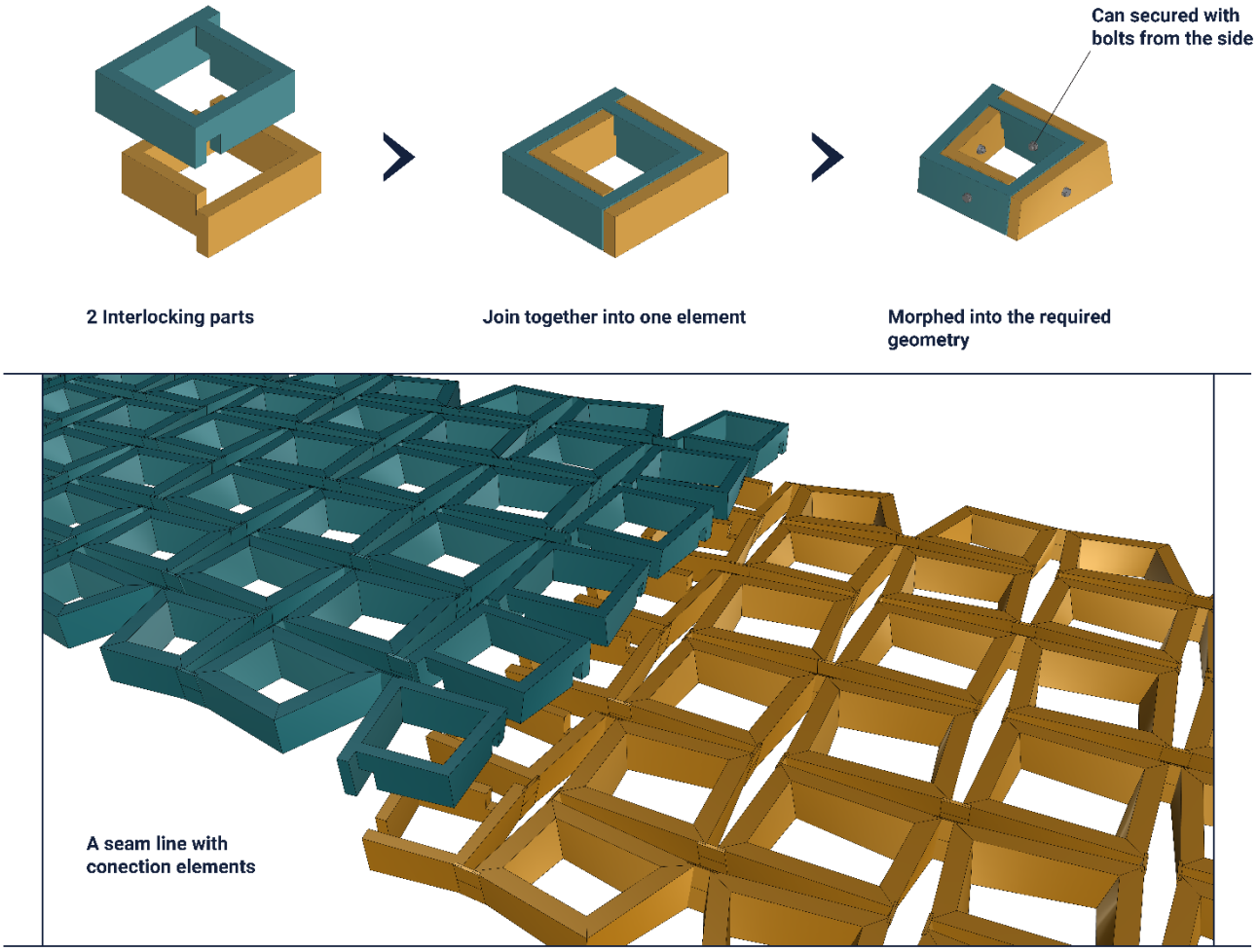

Figure 79: *Connection element*

7.5 Prototype 1:10

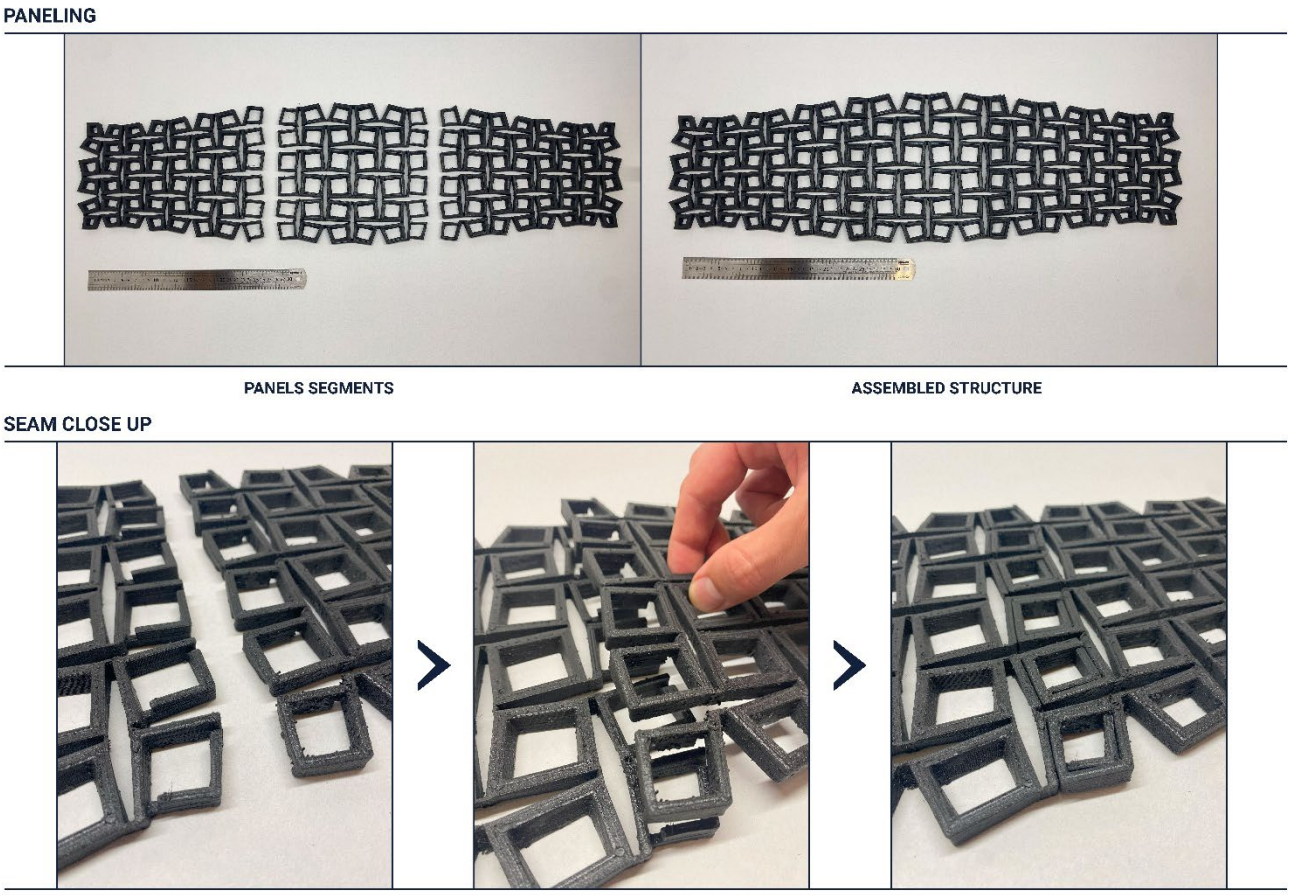

Figure 80: *Panelling 1:10 model*

8 CONCLUSION

The primary aim of this research was to investigate how principles of mechanical metamaterials can be scaled up to design deployable shelters. Through an integrated computational and experimental approach, this research successfully addressed the main research question: "*How can the principles of mechanical metamaterials be scaled up to design deployable shelters?"*

The literature review highlighted the significant potential of mechanical and programmable metamaterials to enable adaptive, deployable structures. However, it also revealed a critical limitation: the lack of predictive modelling tools for such materials. The developed computational method in this project effectively tackled this "inverse design problem," as defined by Panetta et al. (2021), by using dynamic relaxation and form-finding techniques. This method allowed simultaneous optimization of flat and deployed configurations, ensuring accurate predictions of structural transformations and significantly reducing trial-and-error approaches.

In this research, an attempt was made to tackle the inverse design problem as defined by Panetta et al. (2021) by developing a computational method that uses dynamic relaxation. This approach enabled the simultaneous optimization of both flat and deployed configurations, leading to accurate predictions of structural transformations and reducing reliance on trial-and-error methods.

In practice, the developed computational tool improved the efficiency and ease of the design and production processes. Large displacement analyses confirmed that the structures closely approximated the desired target shapes, accounting for material deformation. Nonetheless, the deployment method itself requires further refinement. While the cable-based deployment system proposed in this research was low-cost and reliable for the scale studied, practical considerations such as friction and tensioning forces suggest room for improvement, especially for larger or more complex structures.

Scaling the developed concept of a programmable mechanical metamaterial introduced several challenges. The full-scale (1:1) prototype demonstrated the feasibility of manufacturing compliant hinges at a structural scale using large-format additive manufacturing (LFAM) but also highlighted the critical role of these components. The performance and accuracy of the hinges significantly affect the overall functionality of the deployed structure. Achieving an optimal balance between global structural stiffness and local hinge flexibility proved to be a major challenge. Self-weight remained a limiting factor, prompting the exploration of alternative hinge designs—such as dual-material and reinforced hinges—to reduce weight and enhance performance.

The computational tool was successfully applied to design a functional deployable shelter for events. Structural analyses revealed that while the structure was generally stable and safe under operational loads, significant stress concentrations and deviations were observed during deployment. Several important limitations were noted, such as the lack of consideration for deployment-induced stresses, anisotropic material behaviour of 3D-printed parts, and environmental factors like UV and heat resistance. Further detailed investigation is required, particularly regarding the behaviour of compliant hinges under compressive loads, potential buckling, and delamination risks.

In conclusion, the principles of mechanical metamaterials can indeed be scaled up to create large, safe, and stable deployable shelters. The developed computational tool provides a significant advancement in predictive modelling, enabling efficient design and optimization of adaptive structures. While considerable progress has been made, particularly in design

methodology and manufacturing feasibility, further research into deployment methods, structural optimization, and hinge design is essential to fully realize the potential of deployable metamaterial-based structures at an architectural scale.

9 REFLECTION

Graduation Process

This graduation project is positioned between the Structural Design and Design Informatics studios.

In Design Informatics, the main challenge lies in addressing the inverse design problem, where the goal is to determine a structural configuration that can approximate a given target shape when deployed. This involves applying computational form-finding and optimization techniques.

In Structural Design, the focus is on scaling deployable structures while achieving a balance between flexibility and stiffness. Particular attention is given to material behavior, structural stability, and manufacturability at larger scales.

Both disciplines contribute to the project: computational methods support the generation of deployable systems, while structural considerations ensure their feasibility and performance. The two approaches come together during the structural analysis and optimization phases.

The research approach evolved slightly during the course of the project, although the overall structure remained solid. The main steps were identifying a kinematic system to base the design on, developing a computational tool, optimizing the structure, and applying the method to a case study followed by structural analysis.

The development strategy for the computational tool changed during the project, as discussed in Chapter "Approach." Initially, the plan was to precompute a range of element configurations, analyze their behavior, and apply them piece by piece to the geometry. This method was later replaced by a more integrated, global form-finding approach using dynamic relaxation. This shift proved to be an important improvement, resulting in a more coherent and adaptable method, and can be considered a key breakthrough in the project. Overall, the research approach led to the intended results by producing a working design tool, validating its application on different geometries, and demonstrating its potential through a case study.

The graduation studios of Structural Design and Design Informatics emphasize research-driven, computational approaches combined with structural analysis. This project closely follows that line by developing a parametric design tool, employing dynamic relaxation for form-finding, and validating results through both simulation and prototyping. Minor deviations were made by simplifying the structural analysis during early optimization phases to maintain computational feasibility, resulting in a less extensive optimization process than initially intended.

However, there is an aspect explored in this research that is less commonly addressed within the studio or master program: the design of mechanical or dynamic systems that are intended to change shape and shift between different configurations. This focus on designing structures with multiple stable states is particularly relevant for developing more adaptive, responsive, and potentially more sustainable designs. It highlights the possibilities of integrating dynamic performance into architectural and structural applications.

This project builds on research on mechanical metamaterials from fields such as biomedical engineering (Zadpoor, 2016), where these structures are typically applied at much smaller scales. The goal was to adapt and implement some of these techniques at a structural scale by developing a computational design tool.

Prototyping played a critical role in connecting research and design. Because the project involved dynamic, shape-changing structures, physical behavior could not always be fully predicted through simulation alone. Therefore, rapid prototyping with TPU and compliant hinges

was integrated from the beginning. This allowed for quick validation of design hypotheses and supported an iterative research-through-design approach, where insights gained from physical tests directly informed further development.

No major moral or ethical issues were encountered during the project. One aspect that could be questioned is the choice to create a structure entirely out of plastic, rather than using a more sustainable material. However, the focus of the research was on developing a method to design dynamic, shape-changing structures, not on material selection. The material choice was based on the need for very specific mechanical properties, which are currently only achievable with materials like TPU and TPC. There is, however, ongoing research into more sustainable printable materials, such as PHA, which BouwLab is experimenting with (BouwLab, n.d.), and 3D printing with lignin (Ersoy, 2025), which could potentially offer more sustainable alternatives in the future.

Societal Impact

This project explores a new approach to designing and manufacturing deployable structures, emphasizing the reduction of components, simplified assembly processes, and the potential for automated design and fabrication. These results could be applicable in practice, particularly in contexts where lightweight, adaptable, and quickly deployable structures are required, such as temporary shelters, event spaces, or emergency infrastructure.

The project contributes to sustainable development by promoting more adaptive and responsive design strategies. Structures that can efficiently change shape and function have the potential to reduce material use, extend the usable life of constructions, and enable more flexible responses to changing needs.

In terms of sustainability (people, planet, profit/prosperity), the project supports material efficiency and reduced assembly times, which could lower environmental impacts and production costs. However, the current reliance on plastic materials highlights the need for further research into sustainable alternatives.

The socio-cultural and ethical impact of the project lies in its potential to democratize access to customizable, rapidly deployable architecture. It offers new possibilities for creating spaces that adapt to users' needs, supporting more inclusive and dynamic environments.

In relation to the wider social context, the project aligns with ongoing trends in automation, digital fabrication, and material innovation within architecture and construction. It encourages a shift toward more flexible and efficient building practices.

Overall, the project introduces new ideas for how adaptive systems can influence the future of architecture and the built environment, particularly in areas where mobility, adaptability, and resource efficiency are critical.

10 REFERENCES

1. Aldawood, F. K. (2023). A comprehensive review of 4D printing: State of the arts, opportunities, and challenges. *Actuators, 12*(3), 101. https://doi.org/10.3390/act12030101

2. Ansys. (2024). *Granta EduPack Polymer Level 3 database* [Computer software]. Ansys, Inc.

3. BASF. (2018). *Elastollan® – Physical properties: Thermoplastic polyurethane (TPU)* [PDF]. https://www.basf.com/dam/jcr%3A19c11827-1bc0-3b0f-a3f4-4fc2b986d54f/Elastollan_Properties-Physical-Properties.pdf

4. BASF Polyurethanes GmbH. (n.d.). *Elastollan® C 78 A* [Data sheet]. CAMPUS Plastics. https://www.campusplastics.com/campus/en/datasheet/Elastollan%C2%AE+C+78+A/BASF+Polyurethanes+GmbH/59/c80240a9

5. BASF Polyurethanes GmbH. (n.d.). *Elastollan® C 88 A* [Data sheet]. CAMPUS Plastics. https://www.campusplastics.com/campus/en/datasheet/Elastollan%C2%AE+C+88+A/BASF+Polyurethanes+GmbH/59/e77d2e9c

6. BouwLab Haarlem. (n.d.). *Home*. Retrieved May 12, 2025, from https://bouwlab.com/

7. Campbell, T. A., Tibbits, S., & Garrett, B. (2014). *The next wave: 4D printing* (pp. 1–16). Atlantic.

8. Caracol S.r.l. (2023). *TPE00VEPv1 Natural.std – ENSOFT SO-161-70A* [Material datasheet]. https://caracol-am.com

9. CEAD Group. (n.d.). *Large scale 3D printing solutions*. Retrieved May 12, 2025, from https://www.ceadgroup.com/

10. CEAD Group. (2025). *Guidebook for LFAM design* [Internal company document].

11. Chen, T., Panetta, J., Schnaubelt, M., & Pauly, M. (2021). Bistable auxetic surface structures. *ACM Transactions on Graphics, 40*(4), 1–9. https://doi.org/10.1145/3450626.3459940

12. Connex. (n.d.). *Automatic tension strap with protection* (Model DY270623). Amazon.nl. https://www.amazon.nl/dp/B019ETZWAU

13. Demoly, F., Dunn, M. L., Wood, K. L., Qi, H. J., & André, J. (2021). The status, barriers, challenges, and future in design for 4D printing. *Materials & Design, 212*, 110193. https://doi.org/10.1016/j.matdes.2021.110193

14. Dudte, L. H., Choi, G. P. T., Becker, K. P., & Mahadevan, L. (2023). An additive framework for kirigami design. Nature Computational Science, 3(5), 443–454. https://doi.org/10.1038/s43588-023-00448-9

15. Ersoy, C. (2025). *SYLVA: Advancing bio composite materials through robotic additive manufacturing* [Master's thesis, TU Delft].

16. Fenci, G. E., & Currie, N. G. (2017). Deployable structures classification: A review. *International Journal of Space Structures, 32*(2), 112–130. https://doi.org/10.1177/0266351117711290

17. Guseinov, R., Miguel, E., & Bickel, B. (2017). CurveUps. *ACM Transactions on Graphics, 36*(4), 1–12. https://doi.org/10.1145/3072959.3073709

18. Ion, A., Lindlbauer, D., Herholz, P., Alexa, M., & Baudisch, P. (2019). Understanding metamaterial mechanisms. In *Proceedings of CHI 2019* (pp. 1–14). ACM. https://doi.org/10.1145/3290605.3300877

19. Jiang, C., Rist, F., Pottmann, H., & Wallner, J. (2020). Freeform quad-based kirigami. *ACM Transactions on Graphics, 39*(6), 1–11. https://doi.org/10.1145/3414685.3417844

20. Kadic, M., Milton, G. W., Van Hecke, M., & Wegener, M. (2019). 3D metamaterials. *Nature Reviews Physics, 1*(3), 198–210. https://doi.org/10.1038/s42254-018-0018-y

21. Karamba3D. (n.d.). *Karamba3D – Parametric Engineering Tool*. Retrieved May 17, 2025, from https://www.karamba3d.com/abc

22. Konaković, M., Crane, K., Deng, B., Bouaziz, S., Piker, D., & Pauly, M. (2016). Beyond developable. *ACM Transactions on Graphics, 35*(4), 1–11. https://doi.org/10.1145/2897824.2925944

23. Konaković-Luković, M., Panetta, J., Crane, K., & Pauly, M. (2018). Rapid deployment of curved surfaces via programmable auxetics. *ACM Transactions on Graphics, 37*(4), 1–13. https://doi.org/10.1145/3197517.3201373

24. Lubrizol Corporation. (2019, September 4). *ESTANE® 3D TPU F98A-030 CR HC PL: Technical data sheet* [PDF]. https://www.lubrizol.com/-/media/Lubrizol/Engineered-Polymers/Documents/Engineered-Polymer-TDS/ESTANE-3D-TPU-F98A-030-CR-HC-PL.pdf

25. Maestre, J. S. M., Du, Y., Hinchet, R., Coros, S., & Thomaszewski, B. (2023). Differentiable stripe patterns for inverse design of structured surfaces. *ACM Transactions on Graphics, 42*(4), 1–14. https://doi.org/10.1145/3592114

26. MatWeb, LLC. (n.d.-a). *Ultimaker TPU 95A filament* (Material data sheet). MatWeb – Online Materials Information Resource. Retrieved February 24, 2025, from https://www.matweb.com/search/datasheettext.aspx?matguid=14625939fcbc4d2da97f6d3ac9cbdb7e

27. MatWeb, LLC. (n.d.-b). *Huntsman Iroprint™ F 80213 TPU prototyping filament* (Material data sheet). MatWeb – Online Materials Information Resource. Retrieved February 24, 2025, from https://www.matweb.com/search/datasheettext.aspx?matguid=b56fdda019f1467cae8d4a11d5415791

28. MatWeb, LLC. (n.d.-c). *Overview of materials for thermoplastic polyurethane, elastomer, ether grade* (Property summary). MatWeb – Online Materials Information Resource. Retrieved February 24, 2025, from https://www.matweb.com/search/datasheettext.aspx?matguid=9f5318a1f93b403bbd5748abec70fac1

29. MatWeb, LLC. (n.d.-d). *Covestro Texin® 4210 thermoplastic polyurethane (TPU)* (Material data sheet). MatWeb – Online Materials Information Resource. Retrieved February 24, 2025, from https://www.matweb.com/search/datasheet.aspx?matguid=eb87e516a79f42a69419a5673a06d815

30. MIT's Self-Assembly Lab & Wood-Skin S.r.l. (n.d.). *Programmable Table — Self-Assembly Lab*. Retrieved from https://selfassemblylab.mit.edu/programmable-table

31. NEN. (2005). *NEN-EN 1991-1-4 nl: Eurocode 1: Actions on structures – Part 1-4: General actions – Wind actions* (Nederlandse norm). Nederlands Normalisatie-instituut.

32. Ou, J., Ma, Z., Peters, J., Dai, S., Vlavianos, N., & Ishii, H. (2018). KinetiX – designing auxetic-inspired deformable material structures. *Computers & Graphics, 75*, 72–81. https://doi.org/10.1016/j.cag.2018.06.003

33. Panetta, J., Isvoranu, F., Chen, T., Siéfert, E., Roman, B., & Pauly, M. (2021). Computational inverse design of surface-based inflatables. *ACM Transactions on Graphics, 40*(4), 1–14. https://doi.org/10.1145/3450626.3459789

34. Papadopoulou, A., Laucks, J., & Tibbits, S. (2017). From self-assembly to evolutionary structures. *Architectural Design, 87*(4), 28–37. https://doi.org/10.1002/ad.2192

35. Park, J. J., Won, P., & Ko, S. H. (2019). A review on hierarchical origami and kirigami structure for engineering applications. *International Journal of Precision Engineering and Manufacturing-Green Technology, 6*(1), 147–161. https://doi.org/10.1007/s40684-019-00027-2

36. Pellegrino, S. (2001). Deployable structures in engineering. In S. Pellegrino (Ed.), *Deployable Structures* (pp. 1–35). Springer. https://doi.org/10.1007/978-3-7091-2584-7_1

37. Piker, D. [DanielPiker]. (2021, May 31). *Kangaroo bipartite example file* [Computer software]. McNeel Forum. https://discourse.mcneel.com/t/kangaroo-bipartite/125118

38. Pillwein, S., Leimer, K., Birsak, M., & Musialski, P. (2020). On elastic geodesic grids and their planar to spatial deployment. *ACM Transactions on Graphics, 39*(4), 1–14. https://doi.org/10.1145/3386569.3392490

39. Pillwein, S., & Musialski, P. (2021). Generalized deployable elastic geodesic grids. *ACM Transactions on Graphics, 40*(6), 1–15. https://doi.org/10.1145/3478513.3480516

40. Recreus. (2024). *Filaflex 95 Foamy*. Retrieved May 12, 2025, from https://recreus.com/en/products/filaflex-95-foamy

41. Ren, Y., Kusupati, U., Panetta, J., Isvoranu, F., Pellis, D., Chen, T., & Pauly, M. (2022). Umbrella meshes. *ACM Transactions on Graphics, 41*(4), 1–15. https://doi.org/10.1145/3528223.3530089

42. Shaw, L. A., Sun, F., Portela, C. M., Barranco, R. I., Greer, J. R., & Hopkins, J. B. (2019). Computationally efficient design of directionally compliant metamaterials. *Nature Communications, 10*(1), 1–9. https://doi.org/10.1038/s41467-018-08049-1

43. Silverline. (n.d.). *Heavy Duty Hand Cable Puller 2000 kg / 3 m Cable* (Model 361253). Amazon.nl. https://www.amazon.nl/dp/B016YAJXJ8

44. Tibbits, S. (2012). Design to self-assembly. *Architectural Design, 82*(2), 68–73. https://doi.org/10.1002/ad.1381

45. Ultimaker BV. (2018, November 19). *Technical data sheet – TPU 95A filament* (Version 4.002) [PDF]. https://www.matterhackers.com/r/0HMNp5

46. Whitehead, A. S. (2019, February 3). Asymptotic grid structure of a triply periodic minimal surface – *WeWantToLearn.net*. WeWantToLearn.net. https://wewanttolearn.wordpress.com/tag/monoclastic/

47. Zadpoor, A. A. (2016). Mechanical metamaterials. *Materials Horizons, 3*(5), 371–381. https://doi.org/10.1039/c6mh00065g